

Integrative Gene Regulatory Network Analysis Discloses Key Driver Genes of Fibromuscular Dysplasia

Valentina d'Escamard, PhD,¹ Daniella Kadian-Dodov, MD,² Lijiang Ma, PhD,^{1,3} Sizhao Lu, PhD,^{4,5} Annette King, NP,² Yang Xu, MD,¹ Shouneng Peng, PhD,³ Bhargravi Vonguru, MS,¹ Yu Zhou, MMed,² Allison Thomas, MS,¹ Katherine C. Michelis, MD,¹ Emir Bander, MD,² Rihab Bouchareb, PhD,¹ Adrien Georges, PhD,^{6,7} Aya Nomura-Kitabayashi, PhD,¹ Robert J. Wiener, PhD,¹ Kevin D. Costa, PhD,¹ Elena Chepurko, DVM,¹ Vadim Chepurko, PhD,¹ Marika Fava, PhD,⁸ Temo Barwari, PhD,⁸ Anelechi Anyanwu, MD,⁹ Farzan Filsoufi, MD,⁹ Sander Florman, MD,¹⁰ Nabila Bouatia-Naji, PhD,^{6,7} Lukas E. Schmidt, MSc,¹¹ Manuel Mayr, MD, PhD,^{1,8} Michael G. Katz, MD,^{1,2,3,8} Ke Hao, PhD,³ Mary C.M. Weiser-Evans, PhD,^{4,5,12,13} Johan LM Björkegren, MD, PhD,^{2,3,14} Jeffrey W. Olin, DO,² Jason C. Kovacic MBBS, PhD.^{1,2,15,*}

Running title: A gene regulatory network in FMD

1 - Cardiovascular Research Institute, Icahn School of Medicine at Mount Sinai, New York, NY, USA

2 - The Zena and Michael A. Wiener Cardiovascular Institute, Icahn School of Medicine at Mount Sinai, New York, NY, USA

3 - Department of Genetics & Genomic Sciences, Institute of Genomics and Multiscale Biology, Icahn School of Medicine at Mount Sinai, New York, NY, USA

4 - Department of Medicine, Division of Renal Diseases and Hypertension, University of Colorado Anschutz Medical Campus, Aurora, CO, USA

5 - School of Medicine, Consortium for Fibrosis Research and Translation, University of Colorado Anschutz Medical Campus, Aurora, CO, USA

6 - INSERM, UMR970 Paris Cardiovascular Research Center (PARCC), France.

7 - Paris-Descartes University, Sorbonne Paris Cité, Paris 75006, France

8 - King's British Heart Foundation Centre, King's College London, United Kingdom

9 - Department of Cardiovascular Surgery, Icahn School of Medicine at Mount Sinai, New York, NY, USA

10 - Recanati-Miller Transplantation Institute, Icahn School of Medicine at Mount Sinai, New York, NY, USA

11 - Department of Internal Medicine II, Division of Cardiology, Medical University of Vienna, Währinger Gürtel 18-20, Vienna, Vienna, 1090, Austria

12 - Cardiovascular Pulmonary Research Program, University of Colorado Anschutz Medical Campus, Aurora, CO, USA

13 - Integrated Physiology PhD Program, Anschutz Medical Campus, Aurora, CO, USA

14 - Department of Medicine, Karolinska Institutet, Karolinska Universitetssjukhuset, Huddinge, Sweden

41 15 - Victor Chang Cardiac Research Institute, Darlinghurst, Australia; St Vincent's Clinical
42 School, University of NSW, Australia

43

44 * Corresponding author:

45 Dr Jason Kovacic

46 Cardiovascular Research Institute

47 One Gustave L. Levy Place, Box 1014

48 New York, NY, 10029-6574

49 Telephone: 212.824.9025

50 Fax: 212.241.4080

51 jason.kovacic@mountsinai.org

52

53 **Abstract**

54

55 Fibromuscular dysplasia (FMD) is a poorly understood disease affecting 3-5% of adult females.
56 The pathobiology of FMD involves arterial lesions of stenosis, dissection, tortuosity, dilation and
57 aneurysm which can lead to hypertension, stroke, myocardial infarction and even death.

58 Currently, there are no animal models for FMD and few insights as to its pathobiology. Here, by
59 integrating DNA genotype and RNA sequence data from primary fibroblasts of 83 FMD patients
60 and 71 matched healthy controls, we inferred 18 gene regulatory co-expression networks, four
61 of which were found to act together as an FMD-associated supernetwork in the arterial wall.

62 After *in vivo* perturbation of this co-expression supernetwork by selective knockout of a top
63 network key driver, mice developed arterial dilation; a hallmark of FMD. Molecular studies
64 indicated that this supernetwork governs multiple aspects of vascular cell physiology and
65 functionality, including collagen/matrix production. These studies illuminate the complex causal
66 mechanisms of FMD and suggest a potential therapeutic avenue for this challenging disease.

67

68

69 **Introduction**

70

71 Fibromuscular dysplasia (FMD) is a non-atherosclerotic, non-inflammatory vascular disease that
72 involves fibroblasts and smooth muscle cells (SMCs).¹ Mean age at diagnosis is ~50 years and
73 it is a disease that overwhelmingly affects women, with 80-90% of patients being female.²⁻⁴
74 While the incidence of clinically manifest FMD is debated, the true disease prevalence is
75 estimated to be 3-5% in adult females.^{5,6} Although FMD was first recognized over 80 years
76 ago,⁷ it remains an understudied medical enigma with no animal models, no specific treatments,
77 and very little known about its pathobiology.^{2,4,8,9}

78

79 FMD is classified as being either focal or multifocal, with the more common multifocal form
80 (~75% of cases) known to predominantly involve cellular and collagen/matrix changes arising in
81 the tunica media.^{2-4,8,10} Patients with FMD exhibit a cluster of diffuse alterations in SMC
82 function, arterial geometry, wall characteristics, and mechanical properties,¹¹ which can
83 culminate in the disease hallmarks of arterial fibrosis, stenosis, dissection, tortuosity, dilation,
84 aneurysm and occlusion of medium and large arteries throughout the body (Figs. 1a,b).^{2-4,12-14}
85 FMD commonly affects the renal arteries where it may cause hypertension, while cervical or
86 coronary artery involvement may cause stroke or myocardial infarction, respectively.^{2-4,15} Death
87 from FMD may arise from stroke or myocardial infarction,^{2-4,15} or from the involvement of other
88 arterial beds such as the mesenteric system causing fatal gut ischemia.¹⁶

89

90 Attempts at understanding the etiology of FMD have involved a variety of approaches.¹⁷⁻²⁰ A
91 recent genome-wide association study (GWAS) meta-analysis involving 1556 FMD cases
92 identified five loci that were independently associated with FMD.⁹ Although this was a major
93 advance, the ongoing knowledge gaps regarding this disease are highlighted by the limited
94 number of loci that have been associated with FMD and the lack of mechanistic understanding
95 of how these loci lead to the ensuing vascular pathology.

96

97 Systems genetics has emerged as a tractable and informative parallel approach to GWAS,
98 whereby layers of intermediate functional “omics” data (e.g., RNA sequencing transcriptomic
99 datasets) are integrated with genetics (e.g., DNA genotype datasets) to better elucidate gene-
100 host-environmental interactions leading to differing clinical phenotypes.²¹ Recently, the
101 application of systems genetics has markedly improved our understanding of other complex
102 vascular diseases such as coronary artery disease, by better outlining their broad basis for
103 heritability^{22,23} and, through inference of gene regulatory co-expression networks, by defining
104 new mechanisms of disease causality.²³⁻²⁶ Given the challenges surrounding FMD we initiated
105 DEFINE-FMD (NCT01967511), a systems genetics study leveraging blood samples and
106 fibroblasts obtained by skin biopsy to disclose key FMD gene regulatory co-expression
107 networks with disease drivers and causal pathways.¹⁹ Here, we present the primary DEFINE-
108 FMD findings arising from detailed systems analyses of fibroblasts from FMD cases and
109 matched controls.

110

111 **Results**

112 113 FMD patient fibroblasts exhibit differential gene expression

114 A total of 154 subjects from DEFINE-FMD and its forerunner, the CAUSE study, were included
115 in this analysis, comprising 83 patients with multifocal FMD and 71 healthy, age- and sex-
116 matched controls. Per the study enrollment criteria all cases and controls were female and of
117 self-reported Caucasian ethnicity. Their clinical characteristics are summarized in Table 1 and a
118 data analysis overview is provided in Fig. 1c. Primary fibroblasts were obtained from skin biopsy
119 samples for all subjects. Skin biopsies and their outgrowth fibroblasts were grown in highly
120 standardized explant culture conditions for 6-8 weeks prior to harvesting and downstream
121 analyses. This prolonged period of *ex vivo* culture extended well beyond the half-life of anti-
122 hypertensive medications or other potential confounding effects that might be present in these
123 cells when initially harvested.

124
125 We performed bulk RNA sequencing (RNAseq) on these primary fibroblasts and compared
126 differential gene expression (DGE), which identified 349 genes that were differentially
127 expressed in fibroblasts from FMD cases compared to matched healthy controls (Fig. 1d;
128 Supplementary Table 1). Most transcripts showed moderate differences in expression.
129 However, certain genes showed larger differences, with the greatest fold change for RAB5
130 interacting factor (*RAB5IF*; log₂ fold change 1.0) and pyridoxal phosphatase (*PDXP*; log₂ fold
131 change 0.93). Also, among differentially expressed transcripts there were several genes that
132 play an important role in vascular biology, including hypoxia-inducible factor (HIF)-1 α and matrix
133 metalloproteinase (MMP)-19. Gene Ontology (GO) analysis of this FMD fibroblast DGE identified
134 754 enriched gene sets (Figs. 1e,f; Supplementary Tables 2,3). Among the most markedly
135 upregulated gene sets, many were related to either cell signaling and signal transduction, cell
136 structure and architecture, or cellular biosynthetic processes.

137 138 A gene co-expression supernetwork implicated in FMD

139 Using this primary fibroblast RNAseq data, we combined the data from cases and controls and
140 inferred co-expression networks across the pooled dataset, which resulted in the identification
141 of 18 unique networks (Table 2). To better understand how these co-expression networks
142 interact within cells and because network-network interactions are especially powerful for
143 causing disease,^{23,27} these 18 networks were further combined according to the adjacency of
144 their eigengene values (Supplementary Fig. 1).^{23,27} This led us to identify 3 co-expression
145 supernetworks (SNs), named SN-A, -B and -C, which were comprised of 4, 6 and 8 co-
146 expression networks respectively (Table 2).

147
148 To assess the potential causal roles of these networks and supernetworks for FMD, we initially
149 undertook three independent analyses (Table 2): 1) Determination of network enrichment for
150 genes differentially expressed between FMD cases and controls; 2) Correlation of network gene
151 expression with the number of diseased vessels (controls = 0, FMD cases = 1 – 5 vessels; see
152 Table 1) and enrichment of the number of diseased vessels in each network (the number of

153 vessels affected by FMD is clinically used as a marker of disease severity⁴); 3) Determination of
154 the proportion of genes in each network which reached nominal significance ($P < 0.05$) in a
155 2016 FMD dataset comprising 249 FMD cases and 689 controls who underwent DNA exome-
156 chip array analysis (Kiando et al.¹⁷). Among all networks and supernetworks, SN-A was the only
157 network that was associated with FMD in all 3 analyses, with respective P values of 6.85×10^{-13} ,
158 9.69×10^{-25} , and 0.00026 (Table 2). Accordingly, we elected to focus on SN-A for further study. A
159 complete list of the 775 genes of SN-A is provided in Supplementary Table 4, and a visual
160 representation in Figs. 2a and 2c. Two of the 4 co-expression networks that comprise SN-A are
161 presented in Figs. 2d,e. Evaluation of the functions of SN-A by GO revealed a range of roles
162 that are potentially relevant to the FMD disease phenotype (Fig. 2b; Supplementary Table 5).

163
164 We next undertook an independent validation of SN-A in human tissues using the GTEx²⁸
165 arterial tissue RNAseq datasets. Specifically, we applied permutation connectivity testing²² to
166 validate if the genes of SN-A are also interconnected in these independent human arterial tissue
167 datasets. As a key validation, we found that the SN-A genes are highly interconnected in the
168 tissues of medium and large sized arteries from GTEx, including aorta, coronary artery and tibial
169 artery (Bonferroni corrected $P = 10^{-271}$, 10^{-126} , 10^{-259} , respectively).

170
171 In summary, the DEFINE-FMD study identified a gene co-expression supernetwork (SN-A) that
172 is associated with FMD. In addition, we demonstrated that SN-A replicates in the adult human
173 aorta, coronary artery and tibial artery using the independent GTEx RNAseq datasets. While it
174 was on the basis of the above data that we determined SN-A was likely to be causal for FMD
175 and thus elected to pursue it in detailed mechanistic studies, a subsequent FMD GWAS meta-
176 analysis published in 2021⁹ provided an additional opportunity to validate the association of SN-
177 A with FMD. As with the 2016 FMD exome-chip array dataset,¹⁷ we again looked for enrichment
178 in network genes that were nominally associated with FMD from this 2021 FMD GWAS.⁹ This
179 analysis again validated the strong association of SN-A with FMD ($P = 1.57 \times 10^{-7}$) (Table 2).

181 UBR4 is a key driver of SN-A

182 Gene regulatory networks were inferred from gene expression data using feature selection with
183 machine learning tree-based ensemble methods. A key driver analysis was then performed to
184 identify the high-hierarchy genes that govern the activity and function of SN-A. This identified 89
185 potential key driver genes for SN-A, with the top 14 of these all exhibiting an adjusted P value
186 indicative of their role as a key driver of $< 10^{-11}$ (Figs. 2a and 2c; Supplementary Table 6). We
187 sought to identify which of these top key driver genes might be best suited for further studies of
188 SN-A by first examining expression levels in human arterial tissues in GTEx. *UBR4* (ubiquitin
189 protein ligase E3 component n-recognin 4, also known as *P600*) emerged as exhibiting
190 significantly higher expression in aorta, coronary artery and tibial artery than any other of these
191 top key driver genes, thus making it a logical choice for subsequent knockdown experiments to
192 study and understand SN-A ($P < 4 \times 10^{-8}$ for all comparisons) (Figs. 3a-c; Supplementary Table
193 7).

194

195 An important step was to validate that *UBR4* is a potent key driver of SN-A. We created stable
196 Bj-5ta fibroblast cell lines with knockdown of *UBR4* (*UBR4-kd*) (Supplementary Fig. 2a).
197 Consistent with a key driver role, bulk RNAseq of *UBR4-kd* and control Bj-5ta fibroblasts
198 indicated marked changes in gene expression and cell function (Figs. 3d-f; Supplementary
199 Tables 8-10). Of the 775 genes in SN-A, 509 (65.7%) exhibited significantly altered expression
200 in *UBR4-kd* fibroblasts versus control cells (Supplementary Fig. 2b). We also performed a
201 hypergeometric test that evaluates to what extent a gene assigned a putative key driver role in a
202 network inferred from one dataset (i.e., in DEFINE-FMD) in fact governs the activity of this
203 network also in an independent dataset (i.e., in RNAseq data from *UBR4-kd* Bj-5ta fibroblast
204 cells).²⁷ This showed that compared to randomly selected genes, *UBR4* is a major key driver of
205 SN-A and exerts powerful regulatory control over the genes in this supernetwork ($P = 2.23 \times 10^{-165}$)
206 (Fig. 3g). Taken together, this hypergeometric test result and the differential expression of
207 65.7% of the SN-A genes in the *UBR4-kd* Bj-5ta fibroblast dataset shows that *UBR4* is a potent
208 key driver of SN-A. In a series of *in vitro* studies, we then profiled *UBR4-kd* Bj-5ta fibroblasts
209 (versus control cells). This revealed that knockdown of *UBR4* had a major impact on a range of
210 cellular functions including increased cell proliferation, increased cell contraction, reduced cell
211 adhesion and altered collagen/matrix production, whereas cell senescence and apoptosis were
212 not affected (Extended Data Figs. 1-4).

213
214 Prior histopathological studies suggest an interplay and “morphologic continuum”¹ of the cell
215 types that cause FMD – implicating SMCs, fibroblasts and myofibroblasts.^{1,10,29} Therefore, we
216 also explored *UBR4*'s effects in SMCs, by creating a stable knockdown of *UBR4* in human
217 aortic SMCs (HASMCs) *in vitro*. Similar to Bj-5ta fibroblasts, *UBR4-kd* HASMCs (as compared
218 to control HASMCs) exhibited marked changes in gene expression and cell function (Extended
219 Data Figs. 5-8; Supplementary Tables 11-16). Furthermore, a hypergeometric test validated the
220 findings in Bj-5ta fibroblasts and showed that compared to randomly selected genes, *UBR4* is
221 also a major key driver of SN-A in HASMCs ($P = 2.51 \times 10^{-93}$) (Extended Data Fig. 5e).
222 Importantly, *UBR4-kd* HASMCs exhibited particularly marked changes in collagen/matrix
223 production (Extended Data Fig. 8).

224
225 Immunofluorescence staining of human arterial samples was then performed to evaluate the
226 protein expression pattern of *UBR4*, which has not been well characterized in adult human
227 vascular tissues.³⁰ This showed robust *UBR4* protein staining in the tunica media of the internal
228 mammary and renal arteries, both being medium-sized arteries that are predisposed to
229 developing FMD,^{2,4,8,30,31} with the predominant cell type exhibiting *UBR4* staining being medial
230 vascular SMCs (Figs. 3h-k). *UBR4* expression was also observed in endothelial cells and
231 adventitial fibroblasts (Figs. 3l-o).

232
233 Collectively, these studies identified and validated that *UBR4* is a top key driver of SN-A, and
234 that *UBR4* is implicated in controlling multiple FMD-relevant aspects of cell functionality,
235 including proliferation, contraction, adhesion and collagen/matrix production. Furthermore,
236 *UBR4* shows particularly robust protein expression in vascular SMCs in the tunica media of

237 adult human arteries – which is consistent with the fact that multifocal FMD is also known to
238 arise from this anatomical arterial layer.²⁻⁴

239

240 *In vivo Ubr4* knockout causes a phenotype with features of FMD

241 To understand the role of SN-A *in vivo*, we created mice with inducible SMC-specific knockout
242 of *Ubr4* (*Sm22 α -CreER^{T2};Ubr4^{flox/flox}*; henceforth *Sm22 α -Ubr4^{KO}*). To overcome the previously
243 demonstrated issue that constitutive *Ubr4* knockout is embryonically lethal due to placental
244 vascular malformations,³²⁻³⁴ mice received tamoxifen beginning at 4 weeks of age to delete
245 *Ubr4* in SMCs after the embryonic period (Figs. 4a-e). Given that 80-90% of FMD patients are
246 female,²⁻⁴ studies using *Sm22 α -Ubr4^{KO}* mice were performed using female mice. *Sm22 α -Ubr4^{KO}*
247 mice were examined at two time points, being at 5 months (Fig. 4 [except 4e] and
248 Supplementary Figs. 3-7) and 14 months (Supplementary Figs. 8-11) after tamoxifen
249 administration.

250

251 Recapitulating one of the hallmarks of FMD, female *Sm22 α -Ubr4^{KO}* mice exhibited marked
252 dilation of the entire thoracic and abdominal aorta. By ultrasound, the extent of aortic dilation
253 was ~30-50% at 5 months after tamoxifen administration (Figs. 4f-m), and 40-60% at 14 months
254 after tamoxifen (Supplementary Fig. 8). The extent of arterial dilation was confirmed by
255 histopathological staining (Figs. 4n-v and Supplementary Figs. 5-6 and 9-11). Consistent with
256 the *in vitro* protein data (Extended Data Figs. 4,8), evaluation of collagen/matrix proteins
257 revealed marked changes in aortas from female *Sm22 α -Ubr4^{KO}* mice (Supplementary Fig. 7).

258

259 To validate these findings and although only a minority (~10-20%) of FMD patients are male, we
260 used an alternate SMC-specific Cre driver strain (*SMMHC-CreER^{T2}*) to delete *Ubr4* in male
261 mice (*SMMHC-CreER^{T2};Ubr4^{flox/flox}*; henceforth *SMMHC-Ubr4^{KO}*). This alternate *SMMHC-*
262 *CreER^{T2}* strain was chosen because at that time it was considered the gold standard for
263 studying vascular SMCs in mice,³⁵⁻³⁷ but it has the limitation of carrying the transgene on the Y-
264 chromosome (which precludes analysis in females). These studies in male *SMMHC-Ubr4^{KO}*
265 mice provided almost identical results to those in female *Sm22 α -Ubr4^{KO}* mice (Fig. 5 and
266 Supplementary Figs. 12-15). As an additional finding that is consistent with an FMD phenotype,
267 we observed an increase in collagen content in the tunica media of *SMMHC-Ubr4^{KO}* mice
268 compared to littermate controls throughout the thoracic and abdominal aorta (Fig. 5t,u;
269 Supplementary Figs. 14j,k and 15j,k).

270

271 In terms of other effects of SMC-specific *Ubr4* knockout, an extensive analysis of both *Sm22 α -*
272 *Ubr4^{KO}* and *SMMHC-Ubr4^{KO}* mice (compared to their respective littermate controls) did not
273 reveal any other issues that might account for the arterial dilation phenotype (Supplementary
274 Figs. 3-4, 8, 12-13). In particular, although the effect was inconsistent, blood pressure and
275 cardiac function tended to be lower with SMC-specific *Ubr4* knockout. While the reasons for this
276 are unknown, it appears unlikely to be related to the phenotype observed in *Sm22 α -Ubr4^{KO}* and
277 *SMMHC-Ubr4^{KO}* mice because lower blood pressure and cardiac function would be expected to
278 be protective against arterial dilation.

279

280 Perturbation of matrix and collagen due to SN-A and *Ubr4*

281 To further explore these findings, we performed single cell RNAseq (scRNAseq) of arterial
282 tissues from female mice with inducible SMC-specific knockout of *Ubr4* which also expressed
283 tdTomato (tdT) in SMCs (*Sm22 α -CreER^{T2};tdTomato;Ubr4^{fllox/fllox}*, henceforth *tdT-Sm22 α -Ubr4^{KO}*).
284 Control mice for scRNAseq studies were female *Sm22 α -CreER^{T2};tdTomato* mice, which also
285 expressed tdT in SMCs, but which did not have knockout of *Ubr4*.

286

287 We sorted tdT⁺ and tdT⁻ cells from aortas and carotid arteries of *tdT-Sm22 α -Ubr4^{KO}* and control
288 mice and performed scRNAseq on these populations. Dimension reduction and clustering were
289 performed to visualize the data (Fig. 6a). Expression of marker genes was examined to
290 annotate specific clusters (Extended Data Fig. 9a). As expected, tdT⁺ cells predominantly
291 contributed to SMC clusters, with lesser contributions to fibroblast clusters (Fig. 6b). Importantly,
292 *Ubr4* knockout induced major shifts in SMC clusters (Fig. 6c,d) and in particular, an expansion
293 of clusters SMC_1 and SMC_7 (Extended Data Fig. 9b). In contrast, *Ubr4* knockout had only a
294 minor impact on the composition of major tdT⁻ populations (Extended Data Fig. 9c).

295

296 We further examined differentially expressed genes in *tdT-Sm22 α -Ubr4^{KO}* versus control mice
297 among all SMC clusters, and identified 333 upregulated genes (> 1.5-fold change, FDR < 0.05)
298 and 557 downregulated genes (< 2/3-fold change, FDR < 0.05). As expected, *Ubr4* expression
299 was significantly downregulated when comparing across all SMC clusters in *tdT-Sm22 α -Ubr4^{KO}*
300 versus control mice (FDR = 4.2 x 10⁻¹⁴) (Fig. 6e; Supplementary Table 17). GOBP enrichment
301 analysis of the upregulated genes did not identify significant processes (Supplementary Table
302 18), while the downregulated genes were enriched in GOBPs such as extracellular matrix
303 organization and SMC migration (Fig. 6f; Supplementary Table 19), suggesting that *Ubr4*
304 knockout has a significant impact on SMC migration and the SMC contribution to extracellular
305 matrix content. Among the 775 genes in SN-A, we identified 572 that had known mouse
306 orthologs and which showed expression in the scRNAseq data. A total of 229 of these 572
307 genes in SN-A (40.0%) exhibited altered expression (FDR < 0.05) in tdT⁺ SMCs from *tdT-*
308 *Sm22 α -Ubr4^{KO}* versus control mice, with 148 upregulated (Supplementary Table 20) and 81
309 downregulated genes (Supplementary Table 21). Among these differentially expressed genes,
310 we identified genes related to tissue fibrosis (*Clip1*, *Postn*) and numerous collagen/matrix-
311 related genes (Fig. 6g). In addition, we scored the cells in the scRNAseq data according to the
312 572 SN-A orthologous genes which also showed expression in the scRNAseq data. The results
313 indicated that tdT⁺ cells, and particularly tdT⁺ cells from *tdT-Sm22 α -Ubr4^{KO}* mice, had higher SN-
314 A signature scores compared to tdT⁻ cells from either *tdT-Sm22 α -Ubr4^{KO}* or control mice (Fig.
315 6g). We also examined differentially expressed genes in both SMC_1 (Supplementary Table 22)
316 and SMC_7 (Supplementary Table 23), with SMC_7 comprising a major proportion of the
317 SMCs, against clusters SMC_2-6. GOBP enrichment showed that, with knockout of *Ubr4*,
318 cluster SMC_1 exhibited downregulation of genes involved in extracellular matrix production,
319 SMC migration and proliferation (Extended Data Fig. 10a, right panel), while cluster SMC_7

320 exhibited a gene signature consistent with dysregulated SMC migration and proliferation
321 (Extended Data Fig. 10b).

322
323 Given the contribution of tdT⁺ cells to fibroblast clusters, we looked for effects of *Ubr4* knockout
324 in these cells and identified 255 upregulated and 197 downregulated genes in tdT⁺ fibroblasts
325 from *tdT-Sm22α-Ubr4^{KO}* versus control mice (Fig. 6h; Supplementary Table 24). Although the
326 fold-change for *Ubr4* downregulation in tdT⁺ fibroblasts was only 0.72 (log2 fold change = -
327 0.48), and therefore *Ubr4* was filtered out and is not included in this list of downregulated genes,
328 its downregulation was nevertheless statistically significant (FDR = 0.005). GOBP analysis
329 indicated that genes which are upregulated in tdT⁺ fibroblasts from *tdT-Sm22α-Ubr4^{KO}* mice are
330 enriched in processes related to muscle contraction (e.g., *Acta2*, *Myh11*), extracellular matrix
331 (e.g., *Postn*, *Adamts1*, *Mmp17*) and cell migration (Fig. 6i). A comparison among tdT⁻ fibroblasts
332 from *tdT-Sm22α-Ubr4^{KO}* versus control mice revealed 303 upregulated genes and 249
333 downregulated genes, which included an array of extracellular matrix genes (Fig. 6j;
334 Supplementary Table 25). As expected, no significant difference in *Ubr4* expression was
335 observed between these tdT⁻ populations from *tdT-Sm22α-Ubr4^{KO}* versus control mice (Fig. 6j).
336 GOBP analysis revealed that the upregulated genes in tdT⁻ fibroblasts from *tdT-Sm22α-Ubr4^{KO}*
337 versus control mice were enriched in an array of processes including cell migration (Fig. 6k).

338
339 We also examined the secondary effects of *Sm22α*-driven *Ubr4* knockout on other non-*Sm22α*-
340 expressing cell populations. Endothelial cells from *tdT-Sm22α-Ubr4^{KO}* versus control mice
341 exhibited 62 upregulated and 28 downregulated genes (Extended Data Fig. 10c; Supplementary
342 Table 26). Macrophages from *tdT-Sm22α-Ubr4^{KO}* versus control mice exhibited 310
343 downregulated genes and 200 upregulated genes (Extended Data Fig. 10d; Supplementary
344 Table 27). These downregulated genes in macrophages from *tdT-Sm22α-Ubr4^{KO}* versus control
345 mice were enriched in GOBP terms related to extracellular matrix (Extended Data Fig. 10e).
346 Due to their small cluster sizes, differential expression analysis of dendritic cells
347 (Supplementary Table 28) and T cells (Supplementary Table 29) yielded few genes and/or
348 pathways.

349 FMD heritability due to SN-A

350 Having validated an FMD-relevant phenotype when SN-A is perturbed in mice by SMC-specific
351 knockout of *Ubr4*, we returned to our human datasets to determine the proportion of FMD
352 heritability that is accounted for by SN-A. To this end, methods such as linkage disequilibrium
353 score (LDSC) regression have been developed to determine the component of genetic disease
354 heritability carried by the genetic regulation (i.e., expression quantitative trait loci [eQTLs]) of
355 gene regulatory co-expression networks and supernetworks.^{22,23,38} Applying LDSC to the FMD
356 GWAS meta-analysis dataset,⁹ we determined that eQTLs in SN-A account for 45.4% of FMD
357 heritability (H²). By comparison, eQTLs in SN-B and SN-C accounted for 0% and 2.0% of FMD
358 heritability, respectively.

359
360
361

362 Discussion

363

364 Until recently, it has not been possible to fully understand complex biologic interactions at a
365 depth and resolution that is reflective of their true state.^{21,39} However, advances in technologies
366 like RNAseq, and progress in bioinformatics, have led to the emergence of 'systems genetics',
367 which provides the ability to study the true complexity of pathobiological molecular interactions
368 and processes.^{21,39} In the context of disease pathobiology and causality, multiple genes are
369 understood to cluster together into 'disease modules'.⁴⁰ Specifically, a 'disease module'
370 represents a group of network genes that together contribute to cellular functions - the
371 disruption of which results in a particular disease phenotype.⁴⁰ Moreover, additional recent
372 studies have shown that these gene networks make a direct contribution to the heritability of
373 complex disorders.^{22,23}

374

375 In the context of FMD, which until recently was of entirely unknown cause, certain prior studies
376 had suggested unique changes in dermal fibroblasts from subjects with FMD.⁴¹ Here, we
377 leveraged this knowledge and applied a 'systems genetics' approach to understand this
378 disease. Using samples from the DEFINE-FMD study comprising a total of 83 female FMD
379 patients and 71 healthy matched controls, we identified and validated a gene regulatory co-
380 expression supernetwork (SN-A) that appears to play a causal role in this disease, and which
381 accounts for a significant proportion of FMD heritability (H^2). *UBR4* was found to be a top key
382 driver of this supernetwork, and consequently the knockout of *Ubr4* in SMCs in mice led to a
383 vascular phenotype that recapitulates key clinical features of FMD: arterial dilation^{2-4,12-14} and
384 altered collagen/matrix production.^{9,20,42} Specifically, with regard to the major mouse phenotype
385 of aortic dilation that arose with perturbation of SN-A (Figs. 4,5), two recent independent studies
386 have shown that aortic dilation and aneurysm are key clinical features of FMD.^{13,14} Furthermore,
387 while *in vitro* and *in vivo* molecular profiling revealed that *UBR4* and SN-A govern a range of
388 disease-relevant cellular processes, several of these experiments showed that changes in
389 extracellular matrix and collagen are particularly important aspects of their effects (Figs. 5,6;
390 Extended Data Figs. 4,5,8,10; Supplementary Fig. 7).

391

392 *UBR4* is an N-recognin of the N-end rule pathway, which is a proteolytic system in which
393 destabilizing N-terminal residues of short-lived proteins act as degradation determinants (N-
394 degrons). Substrates carrying N-degrons are recognized by N-recognins (e.g., *UBR4*) that
395 mediate ubiquitylation-dependent selective proteolysis.^{33,43} As well as exhibiting robust
396 expression levels in arterial tissues (Figs. 3a-c, Supplementary Table 7) and therefore being
397 ideal for subsequent knockdown studies to understand SN-A *in vitro* and *in vivo*, *UBR4* was also
398 a particularly interesting candidate key driver for SN-A because it had previously been
399 described as regulating vascular development and angiogenesis.³²⁻³⁴ Specifically, and although
400 unstudied in the adult cardiovascular system, constitutive total *Ubr4* knockout in mice had been
401 shown to cause embryonic lethality due to placental vascular malformations, with a failure of
402 vascular mesenchymal cells and vessel dilation.³²⁻³⁴ Knowing also from our results that the
403 effects of *UBR4* are very strongly linked to SN-A activity (see hypergeometric test results; $P =$

404 2.23 x 10⁻¹⁶⁵ in Bj-5ta fibroblasts and $P = 2.51 \times 10^{-93}$ in HASMCs) it was a logical choice to
405 further investigate the role of this supernetwork.

406
407 Interestingly, while we were already conducting *in vivo* studies of SN-A and *UBR4* in mice, a
408 series of manuscripts emerged regarding the role of *UBR4* in adult skeletal muscle,^{44,45} showing
409 that *UBR4* promotes skeletal myofiber hypertrophy without change in the number of muscle
410 fibers or increase in muscle strength. However, the specific effect of *UBR4* deletion on different
411 skeletal muscle fiber types (i.e., types 2A, 2X, 2B) was dependent on the age of the mice and
412 whether acute versus chronic *UBR4* loss was induced.^{44,45} By comparison, in our *in vitro* studies
413 we found that *UBR4* knockdown was associated with a number of disease-relevant cellular
414 changes, including increased cell contraction in Bj-5ta fibroblasts (Extended Data Fig. 1d).
415 However, it is critical to note that our studies with *UBR4* were not undertaken to understand
416 *UBR4 per se*, but as a tool to modulate and understand SN-A. Furthermore, while the collective
417 data from our manuscript points to a causal role for SN-A in FMD, we cannot specifically ascribe
418 causality to *UBR4* based on our data. As a factor that will require further study, in human
419 physiology and disease a multitude of other factors might also control SN-A and its activity (i.e.,
420 alternate key drivers). Nevertheless, the fact that *UBR4* can act as a key driver of SN-A was
421 robustly demonstrated in our study, with the aforementioned hypergeometric test showing a P
422 value of 2.23 x 10⁻¹⁶⁵ in Bj-5ta fibroblasts and $P = 2.51 \times 10^{-93}$ in HASMCs.

423
424 Several recent studies have indicated that FMD, and the closely related disease spontaneous
425 coronary artery dissection (SCAD), are both related to other connective tissue disorders in their
426 pathologic basis. In particular, *COL3A1* (causative in vascular Ehlers Danlos Syndrome) and
427 *Fibrillin-1* (*FBN1*; causative in Marfan disease) have both been implicated in SCAD.⁴⁶⁻⁴⁸ It is
428 notable that when SN-A was perturbed, this was associated with altered levels of both *COL3A1*
429 and *FBN1* (Extended Data Figs. 4,5,8). Also of note, FMD and SCAD are increasingly
430 recognized as arising largely due to alterations in extracellular matrix and collagen^{9,20,42,47,48} –
431 which was again consistent with the effects of SN-A (Fig. 6; Extended Data Figs. 4,5,8,10;
432 Supplementary Fig. 7). Furthermore, perturbation of SN-A was associated with altered gene
433 expression levels of *ADAMTSL4*, *COL3A1*, *COL4A1*, *COL4A2*, *COL5A1*, *COL5A2*, *F3*, *FBN1*,
434 *HTRA1*, *ITGA1*, *LOX*, *LRP1*, *MYH11*, *NOTCH1*, *SLC24A3*, *TGF-βR1*, *TGF-βR2*, *TLN1*, *TIMP3*
435 (Fig. 3d, Supplementary Table 8) – with each of these genes being implicated in FMD and/or
436 SCAD.^{9,20,46-48} Collectively, this confirms that SN-A governs multiple key vascular genes and
437 functions that are related to FMD and also to SCAD.

438
439 As discussed, FMD is associated with alterations in extracellular matrix and collagen,^{9,20,42}
440 vascular cell function, arterial geometry, wall characteristics, and mechanical properties,¹¹ which
441 can lead to the disease hallmarks of arterial fibrosis, stenosis, dissection, tortuosity, dilation,
442 aneurysm and occlusion.^{2-4,12-14} Our *Sm22α-Ubr4*^{KO}, *tdT-Sm22α-Ubr4*^{KO} and *SMMHC-Ubr4*^{KO}
443 mice exhibited several but not all of these features, and there are a number of likely factors
444 accounting for the phenotypic differences between our mouse models and the human disease.
445 First, clinical FMD is very rarely associated with all of the abovementioned features in individual

446 patients (see Table 1 and refs^{2-4,12,13}), therefore, it is unrealistic to expect that *Sm22α-Ubr4^{KO}*,
447 *tdT-Sm22α-Ubr4^{KO}* or *SMMHC-Ubr4^{KO}* mice would also exhibit all of these vascular
448 perturbations. Second, we determined that SN-A accounts for 45.4% of FMD heritability and
449 therefore other genes, networks and additional heritable elements are also involved in the
450 clinical FMD phenotype. Third, as with all murine arterial disease models, the major differences
451 between humans and mice in terms of arterial dimensions, shear forces, stiffness, pressure,
452 effects of Laplace's law and other factors undoubtedly played a role in the final murine
453 phenotype. Fourth, FMD commonly involves the internal carotid and renal arteries, but despite
454 differing approaches we were not satisfied that these vessels could be harvested without undue
455 traction / manipulation / trauma to these arteries that would likely cause distortion for
456 histopathologic analysis. Beyond differences between the human FMD phenotype and our
457 mouse models, there are additional potential limitations to this study. Among these, we did not
458 explore protein-protein interactions that may be involved in FMD (only RNA-RNA interactions in
459 the context of genes in SN-A were studied), and other key drivers that might also govern SN-A
460 were not explored. Nevertheless, and despite these limitations, our discovery that *Sm22α-*
461 *Ubr4^{KO}*, *tdT-Sm22α-Ubr4^{KO}* and *SMMHC-Ubr4^{KO}* mice recapitulate key network changes and
462 several aspects of the clinical FMD phenotype is a major advance for the field, which will be of
463 significant value for understanding this complex disease.

464

465 In summary, using patient-derived samples from the DEFINE-FMD study we applied a state-of-
466 the-art systems genetics approach to study this common but poorly understood disease that
467 overwhelmingly affects women. This led us to identify a disease-relevant gene regulatory co-
468 expression supernetwork that appears causal for FMD and which accounts for a substantial
469 proportion of FMD disease heritability. By targeting *UBR4*, a top key driver of this supernetwork,
470 we created the first mouse model for FMD and provide detailed insights into the specific
471 pathobiological processes that cause this disease, suggesting a complex interplay between
472 altered vascular cell functionalities and collagen/matrix balance. This study opens the door to
473 targeted modulation of *UBR4* and SN-A, which may hold promise as a clinical therapeutic
474 approach for FMD.

475

476 **Methods**

477

478 **The DEFINE-FMD clinical study**

479 The details of the DEFINE-FMD study have previously been published.¹⁹ In brief, DEFINE-FMD
480 is a systems biology study aiming to define key disease drivers and mediators of FMD. Its
481 forerunner pilot study, the CAUSE study (ClinicalTrials.gov Identifier: NCT01808729), enrolled
482 its first 'run-in' control subject on October 31st 2012, and first FMD patient on February 22nd
483 2013. As the CAUSE study approached target enrollment it was closed (at n=34 subjects) and
484 we initiated DEFINE-FMD (ClinicalTrials.gov Identifier: NCT01967511). DEFINE-FMD continues
485 to recruit subjects and as of May 2024 over 440 subjects have been enrolled (approximately
486 60% cases, 40% controls). Both the CAUSE and DEFINE-FMD studies are observational, case-
487 controlled, cross-sectional studies, and both were approved by the institutional review board of
488 the Icahn School of Medicine at Mount Sinai. All subjects gave written informed consent.

489 For this primary fibroblast analysis, in early 2015 we identified 57 FMD cases and 47
490 matched controls from the CAUSE (24 cases) and DEFINE datasets (33 cases and all 47
491 controls) for initial studies of fibroblast gene expression (total = 104 subjects). After pilot
492 analyses, we elected to increase the subject numbers by adding an additional 26 FMD cases
493 and 24 controls (all from the DEFINE study), giving a total study sample size of 83 FMD cases
494 and 71 controls (total = 154 subjects) (Table 1).

495 Inclusion criteria for entry into DEFINE-FMD include ≥ 18 years of age, being freely
496 willing to participate, and fluency in English. FMD cases are required to have a clinical diagnosis
497 of multifocal FMD that is confirmed by imaging (computed tomographic angiography, magnetic
498 resonance angiography or catheter-based angiography). Similar inclusion criteria also applied
499 for FMD cases in the CAUSE study. While DEFINE-FMD was recently expanded and is now
500 also enrolling subjects with spontaneous coronary artery dissection (SCAD) or cervical artery
501 dissection (CvAD) in the absence of typical multifocal FMD, these subjects with isolated SCAD
502 or CvAD were not included in this analysis. However, for this analysis, confirmed multifocal
503 FMD cases were permitted to have had SCAD and/or CvAD. In addition, per our original
504 enrollment criteria through until early 2017, only females were included in this analysis.
505 Furthermore, for this analysis we imposed the additional inclusion/exclusion criteria that controls
506 cannot be related to FMD cases.

507 Healthy control females were recruited from the general population that broadly matched
508 the age distribution of FMD cases. Inclusion criteria for healthy controls include no clinical
509 features of FMD, CvAD or SCAD (including no cervical or abdominal bruits, an absence of
510 family history of sudden death or aneurysm) and absence of any major ongoing systemic
511 disease including any condition requiring hospitalization, immune suppression, intravenous or
512 injected medications or that result in functional impairment in the performance of activities of
513 daily living. Healthy controls are pre-screened and matched to FMD cases according to age,
514 sex, race/ethnicity, and body mass index (BMI). However, because it would be almost
515 impossible to identify and recruit control subjects that are of precisely the same age as every
516 FMD case, healthy control females are recruited that broadly match the age and BMI
517 distribution of FMD cases. FMD cases and controls were enrolled concurrently, at the same site

518 and by the same investigative team, over the same time period, and with all samples handled
519 identically.

520 Exclusion criteria (for cases and controls) include: co-morbidities which reduce life
521 expectancy to one year; any solid organ or hematological transplantation, or those in whom
522 transplantation is considered; active autoimmune disease; illicit drug use; HIV positive; prior
523 malignancy. In controls, an additional exclusion criteria is an early-onset family history of any
524 form of vascular disease. Healthy controls also undergo screening clinical assessment, with
525 specific attention paid to any history or physical examination findings suggestive of FMD or
526 other vascular disease, by two clinical experts in FMD (JWO, DKD). Notably, 3 patients who
527 agreed to be a healthy control have been diagnosed with FMD after the screening history and
528 physical exam.

529 If the above entry criteria are met and following informed consent, venesection and 3 mm
530 skin punch-biopsy (from the medial aspect of the upper arm) are performed. At venesection, 20
531 ml of blood are collected: 10 ml is collected into EDTA tubes and is reserved for DNA extraction,
532 while 10 ml is collected in EDTA-anticoagulated (plasma) and non-anticoagulated (serum) tubes
533 (5ml each) and reserved for plasma/serum preparation. Samples are transported at room
534 temperature for processing within 15 mins.

535

536 Plasma, serum and DNA preparation

537 To obtain plasma, EDTA-anticoagulated blood is centrifuged at 2,000 g for 10 min. Blood for
538 preparation of serum is also centrifuged at 2,000 g for 10 min. Plasma and serum are then
539 aliquoted and immediately frozen at -80°C pending batched analysis. DNA is isolated from
540 whole blood using the Puregene Blood Core kit B (Qiagen, #158467 [since changed to
541 #158023]), according to the manufacturer's instructions. DNA is aliquoted and frozen at -80°C.

542

543 Primary fibroblast culture

544 Skin biopsy samples are kept in 10 ml of sterile PBS (Thermo Fisher Scientific, 10010023) at
545 room temperature and processed within 15 min after collection. Briefly, skin biopsy samples are
546 washed twice with 10 ml of sterile PBS, then cut into 4 pieces using a sterile scalpel, and plated
547 one piece/well onto a 6 well plate previously coated with gelatin (Millipore Sigma, SF008). The 4
548 pieces of skin are then covered with a sterile coverslip (Fisher Scientific, 12-546-2) and cultured
549 at 37°C in 5% CO₂ in fibroblast medium (Supplementary Table 30). The fibroblast medium is
550 changed every 2-3 days. The fibroblasts begin to migrate out of the tissue within the first several
551 days and are collected beginning at 3-4 weeks when they reach 80-90% confluency. For
552 fibroblast harvesting and collection, cells are washed with 1 ml of PBS/well, then trypsinized
553 using 0.5 ml of Trypsin-EDTA (0.25%) (Thermo Fisher Scientific, 25200056) per well. After 5
554 min incubation at 37°C, trypsin is neutralized with 1 ml of fibroblast medium. The detached cells
555 are then transferred to a sterile 15 ml falcon tube and centrifuged at 272 g for 5 min. The cell
556 pellet is resuspended with 500 µl of Recovery Cell Culture Freezing Medium (Thermo Fisher
557 Scientific, 12648010) and immediately frozen at -80°C, before being transferred within 1-2 days
558 to storage in liquid nitrogen for future use. The pieces of skin continue to produce fibroblasts

559 after successive rounds of cell harvesting as described above. An average of 10-15
560 vials/subject at different outgrowths are collected and stored.

561

562 Primary fibroblast RNA extraction and supernatant collection

563 For harvesting of RNA from primary human fibroblasts for downstream use in network analyses
564 as described in this manuscript, fibroblasts from the second outgrowth (6-8 weeks after the skin
565 samples were harvested and placed into culture) were trypsinized as described above and
566 2×10^6 fibroblasts in total were replated across 6 wells of a 6 well plate. When the fibroblasts
567 reached 90% confluency, cells were washed twice with PBS (2 ml/well) and incubated with 1.5
568 ml/well of DMEM/F-12 HEPES (Supplementary Table 30) for 24 hours. Cells were then washed
569 with PBS (2 ml/well) and incubated at 37°C with fibroblast medium for 8 hours. The fibroblasts
570 were washed twice with PBS (2 ml/well), and lysates from fibroblasts were collected adding 350
571 μ l/well of buffer RLT (Qiagen, RNeasy Mini Kit, 74104) supplemented with 1% of 2-
572 Mercaptoethanol (Thermo Fisher Scientific, 21985-023). The lysates were frozen and stored at -
573 80°C. RNA from cells lysates was extracted using an RNeasy Mini Kit (Qiagen, 74104) following
574 the manufacturer's instructions and stored at -80°C. RNA quantity and quality were analyzed
575 using a NanoDrop 2000c Spectrophotometer (Thermo Scientific).

576

577 Human renal and internal mammary artery collection

578 Adult human arterial samples were obtained under a separate study protocol that was approved
579 by the institutional review board of the Icahn School of Medicine at Mount Sinai. Full details of
580 this protocol have previously been published.^{19,49} Human renal and internal mammary artery
581 samples used in the current study were pre-existing and no subjects were recruited or enrolled
582 for the purposes of vascular tissue donation.

583

584 UBR4 knockdown in immortalized human Bj-5ta fibroblasts

585 Immortalized human Bj-5ta fibroblasts (ATCC, CRL-4001) were cultured at 37°C in 5% CO₂ in
586 fibroblast medium. Transduction of *UBR4* shRNA lentiviral particles and non-silencing Lentiviral
587 shRNA Control (scramble) into Bj-5ta fibroblasts was performed using the GIPZ *UBR4* ShRNA
588 Viral particle Starter Kit (Horizon/Dharmacon, VGH5518-200205973, source clone ID: V2LHS
589 238957) according to the manufacturer's instructions using MOI=3. *UBR4* knockdown (*UBR4*-
590 *kd*) and scramble control cells were cultured in fibroblast medium. Bj-5ta fibroblasts are not
591 among the known misidentified cell lines in the list maintained by the International Cell Line
592 Authentication Committee. Authentication was conducted by the supplier, but morphology and
593 experimental results, particularly RNAseq data, were consistent with these being human
594 fibroblasts.

595

596 UBR4 knockdown in human aortic smooth muscle cells (HASMCs)

597 Immortalized human aortic smooth muscle cells (HASMCs) (Applied Biological Materials,
598 T0515) were cultured at 37°C in 5% CO₂ in Prigrow I medium (Applied Biological Materials,
599 TM001) supplemented with 10% FBS (ThermoFisher Scientific, 16000044) and 1% antibiotic
600 antimycotic (ThermoFisher Scientific, 15240062). Transduction of *UBR4* shRNA lentiviral

601 particles and non-silencing Lentiviral shRNA Control (scramble) into HASMCs was performed
602 using the GIPZ UBR4 ShRNA Viral particle Starter Kit (Horizon/Dharmacon, VGH5518-
603 200238568, source clone ID: V3LHS 318553) according to the manufacturer's instructions using
604 MOI=3. Note that this is the same kit as was used for *UBR4* knockdown in Bj-5ta fibroblasts,
605 only a different clone showed superior knockdown efficacy that was used for HASMCs. *UBR4*
606 knockdown (*UBR4-kd*) and scramble control HASMCs were cultured in complete Prigrow I
607 medium supplemented with 10% FBS. HASMCs as use here are not among the known
608 misidentified cell lines in the list maintained by the International Cell Line Authentication
609 Committee. Authentication was conducted by the supplier, but morphology and experimental
610 results, particularly RNAseq data, were consistent with these being HASMCs.

611

612 RNA extraction and qRT-PCR for Bj-5ta fibroblasts and HASMCs

613 Total RNA was extracted from *UBR4-kd* and control cells (using the RNeasy Mini Kit as
614 described for primary human fibroblasts). Reverse transcription was performed using the iScript
615 cDNA Synthesis Kit (Bio-Rad, 1708891) according to the manufacturer's instructions. Reaction
616 conditions were 25°C for 5 mins, 46°C for 20 mins, 95°C for 1 min and 4°C hold temperature.
617 cDNA quantity and quality were analyzed using a Nano Drop 2000c Spectrophotometer. qRT-
618 PCR was performed using PerfeCTa SYBR Green FastMix Reaction Kit (VWR, 101414-292)
619 according to the manufacturer's instructions and was performed at 95°C for 3 mins, followed by
620 39 cycles of 95°C for 10 seconds and 55°C for 30 seconds. 18S rRNA was used as a control,
621 and gene expression was analyzed using the $\Delta\Delta C_t$ method. Real time PCR was performed
622 using a CFX96 Real-time PCR detection system with Maestro 1.1 software 4.1 (Bio-Rad).
623 Primers for human *UBR4* amplification and control were: *UBR4* fwd 5'-
624 TGTGAAGCTCATTGGCAGTC-3' and rev 5'-GCTGAACCTTCTTGGCTTTG-3';
625 18S fwd 5'-TTTCGGAAGTGAAGCCATGA-3' and rev 5'-GCAAATGCTTTCGCTCTGGTC-3'.

626

627 Subject genotyping

628 DNA samples were processed in two batches of 112 and 128 samples (240 in total),
629 respectively, which included additional CAUSE and DEFINE study subjects that were not
630 included in this analysis. All samples showed a call rate >99%, and were thus retained. No
631 genetically identical pairs were found, no outliers were identified in a Principal Components
632 Analysis (run using eigenstrat⁵⁰), and all samples were correctly predicted as females. Further
633 inspection of the samples' heterozygosity also revealed no outliers. Genotyping array probes
634 were filtered according to call rate (>95%) and Hardy-Weinberg equilibrium test *P* value (>1x10⁻⁶).
635 In the first batch, 961,962 probes passed the filters, and 2,231 failed. In the second batch
636 958,840 probes passed the filters, and 2,079 failed. Data from the two batches were then
637 merged along 949,070 shared variants.

638 In order to identify subject ethnicity, we projected the assayed genotype data on the first
639 two genetic principal components from the hapmap panel. Of the 240 subjects with genotype
640 data, we visually identified 214 subjects of Caucasian ancestry, and 26 of other ancestry. Of the
641 84 FMD cases and 71 controls in this study (154 total), 140 were identified as Caucasian while
642 14 were found to have at least partial non-Caucasian ancestry (8 cases and 6 controls).

643 Genotyping data was imputed using the 1000 Genomes panel (phase 3) and the Michigan
644 Imputation Server, using the minimac imputation pipeline. We successfully imputed 17,378,389
645 variants.

647 RNA sequencing

648 For both primary fibroblasts from study subjects and also Bj-5ta fibroblasts, samples were
649 prepared for RNA sequencing (RNAseq) using the TruSeq RNA Library according to the
650 manufacturer's instructions (Illumina, San Diego, CA), and RNAseq was performed on an
651 Illumina HiSeq2000. For HASMCs, samples were prepared using the Illumina Stranded mRNA
652 kit according to the manufacturer's instructions and RNAseq was performed on an Illumina
653 NovaSeq 6000. For primary fibroblasts derived from study subjects, a single end 100bp
654 sequencing strategy was used. For *UBR4-kd* and control cells, for both Bj-5ta fibroblasts and
655 HASMCs, a paired end 100bp sequencing strategy was used. All bulk RNAseq was performed
656 in the Genomics Core Facility of the Icahn School of Medicine at Mount Sinai (New York, USA).
657 Quality control was performed using FASTQC that checks raw sequence data for per-base
658 quality, per-sequence quality, number of duplicate reads, number of reads with an adaptor,
659 sequence length distribution, per-base GC content, per-sequence GC content and Kmer
660 content.⁵¹ GENCODE 29 was used as the reference annotation to quantify gene expression.
661 Sequencing reads (fastq files) for RNAseq data derived from primary fibroblasts and Bj-5ta
662 fibroblasts were mapped to GRCh38 human reference genome using STAR aligner version
663 3.6.0c with default mapping parameters,⁵² while for HASMCs sequencing reads were mapped
664 to GRCh38 human reference genome using STAR aligner version 2.7.5b. Low counts were
665 removed by retaining genes where the count per million (cpm) was greater than 1 in at least two
666 samples.

667 Primary human fibroblast RNAseq was performed as two cohorts and genes common in
668 two datasets were selected for subsequent data analysis. Batch effects were removed by R
669 (3.5.1) package sva.⁵³ After filtering zero and low counts, an average of 34 million reads were
670 retained per sample and 12,473 genes were presented. For the *UBR4* knockdown RNAseq
671 analysis in Bj-5ta fibroblasts, an average of 58 million reads were retained per sample and
672 13,381 genes were detected after filtering. For *UBR4* knockdown RNAseq analysis in HASMCs,
673 an average of 67 million reads were retained per sample and 27,759 genes were detected after
674 filtering. All samples from all RNAseq experiments passed quality control and had more than
675 10,000,000 uniquely mapped reads. Weighted trimmed mean of the log expression ratios
676 (trimmed mean of M values (TMM)) was applied for normalization.⁵⁴

678 Differential gene expression

679 Differential gene expression was analyzed using R package limma (3.38.2)⁵⁵ and sva. Age and
680 batch were covariates, and were adjusted by linear regression modeling. Statistical significance
681 was defined as combat Q value < 0.05 (primary fibroblasts) using sva analysis or adjusted *P*
682 value < 0.05 (*UBR4-kd* and control cells for Bj-5ta fibroblasts and HASMCs) using limma.
683 Differential protein abundance for *UBR4-kd* and control HASMCs was determined using the
684 same method.

685
686 Gene Ontology (GO) analysis (excluding scRNAseq data)

687 Gene functions for differentially expressed genes were analyzed and classified using Gene
688 Ontology (GO),⁵⁶ and enriched GO terms were analyzed by PANTHER.⁵⁷ For DGE between
689 primary fibroblasts from FMD cases and controls, a Binomial test without correction for multiple
690 comparison was performed for identifying significant GO terms. Bonferroni correction for
691 multiple testing was used for identifying significant GO terms (adjusted P value < 0.05) for
692 genes in SN-A, for DGE between *UBR4-kd* Bj-5ta fibroblasts and control cells, and for DGE
693 between *UBR4-kd* HASMCs and control cells. GO terms that had a fold enrichment of < 0.1
694 were removed from the final results, even if the adjusted P value was < 0.05 . For the visual
695 representation of these results, we present the top 10 GO terms based upon smallest P value
696 for both genes that show upregulation and also for gene with downregulation, that includes
697 gene ontology biological process (GOBP), molecular function (GOMF) and cellular component
698 (GOCC). For GO terms related to SN-A (Fig. 2b; Supplementary Table 5), only a single set of
699 GO results are presented related to the genes in SN-A.

700 For GO terms related to mass spectrometry proteomics data from *UBR4-kd* HASMCs
701 and control cells (see methods below) (Extended Data Fig. 8; Supplementary Tables 15 and
702 16), GO terms were obtained using the same analytic pipeline. Bonferroni correction for multiple
703 testing was applied to identify significant GO terms (adjusted P value < 0.05), and results are
704 presented as described above based upon proteins showing either increased or reduced
705 abundance.

706
707 Co-expression modules, network and key driver analyses

708 R package Weighted Gene Co-expression Network Analysis (WGCNA) was used to identify
709 correlation patterns among genes across RNAseq data from primary human fibroblasts from
710 FMD cases and controls, to construct correlation networks and identify co-expression
711 modules.⁵⁸ Sample clustering based on Euclidean distance as part of the R package WGCNA
712 analysis showed one control sample was an outlier, which was removed from the analysis
713 based on the recommendations of this software package. Expression matrices from the two
714 cohorts of fibroblast RNAseq data were normalized and adjusted for batch effects. By analyzing
715 expression matrices, highly correlated genes were identified as co-expression modules
716 according to eigengene values and co-expression modules were further grouped into tight
717 clusters of three meta-modules according to their mutual correlations with other modules in the
718 eigengene dendrogram for downstream analysis. These three meta-modules were named
719 supernetworks (SN) in this study (SN-A, SN-B, SN-C) (Supplementary Fig. 1). Permutation
720 connectivity testing was performed to validate module connectivity in the independent GTEx
721 dataset.²⁸ The built-in function in WGCNA for permutation connectivity testing was used to
722 examine module preservation between two datasets: gene expression in the aorta, coronary
723 artery and tibial artery tissues from GTEx were compared against our primary human fibroblast
724 RNAseq data for module connectivity of SN-A (numbers of subjects from GTEx in this analysis
725 were: aorta 197, tibial artery 285, coronary artery 118).

726 Association of network genes with number of diseased vessels was performed using
727 Poisson regression in R by setting the number of diseased vessels as the outcome variable
728 (controls = 0; FMD cases = 1 – 5 vessels per their clinical history) and gene expression level
729 from the primary fibroblast RNAseq data of each network gene as the explanatory variable.
730 Genes that were significantly associated with number of diseased vessels in each network and
731 supernetwork were counted, and an enrichment analysis of the number of significantly
732 correlated genes with number of diseased vessels in each network and supernetwork was
733 conducted using Fisher's exact test.

734 FMD GWAS single nucleotide polymorphisms (SNPs)^{9,17} with P value < 0.05 were
735 annotated and mapped to genes based on their SNP positions. The enrichment of genes that
736 have FMD GWAS loci in each network and supernetwork was analyzed by Fisher's exact test. P
737 value < 0.05 was considered statistically significant for enrichment analysis.

738 R package GENIE3 was used to infer gene regulatory networks from expression data
739 using the machine learning tree-based ensemble method Random Forests.⁵⁹ Weighted key
740 driver analysis (wKDA) for the meta-module SN-A was performed using Mergeomics
741 (<http://mergeomics.research.idre.ucla.edu>) wKDA tool which was built for integrative network
742 analysis of omics data.⁶⁰

743 A hypergeometric test in R was performed on *UBR4-kd* and relevant control cell RNAseq
744 data, for both Bj-5ta fibroblasts and HASMCs, to examine if *UBR4* knockdown significantly
745 affects the expression of genes in SN-A as compared to randomly selected group of genes in
746 the whole transcriptome.

747

748 Heritability analysis

749 We used the published 2021 FMD GWAS meta-analysis as the basis for determining the
750 heritability of SN-A, SN-B and SN-C.⁹ GWAS partitioning of SNP-heritability for SNs was
751 calculated using linkage disequilibrium (LD) score regression (LDSC),⁶¹ a software that requires
752 only GWAS summary statistics and LD information from an external reference panel that
753 matches the population studied in the GWAS. Only GWAS SNPs located on chromosomes 1 -
754 22 and with cut off nominal P value < 0.05 were used for the heritability analysis.

755

756 Cell proliferation assay

757 For assessment of cell proliferation in *UBR4-kd* and control Bj-5ta fibroblasts, we initially plated
758 control fibroblasts, fibroblasts treated with lentiviral vector containing scrambled shRNA (Scr)
759 and *UBR4-kd* fibroblasts onto 24 well plates in complete fibroblast medium (with FBS) at a
760 density of 120,000 cells/well in replicates of 3. After 24 hours, to synchronize the cells, for all
761 cells the medium was changed to fibroblast medium without FBS (serum free DMEM/F-12
762 HEPES medium). Next, cells were cultured for 18 hours under 3 different conditions: 1)
763 Starvation - culture in serum free DMEM/F-12 HEPES medium only; 2) Stimulation with FBS -
764 culture in DMEM/F-12 HEPES medium with 20% FBS; 3) Stimulation with TGF- β 1 - serum free
765 DMEM/F-12 HEPES medium supplemented with Recombinant Human TGF- β 1 (Peprotech,
766 100-21) at a final concentration of 20 ng/ml. Cells were then labeled with 10 μ M BrdU (Abcam,
767 ab142567) and cultured at 37°C in 5% CO₂ for 3 hours. Cells were then washed 4 times with

768 PBS, fixed with 4% paraformaldehyde (ThermoFisher Scientific, J61899.AP) for 10 mins and
769 permeabilized with 0.3% Triton X-100 for 10 mins. After incubation with 1M HCl for 10 mins at
770 room temperature, cells were washed 3 times with PBS and blocked with DAKO antibody
771 diluent (Agilent, S302283-2) for 1 hour at room temperature followed by overnight incubation at
772 4°C with anti-BrdU antibody (Novus Biologicals, NBP2-14890) in DAKO antibody diluent
773 (1:100). After 3 washes with PBS, cells were incubated with a secondary antibody (Thermo
774 Fisher Scientific, A10040) diluted 1:200 in DAKO antibody diluent for 1 hour at room
775 temperature and then washed and incubated with DAPI (Thermo Fisher Scientific, D3571)
776 diluted 1:1000 in PBS for 5 mins. The DAPI solution was then replaced with PBS and cells were
777 imaged on an inverted microscope (Leica, DMI8). For each condition, total and BrdU positive
778 cells were counted in 3 experimental replicates with ImageJ software (NIH, version 1.53e for
779 windows).

780 For assessment of cell proliferation in *UBR4-kd* and control HASMCs, the same methods
781 as above were used, with the only differences being that HASMCs were cultured in Prigrow I
782 medium supplemented with 10% FBS and 1% antibiotic antimycotic. HASMCs were cultured
783 under 3 different conditions: 1) Starvation - culture in serum free Prigrow I medium only; 2)
784 Stimulation with FBS - culture in Prigrow I medium with 10% FBS; 3) Stimulation with TGF- β 1 -
785 serum free Prigrow I medium supplemented with Recombinant Human TGF- β 1 at a final
786 concentration of 20 ng/ml.

787

788 Cell senescence assay

789 For Bj-5ta fibroblasts, we plated control fibroblasts, fibroblasts treated with lentiviral vector
790 containing scrambled shRNA (Scr), and *UBR4-kd* fibroblasts, onto a 24 well plate at a density of
791 72,000 cells/well in replicates of 3, and they were cultured under 3 different conditions as
792 described for the proliferation assay. A Senescence Cells Histochemical Staining Kit (Sigma,
793 CS0030) was used according to the manufacturer's instructions. In brief, cells were fixed for 7
794 mins at room temperature and stained with X-gal solution for 4 hours at 37°C without CO₂. Total
795 and senescent cells were imaged on an inverted microscope (Leica, DMI8) and counted in 3
796 experimental replicates using Image J software.

797 For HASMCs the same protocol was followed except that HASMCs were cultured in
798 Prigrow I medium supplemented with 10% FBS and 1% antibiotic antimycotic. The HASMCs
799 were cultured under 3 different conditions as described for the proliferation assay.

800

801 Cell contraction assay

802 For Bj-5ta fibroblasts, we plated control fibroblasts, fibroblasts treated with lentiviral vector
803 containing scrambled shRNA (Scr), and *UBR4-kd* fibroblasts as per the 3 conditions described
804 for the proliferation assay. Cells were then trypsinized and resuspended in the same original
805 medium (per the 3 conditions of starvation, stimulation with FBS or stimulation with TGF- β 1,
806 respectively) at 2.5×10^6 cells/mL for each condition. Cell suspensions were mixed 1:4 with a
807 collagen solution following the manufacturer's protocol (Cell Biolabs, CBA201) and plated onto
808 24 well plates in replicates of 4. After 1 hour incubation at 37°C, 1 ml of culture medium
809 (according to the different culture conditions) was added atop of the collagen gel. Cells were

810 incubated for 24 hours, and then contraction was initiated by releasing the collagen gels from
811 the side of the culture dish. Cells were incubated for an additional 48 hours, and the percentage
812 of collagen gel size change was measured with ImageJ software.

813 For HASMCs the same methods were used, with the only difference being that HASMCs
814 were cultured in Prigrow I medium supplemented with 10% FBS and 1% antibiotic antimycotic,
815 and then cultured under 3 different conditions as described for the proliferation assay. However,
816 unlike Bj-5ta fibroblasts that continued to grow and to contract under all 3 conditions, we noted
817 that HASMCs grown without FBS (i.e. conditions of either starvation or stimulation with TGF- β 1)
818 did not contract. We therefore assessed the viability of HASMCs in this contraction assay when
819 cultured without FBS using a Calcein AM kit (Thermo Fisher Scientific, C3099) according to the
820 manufacturer's instructions. Briefly, after performing the contraction assay, collagen gels
821 containing the HASMCs were moved to 4 wells of a new 24 well plate. Each well was washed
822 twice with PBS and cultured at 37°C in 5% CO₂ for 1 hour with 2 μ M Calcein AM. The cells were
823 imaged on an inverted microscope (DMI8, Leica). Upon analysis, the nonfluorescent calcein AM
824 was not converted to a green-fluorescent calcein, proving that HASMCs were not viable for this
825 assay under these conditions of either starvation or stimulation with TGF- β 1. Therefore, we
826 could not reach any reliable conclusion regarding the contraction of HASMCs grown under
827 these conditions, and only contraction data for HASMCs with FBS is presented (Extended Data
828 Fig. 6d).

829 830 Cell apoptosis assay

831 For Bj-5ta fibroblasts, we plated control fibroblasts, fibroblasts treated with lentiviral vector
832 containing scrambled shRNA (Scr), and *UBR4-kd* fibroblasts onto a 48 well plate at 50,000
833 cells/well in replicates of 3 and cultured under 3 different conditions as described for the
834 proliferation assay. As per the manufacturer's protocol (Millipore Sigma - Roche, 12156792910)
835 cells were fixed for 1 hour at room temperature. After permeabilization in 0.3% Triton X-100
836 solution, cells were stained with TUNEL reaction mixture for 1 hour at 37°C. Cells were then
837 incubated with DAPI solution as described in the proliferation assay. Total and red labeled cells
838 were imaged on an inverted microscope (DMI8, Leica) and counted manually by a blinded
839 observer.

840 For HASMCs the same methods were used, with the only difference being the HASMCs
841 were cultured in Prigrow I medium supplemented with 10% FBS and 1% antibiotic antimycotic,
842 and then cultured under 3 different conditions as described for the proliferation assay.

843 844 Cell adhesion assays

845 Bj-5ta fibroblasts treated with lentiviral vector containing scrambled shRNA (Scr) or *UBR4-kd* Bj-
846 5ta fibroblasts were cultured under 3 different conditions as described for the proliferation
847 assay. The CytoSelect 48-well Cell Adhesion Assay (Cell Biolabs CBA-070) was used
848 according to manufacturer's instructions. Briefly, cells were trypsinized, resuspended and plated
849 at 100,000 cells per well onto protein-coated 48 well plates in replicates of 3. Wells were pre-
850 coated with either Bovine Serum Albumin, Fibronectin, Collagen I, Collagen IV, Laminin I, or
851 Fibrinogen. Cells were then incubated for 1 hour at 37°C and the unbound cells were washed

852 away. Adherent cells were then stained, and the stain extracted and transferred to a 96 well
853 microtiter plate. The absorbance was measured at 560 nm using a SpectraMax M5 microplate
854 reader. For HASMCs the same protocol was followed except the HASMCs were cultured in
855 Prigrow I medium supplemented with 10% FBS and 1% antibiotic antimycotic, and then cultured
856 under 3 different conditions as described for the proliferation assay.

857 As an alternate way to assess adhesion, control Bj-5ta fibroblasts, Bj-5ta fibroblasts
858 treated with lentiviral vector containing scrambled shRNA (Scr), and *UBR4-kd* Bj-5ta fibroblasts
859 were cultured in 3 different conditions as per the proliferation assay and were trypsinized,
860 resuspended and plated at 500,000 cells per well onto a 6 well plate, with 2 ml of the respective
861 media, in replicates of 4. After overnight incubation, the medium (including all floating/detached
862 cells) was collected and centrifuged at 320 g for 5 mins. The cell-free medium was discarded,
863 and the pellet resuspended in 50 μ l of PBS and the cells counted using a Hemacytometer
864 (Fisher Scientific, 0267151B). For HASMCs we attempted this method but there were too few
865 cells identified in the pellet to be counted with accuracy.

866 Proteomics analysis of supernatant from Bj-5ta fibroblasts

867 Bj-5ta fibroblasts treated with lentiviral vector containing scrambled shRNA (Scr) or *UBR4-kd* Bj-
868 5ta fibroblasts were cultured with fibroblast medium on a 6 well plate in replicates of 5 until they
869 reached 80% confluency. Cells were then washed 5 times with PBS and cultured with serum
870 free DMEM/F-12 HEPES medium for 4 hours. Cells were washed again 5 times with PBS and
871 cultured again for 24 hours with serum free DMEM/F-12 HEPES medium. The supernatants
872 were then collected, centrifuged at 4,700 g for 10 mins, transferred to a new clean tube and
873 immediately frozen at -80°C pending analysis.

875 For analysis, samples were concentrated using 3kDa molecular weight cut off spin filters
876 (Merck, Amicon), denatured by 6 M urea, 2 M thiourea, and reduced with 10 mM dithiothreitol at
877 37°C for 1 hour. Then, proteins were alkylated with 50 mM iodoacetamide and incubated in the
878 dark for 1 hour at room temperature. Next, proteins were precipitated by adding 10x volume of
879 pre-chilled acetone and incubated at -20°C overnight. Samples were centrifuged at 16,000 g at
880 4°C for 30 mins and the supernatant was discarded. The pellets were dried with a SpeedVac
881 (Thermo Fisher Scientific) for 10 mins and resuspended in 0.1M triethylammonium bicarbonate
882 (TEAB, pH=8.5). Samples were digested with Trypsin/LysC (protein:enzyme = 40:1) at 37°C
883 overnight. Digestion was stopped by 1% trifluoroacetic acid (TFA) and the samples were
884 purified on a Bravo AssayMAP robot (Agilent) using C18 cartridges following the manufacturer's
885 instructions. Eluted peptides were dried with a SpeedVac and resuspended in 2% acetonitrile
886 (ACN), 0.05% TFA in LC-MS grade H₂O.

887 Peptide samples were separated on an UltiMate3000 RSLCnano system (EASY-Spray
888 C18 reversed phase column, 75 μ m x 50 cm, 2 μ m, Thermo Fisher Scientific) using the
889 following LC gradient: 0-10 min: 4-10% B; 10-75 min: 10-30% B; 75-80 min: 30-40% B; 80-85
890 min: 40-99% B; 85-89.8 min: 99% B; 89.8-90 min: 99-4% B; 90-120 min: 4% B (A=0.1% formic
891 acid in H₂O, B=80% ACN, 0.1% formic acid in H₂O) interfaced to an Orbitrap Q Exactive HF
892 mass spectrometer (Thermo Fisher). Full MS spectra were collected using an Orbitrap scan
893 with a range of 350-1600 m/z and a resolution of 60,000. The most abundant 15 ions from the

894 full MS scan were selected for data-dependent MS2 with HCD fragmentation and acquired
895 using an Orbitrap scan with a resolution of 15,000 and isolation windows of 2 m/z. Dynamic
896 exclusion of 40 seconds and lock mass of 445.12003 m/z were used.

897 Raw files of the proteomic analysis for conditioned media were processed using
898 Proteome Discoverer 2.2 (Thermo Fisher Scientific) and searched against UniProt/SwissProt
899 human and bovine database (2017_01, 26169 protein entries) using Mascot 2.6.0 (Matrix
900 Science). Trypsin was used for the enzymatic digestion and 2 missed cleavages were allowed.
901 Carbamidomethylation on cysteines was selected as a static modification and oxidation on
902 methionine, proline, lysine as dynamic modifications. Precursor ion mass tolerance was set at
903 10 ppm and for fragment ion at 20 milli mass unit (mmu). Search results were loaded into
904 Scaffold 4.8.6 and the following filters were applied: a peptide probability of greater than 95.0%
905 (as specified by the Peptide Prophet algorithm), a protein probability of greater than 99.0%, and
906 at least two unique peptides per protein. The precursor intensity values were used for
907 quantitation.

908 Proteomics analysis of supernatant from HASMCs

909 • *Sample collection.* HASMCs treated with lentiviral vector containing scrambled shRNA (Scr) or
910 *UBR4-kd* HASMCs were cultured with Prigrow I medium supplemented with 10% FBS and 1%
911 antibiotic antimycotic on a 6 well plate in replicates of 6 until they reached 80% confluency.
912 Cells were then washed 5 times with PBS and cultured with serum free Prigrow I medium for 4
913 hours. Cells were washed again 5 times with PBS and cultured again for 24 hours with serum
914 free Prigrow I medium. The supernatants were then collected, centrifuged at 4,700 g for 10 min,
915 transferred to a new clean tube and immediately frozen at -80°C.

917 • *Protein digestion and peptide clean-up.* HASMC cell culture supernatants were thawed and
918 concentrated using Amicon Ultra centrifugal filter units with a 3 kDa molecular weight cut-off
919 (Millipore, UFC5003). The volume-normalized concentrated supernatants were then subjected
920 to in-solution digestion as described above for Bj-5ta fibroblasts. Peptides were purified using
921 Pierce Peptide Desalting Spin Columns (Thermo Scientific, 89852).

922 • *Liquid chromatography–mass spectrometry (LC–MS).* The purified peptides were analyzed
923 using an UltiMate 3000 LC system which was coupled via a Nanospray Flex source to an
924 Exploris 480 mass spectrometer equipped with a high-field asymmetric waveform ion mobility
925 spectrometry (FAIMS) Pro interface (all Thermo Scientific). An 80-min gradient with increasing
926 strength of mobile phase B (90% acetonitrile, 0.4% formic acid in water) was used to elute the
927 peptides from a trap cartridge (Thermo Scientific, 174500) at 230 nL/min. The peptides were
928 separated on a reversed-phase analytical column (packed in-house, 75 µm inner diameter x 50
929 cm length, ReproSil-Pur 120 C18-AQ phase, particle size 3 µm, pore size 120 Å). FAIMS
930 compensation voltages of -40 and -60 V were applied. Precursor spectra were acquired in the
931 Orbitrap (resolution 60,000 at 200 m/z, scan range 375–1,500). Data-dependent fragment
932 spectra of the most abundant precursor ions were obtained after higher-energy collisional
933 dissociation and Orbitrap detection (resolution 15,000 at 200 m/z) using a fixed cycle time of 1.5
934 sec and a dynamic exclusion duration of 90 sec.

935 • *Database search of LC-MS data.* RAW files were processed using Proteome Discoverer
936 (Thermo Scientific, version 2.5.0.400) and Mascot (Matrix Science, version 2.6.0). The files
937 were searched against a human database (UniProtKB/Swiss-Prot, version from March 2022,
938 20,376 proteins) and an in-house contaminant database compiled from mass spectrometric
939 analyses of FBS-containing growth medium (768 bovine proteins, porcine trypsin, and Lys-C
940 from *P. aeruginosa*). Mass tolerances were set at 10 ppm for precursor ions and 0.02 Da for
941 fragment ions. Trypsin was set as the protein-digesting enzyme, with up to two allowed missed
942 cleavages. Carbamidomethylation of cysteine (static) and oxidation of lysine, methionine, and
943 proline (dynamic) were selected as modifications. The quality of peptide-spectrum matches
944 (PSMs) obtained from the Mascot target/decoy search was assessed using Percolator. PSM
945 and peptide validation were conducted with Peptide Validator, maintaining a target false
946 discovery rate of 0.01 for both PSMs and peptides. Quantification was based on precursor
947 intensity.

948 • *Data preprocessing.* Search results were filtered to include Master proteins with a high Protein
949 FDR Confidence, as determined by Proteome Discoverer's Protein FDR Validator node (FDR
950 confidence threshold of 0.01 for high confidence), and a minimum number of two unique
951 peptides. Bovine proteins, contaminant proteins from human skin, trypsin, and Lys-C were
952 removed. To retain proteins in cases of pronounced up- or downregulation, proteins displaying
953 low ($\leq 1/6$) missingness in one group and high ($\geq 5/6$) missingness in the other were identified
954 and missing protein abundance values were imputed with 0.5 times the lowest quantified value.
955 For all other proteins, a missing value threshold of 1/3 was applied and proteins with a higher
956 proportion of missing values were dropped. Remaining missing values were imputed with 0.5
957 times the lowest quantified value. Finally, proteins were classified as secreted proteins using
958 SignalP (version 6.0)⁶² or matrisome and matrisome-associated proteins using MatrisomeDB
959 (version 2.0).⁶³

960

961 Mice

962 All mice were housed in the animal facility at the Icahn School of Medicine at Mount Sinai and
963 handled according to institutional animal care and use committee-approved protocols. Mice
964 were housed at between 20-26°C with 30%-70% humidity, with a 7am-7pm (12hr) day/night
965 cycle, and were fed with regular rodent's chow diet and water ad libitum. The following mouse
966 lines were used: *Ubr4^{flox/flox}* mice³² purchased from The Jackson Laboratory (strain #024844);
967 *Sm22 α -CreER^{T2}* mice^{64,65} obtained under material transfer agreement from Institut für
968 Pharmakologie und Toxikologie, Technische Universität München, Germany; *SMMHC-CreER^{T2}*
969 mice⁶⁶ (also known as *Myh11-iCreER^{T2}*) obtained under material transfer agreement from
970 Department of Pharmacology, Max-Planck-Institute for Heart and Lung Research, Bad
971 Nauheim, Germany (these mice are now available directly from The Jackson Laboratory as
972 strain #019079); tdTomato reporter mice⁶⁷ purchased from The Jackson Laboratory (strain
973 #007914). All strains were obtained on a C57BL6 background except *SMMHC-CreER^{T2}* mice,
974 which were back-crossed onto a C57BL6 background prior to use. Mice were interbred to create
975 *Sm22 α -CreER^{T2};Ubr4^{flox/flox}* and *SMMHC-CreER^{T2};Ubr4^{flox/flox}* mice (termed *Sm22 α -Ubr4^{KO}* and
976 *SMMHC-Ubr4^{KO}*, respectively). Female and male littermate *Ubr4^{flox/flox}* mice were used as

977 controls for these lines. Note that these two mouse lines, specifically *Sm22 α -CreER^{T2};Ubr4^{flox/flox}*
978 (termed *Sm22 α -Ubr4^{KO}*) and *SMMHC-CreER^{T2};Ubr4^{flox/flox}* (termed *SMMHC-Ubr4^{KO}*) were used
979 for all experiments except single cell RNAseq (scRNAseq). Unique for the scRNAseq
980 experiments, mice were interbred to create *Sm22 α -CreER^{T2};tdTomato;Ubr4^{flox/flox}* mice (termed
981 *tdT-Sm22 α -Ubr4^{KO}*). For this specific line used only in scRNAseq experiments, *Sm22 α -*
982 *CreER^{T2};tdTomato* mice were used as controls. These mice used in scRNAseq experiments
983 were born, housed, genotyped and received tamoxifen at the animal facility at the Icahn School
984 of Medicine at Mount Sinai. When nearing the age required for experimentation, these mice
985 were transferred to the Center for Comparative Medicine at the University of Colorado Denver
986 where they were acclimatized, prior to scRNAseq studies as described.

987 Genotyping of all mice was validated by PCR of DNA samples collected at 3 weeks of
988 age (Supplementary Table 31). Beginning at 4 weeks of age, all mice (including all control mice)
989 received intraperitoneal injections of 1 mg of tamoxifen (Sigma, T5648) reconstituted in ethanol
990 and diluted in peanut oil (Millipore Sigma, P2144) daily for 7 days. After 7 days off,
991 intraperitoneal tamoxifen injections were repeated for 7 more consecutive days, as described.⁶⁸
992

993 Blood pressure measurements in mice

994 At 22 weeks and at 14 months of age, blood pressure was measured non-invasively in mice
995 using a CODA noninvasive mouse blood pressure system (Kent Scientific Corp.). Four
996 parameters were recorded (systolic, diastolic, and mean blood pressure; heart rate), measured
997 10 times per mouse and the mean was calculated.
998

999 Mouse echocardiography and ultrasonography

1000 Mice underwent echocardiography under light anesthesia, by first placing the mouse in an
1001 induction chamber using 3% isoflurane and 1 L/min 100% oxygen for 2 mins. Once the animal
1002 lost its reflexes, it was laid supine on a heated platform with its nose enveloped in a nosecone
1003 to keep the mouse anesthetized by 2% isoflurane. The mouse limbs were taped to four
1004 electrocardiogram (ECG) electrodes, which were embedded in the platform for the
1005 measurement of heart rate, ECG and respiratory rate. A Vevo 2100 ultrasound system
1006 (VisualSonics, Toronto, ON, Canada) equipped with a MS550 transducer was used for mouse
1007 echocardiography. The transducer had a central frequency of 40 MHz, a focal length of 7.0 mm,
1008 and a frame rate of 557 frames/second (single zone, 5.08 mm width, B-mode). The maximum
1009 field of view of two-dimensional (2D) imaging was 14.1 x 15.0 mm with a spatial resolution of 90
1010 μ m (lateral) by 40 μ m (axial). All parameters were assessed using a three consecutive cardiac
1011 cycle-averaged value. All data were acquired and analyzed by two blinded observers.

1012 • *Assessment of thoracic and abdominal aorta dimensions.* The left parasternal long-axis view
1013 was used to image and measure aortic annulus (immediately after the left ventricular (LV)
1014 outflow tract), sinuses of Valsalva, sinotubular junction, and the tubular (proximal) ascending
1015 aorta. The right parasternal long-axis view was used to image and measure the aortic arch.
1016 Using apical short- and long-axis views the descending aorta at the level of the left common
1017 carotid and left subclavian artery was measured. The abdominal aorta at the level of the
1018 diaphragm was measured by subcostal short- and long-axis views. The aortic diameter was

1019 measured using the leading edge-to-edge convention at end-systole (maximal diameter) in B-
1020 mode according to guideline recommendations.⁶⁹

1021 • *Assessment of global cardiac function.* Short-axis parasternal views of the LV at the mid-
1022 papillary level and long-axis parasternal views of the LV were obtained at a frame rate ranging
1023 from 25 to 28 frames/second for 2-dimensional echocardiography. LV end-diastolic and end-
1024 systolic volumes (LVEDV and LVESV, respectively) were calculated as follows: $V = 5/6 \times A \times L$,
1025 where V is the volume of the LV cavity in milliliters, A is the cross-sectional area of the LV cavity
1026 in cm^2 obtained from a parasternal short-axis image at the mid-papillary level, and L is the
1027 length of the LV cavity in cm measured as the distance from the endocardial LV apex to the
1028 mitral-aortic junction on the parasternal long-axis image. Additional planimetry was performed
1029 on the parasternal long-axis view to obtain LV volumes by application of a modified Simpson's
1030 rule (programmed in the software package of the ultrasound device). Both fractional shortening
1031 (FS) and ejection fraction (EF) were derived from 2-dimensional guided M-mode short-axis
1032 measurements. FS and EF were calculated according to the following equations: FS
1033 (%) = $[(LVEDD - LVESD)/LVEDD] \times 100\%$, where LVEDD is LV end-diastolic and LVESD is LV
1034 end-systolic diameter. EF (%) = $[(LVEDV - LVESV)/LVEDV] \times 100\%$. Cardiac output (CO) was
1035 calculated using color-flow directed Doppler pulsed-wave traces of mitral and aortic flow
1036 measured at the level of the LV outflow tract from the apical 4-chamber view. Aortic outflow and
1037 mitral inflow waveforms were recorded when the mitral and aortic flows were distinct and aortic
1038 and mitral valve clicks were clearly visible. CO was estimated as follows: $CO = VTI \times \pi \times (\text{aortic}$
1039 $\text{diameter}/2)^2 \times HR$, where VTI is the velocity-time integral of aortic flow, HR is heart rate, and
1040 the aortic diameter was measured from the parasternal long-axis 2-dimensional view. The total
1041 body surface area of each animal was calculated using Meeh's formula (surface area = $kW^{2/3}$),
1042 where k value is a constant (9.83), and W=weight.⁷⁰ Cardiac index was calculated by dividing
1043 CO by body surface area. Stroke volume was calculated by dividing CO by heart rate, while
1044 stroke volume index was calculated by dividing CO by heart rate and body surface area. The
1045 LVEDV index (LVEDVI) and LVESV index (LVESVI) were calculated by dividing LVEDV and
1046 LVESV by body surface area, respectively.⁷¹

1047

1048 Mouse tissue collection and processing

1049 Animals were euthanized by cardiac puncture and exsanguination under Ketamine/Xylazine
1050 anesthesia. Blood was collected from each mouse, with 100 μl placed into an EDTA
1051 anticoagulated tube and analyzed immediately for complete blood count (CBC), while the
1052 remaining blood (usually $\sim 400 \mu\text{l}$) was centrifuged at 2,000 g for 10 mins to prepare the plasma
1053 fraction that was immediately frozen at -80°C pending analysis. Exsanguinated mice were
1054 perfused with 4% paraformaldehyde (Fisher Scientific, AAJ61899AP) in PBS via the LV for 15
1055 mins at 3 ml/min using an infusion pump (Braintree Scientific, BS-300). The heart, aorta and
1056 great vessels were then carefully dissected from the surrounding tissues. The aortic arch,
1057 carotids, upper thoracic aorta, and upper abdominal aorta were placed in 20% sucrose
1058 overnight before embedding in OCT (Electron Microscopy Science, 62550-01) and then stored
1059 at -80°C . Samples in OCT were cryosectioned at 10 μm thickness (Leica, CM3050S) onto glass
1060 slides (Fisher Scientific 12-550-19) and stored at -80°C . The ascending aorta, lower thoracic

1061 aorta and lower abdominal aorta, plus also the lungs and heart, were fixed in 4%
1062 paraformaldehyde at 4°C overnight. These tissues were then processed and embedded in
1063 paraffin by the Biorepository and Pathology department at the Icahn School of Medicine at
1064 Mount Sinai. Paraffin blocks were sectioned at 10 µm thickness (Leica, RM2255) onto glass
1065 slides (Fisher Scientific, 12-550-19) and stored at room temperature.

1066 CBC and chemistry analysis

1067 CBC analysis on mouse blood was performed by the Comparative Pathology Laboratory at the
1068 Icahn School of Medicine at Mount Sinai using an IDEXX ProCyte Dx Hematology Analyzer
1069 (IDEXX BioResearch). Cell counts of RBCs, WBCs, platelets, monocytes, lymphocytes, and
1070 neutrophils were obtained using standard procedures according to the manufacturer's
1071 instructions. Plasma was sent to IDEXX laboratories (IDEXX Bioresearch) for clinical chemical
1072 analysis.
1073

1074 Immunohistochemistry, imaging and quantifications of mouse vessels

1075 • *Hematoxylin and Eosin staining*. Paraffin sections were stained with Hematoxylin and Eosin.
1076 Briefly, slides were deparaffinized in Xylene substitute (Sigma-Aldrich, 78475), rehydrated and
1077 stained in Hematoxylin (Sigma-Aldrich, GHS1128) for 3 mins. After a wash in running water,
1078 slides were stained with Eosin Y (Ricca Chemical Company, 2845-32) for 2 mins. Slides were
1079 then dehydrated, cleared with xylene substitute, and mounted with DPX mounting medium
1080 (Electron Microscopy Science, 13510). Images were acquired using a Leica DMI8 microscope.
1081 Outer and inner perimeter, and medial area were measured on 2 separate hematoxylin and
1082 eosin stained sections per mouse using ImageJ software by a blinded observer, with the results
1083 then averaged for each mouse. The calculated lumen area was derived mathematically based
1084 on the knowledge that the inner perimeter (circumference) = $2 \pi r$, where r is the radius of the
1085 vessel (assuming a circular cross-section), and the area of the vessel (assuming a circular
1086 cross-section) = πr^2 . This can be expressed as $\text{Area} = (\text{circumference})^2 / 4 \pi$. The tortuosity of
1087 the elastic laminae (EL tortuosity index) was determined on hematoxylin and eosin stained
1088 sections by selecting a relatively straight section of the vessel measuring 200 µm in length.
1089 ImageJ software was used to measure the total length of the elastic lamina between the
1090 endpoints (i.e., over a straight distance of 200 µm). 4 - 8 measurements per vessel were taken,
1091 and the mean calculated. Using a standard formula,⁷² tortuosity index was calculated as:
1092 $\text{Tortuosity index} = ((L/D)-1)*100$; L = mean of different total length measurements calculated
1093 with image J; D = the straight line distance between the endpoints (200 µm).
1094 • *Masson's trichrome staining*. Paraffin sections were stained using Masson's trichrome stain
1095 (Sigma-Aldrich, HT15) as described by the manufacturer but using a longer incubation time (10
1096 min) for Hematoxylin and Scarlet-Acid Fuchsin. Slides were mounted with DPX mounting
1097 medium. Images were acquired using a Leica DMI8 microscope. Quantification of collagen
1098 content on Masson's trichrome stained sections was made using ImageJ software (NIH, version
1099 1.53e for windows) by a blinded observer.
1100 • *Elastic lamina staining (Van Gieson's stain)*. Slides were deparaffinized in Xylene substitute
1101 (Sigma-Aldrich, 78475), rehydrated and stained in working elastic stain solution (Abcam,
1102

1103 ab150667) for 14 mins. After washing in running water, slides were differentiated in
1104 Differentiating Solution (Sigma-Aldrich, HT25A) for 1 min. Slides were then rinsed in tap water
1105 and then in 95% alcohol to remove iodine. After a brief rinse in distilled water, slides were
1106 stained in Van Gieson solution (Sigma-Aldrich, HT254) for 3 mins. Slides were then rinsed in 2
1107 changes of 95% alcohol, and dehydrated, cleared with xylene substitute, and mounted with
1108 DPX mounting medium (Electron Microscopy Science, 13510). Images were acquired using a
1109 Leica DMI1 microscope. The number of breaks in the elastic lamina were counted on sections
1110 of ascending, thoracic and abdominal aorta by a blinded observer.

1111

1112 RNA scope fluorescent hybridization in situ of mouse vessels

1113 For hybridization in situ staining of mouse vessels, the RNA scope multiplex fluorescence
1114 hybridization in situ kit (Advanced Cell Diagnostics, 323280) was used according to
1115 manufacturer's instructions. Briefly, mouse aortas were dissected out and trimmed of excess
1116 tissues, and then fixed in 4% paraformaldehyde at 4°C for 24 hours. Aortas were then
1117 immersed in 10%, 20% and 30% sucrose in 1x PBS, each time allowing the tissue to sink to the
1118 bottom of the container. Aortas were then embedded in OCT (Electron Microscopy Science,
1119 62550-01), and stored at -80°C. Samples in OCT were cryosectioned at 10 µm thickness (Leica,
1120 CM3050S) onto glass slides (Fisher Scientific 12-550-19), stored at -80°C and analyzed within 1
1121 week.

1122 OCT sections were thawed and washed with PBS to remove residual OCT. Slides were
1123 then baked for 30 mins at 60°C and immersed in prechilled 4% paraformaldehyde at 4°C for 15
1124 mins. Next, slides were dehydrated in changes of 50%, 70% and 100% alcohol and dried at
1125 room temperature for 5 min. Slides were then incubated with Hydrogen Peroxide (Advanced
1126 Cell Diagnostics, 322381) for 10 min at room temperature, and washed twice with distilled
1127 water.

1128 RNA scope target antigen retrieval was performed by submerging the slides into a mildly
1129 boiling RNA scope 1x Target Retrieval Reagent solution (Advanced Cell Diagnostics, 322000)
1130 for 5 mins. The slides were cooled in distilled water, transferred to a 100% alcohol solution for 3
1131 min and dried at 60°C for 5 min. A hydrophobic barrier was created around each section with
1132 ImmEdge Hydrophobic Barrier pen (Vector laboratories, H4000), and the samples were allowed
1133 to dry overnight at room temperature.

1134 The following day, slides were loaded into the ACD EZ-Batch Slide Holder (Advanced
1135 Cell Diagnostics, 321716) and incubated with 5 drops of Protease III (Advanced Cell
1136 Diagnostics, 322381) in an HYbEZ Oven (Advanced Cell Diagnostics, 321721) equipped with
1137 HybEZ Humidity Control Tray (Advanced Cell Diagnostics, 310012) for 30 min at 40°C. Slides
1138 were washed twice with 200 ml distilled water in an ACD EZ-Batch Wash Tray (Advanced Cell
1139 Diagnostics, 321717) After removing excess liquid from the slides, each section was entirely
1140 covered with a probe mix. The probe mix comprised Probe C1: Ubr4 mouse (Advanced Cell
1141 Diagnostics, 415971); and Probe C2: Tagln mouse (Advanced Cell Diagnostics, 480331-C2).
1142 Slides covered with this probe mix were incubated in the HYbEZ Oven equipped with HybEZ
1143 Humidity Control Tray for 2 hours at 40°C. The slides were then washed twice with 200 ml of 1x

1144 Wash Buffer for 2 mins at room temperature. The slides were stored overnight in a 5x SSC
1145 Buffer (ThermoFisher, AM 9770) at room temperature.

1146 The following day, slides were washed once with 200 ml of 1x Wash Buffer (Advanced
1147 Cell Diagnostics, 310091) for 2 min at room temperature. To hybridize AMP1, slides were
1148 incubated with RNA scope Multiplex FL v2 Amp1 (Advanced Cell Diagnostics, 323110) in the
1149 HYbEZ Oven equipped with HybEZ Humidity Control Tray for 30 min at 40°C and washed twice
1150 with 200 ml of 1x Wash Buffer for 2 min at room temperature. The hybridization and wash steps
1151 were repeated to hybridize AMP2 with RNA scope Multiplex FL v2 Amp2 (Advanced Cell
1152 Diagnostics, 323110). To develop HRP-C1 signal, slides were incubated with RNA scope
1153 Multiplex FL v2 HRP-C1 (Advanced Cell Diagnostics, 323110) in the HYbEZ Oven equipped
1154 with HybEZ Humidity Control Tray for 15 min at 40°C and washed twice with 200 ml of 1x Wash
1155 Buffer for 2 mins at room temperature. The slides were then incubated with diluted fluorophore
1156 for labeling the C1 probe (TSA Vivid Fluorophore 520, Advanced Cell Diagnostics, 323271,
1157 diluted 1:1500 in TSA buffer) in the HYbEZ Oven equipped with HybEZ Humidity Control Tray
1158 for 30 min at 40°C and washed twice with 200 ml of 1x Wash Buffer for 2 min at room
1159 temperature. The slides were then incubated with RNA scope Multiplex FL v2 HRP blocker
1160 (Advanced Cell Diagnostics, 323110) in the HYbEZ Oven equipped with HybEZ Humidity
1161 Control Tray for 15 mins at 40°C and washed twice with 200 ml of 1x Wash Buffer for 2 min at
1162 room temperature. To develop HRP-C2 signal, slides were incubated with RNA scope Multiplex
1163 FL v2 HRP-C2 (Advanced Cell Diagnostics, 323110) in the HYbEZ Oven equipped with HybEZ
1164 Humidity Control Tray for 15 min at 40°C and washed twice with 200 ml of 1x Wash Buffer for 2
1165 min at room temperature. The slides were then incubated with diluted fluorophore for labeling
1166 the C2 probe (TSA Vivid Fluorophore 570, Advanced Cell Diagnostics, 323272, diluted 1:1500
1167 in TSA buffer) in the HYbEZ Oven equipped with HybEZ Humidity Control Tray for 30 min at
1168 40°C and washed twice with 200 ml of 1x Wash Buffer for 2 min at room temperature. Slides
1169 were then incubated with RNA scope Multiplex FL v2 HRP blocker in the HYbEZ Oven
1170 equipped with HybEZ Humidity Control Tray for 15 min at 40°C and washed twice with 200 ml of
1171 1x Wash Buffer for 2 min at room temperature. Each section was then incubated with DAPI for
1172 30 sec at room temperature. After removing excess liquid, slides were mounted with ProLong
1173 Gold Antifade Mountant (Thermofisher, P10144) and stored at 4°C in the dark.
1174 Immunofluorescence images were acquired after approximately 19 hours using a confocal
1175 microscope (Zeiss, LSM 780).

1176
1177 Immunofluorescence staining of mouse and human vessels

1178 For all immunofluorescence staining, OCT sections were thawed and washed with PBS to
1179 remove residual OCT. Slides were then fixed in 4% PFA for 20 mins (in addition to the perfusion
1180 fixation done for mice) and washed twice with PBS after fixation. Sections were permeabilized
1181 with 0.3% Triton X-100 in PBS for 10 mins at room temperature, washed once with PBS and
1182 blocked with DAKO antibody diluent (Agilent, S302283-2) for 1 hour at room temperature.
1183 Sections were then incubated overnight at 4°C with primary antibody in DAKO antibody diluent
1184 (for primary antibodies see Supplementary Table 32). Afterwards, slides were washed 3 times
1185 in PBS and incubated for 1 hour at room temperature with appropriate secondary antibody (for

1186 secondary antibodies see Supplementary Table 33). Next, slides were washed 3 times with
1187 PBS and incubated with DAPI (Thermo Fisher Scientific-Invitrogen, D3571) diluted 1:1000 in
1188 PBS for 5 mins. Finally, sections were washed twice with PBS and mounted with
1189 VECTASHIELD Mounting Medium (Vector Laboratories, H-1000). Immunofluorescence staining
1190 was performed on at least 3 replicates for both human and mouse samples. All
1191 immunofluorescence images were acquired using a confocal microscope (Zeiss, LSM 780),
1192 except for CD3, CD45 and CD68 images that were acquired using a Leica, DMI8 microscope.
1193

1194 RNA isolation from mouse and qRT-PCR for *Ubr4* expression

1195 Aorta samples were carefully dissected, cleaned from the surrounding tissues, quick-frozen in
1196 liquid nitrogen and stored at -80°C. For RNA extraction, aortas were thawed in ice using 100 µl
1197 of Trizol (Thermo Fisher Scientific, 15596026) and transferred to a glass homogenizer (Radnoti,
1198 440613) with an additional 400 µl of Trizol at 4°C. After complete lysis with the homogenizer,
1199 samples were left at room temperature for 5 mins. 500 µl of chloroform (Sigma-Aldrich, C2432)
1200 was then added to the samples, and after shaking vigorously the samples were incubated at
1201 room temperature for 5 mins. Samples were then centrifuged at 13,800 g for 15 mins at 4°C.
1202 After centrifugation, the aqueous phase was carefully transferred to a clean microcentrifuge
1203 tube, and an equal volume of 70% ethanol was added to the lysate. The total RNA was then
1204 extracted using RNeasy Mini Kit (Qiagen, 74104) according to the manufacturer's instructions.
1205 Reverse transcription and qRT-PCR were performed as described above for human *UBR4-kd*
1206 and control fibroblasts. Primers for mouse *Ubr4* and 18S were: *Ubr4* fwd 5'-
1207 GTCCTACTCCGCCTTCGAG-3' and rev 5'-TGCAGACCGTGGTGATGTAG-3'. 18S fwd 5'-
1208 TTTCCGGAAGTGGCCATGA-3' and rev 5'-GCAAATGCTTTCGCTCTGGTC--3'.
1209

1210 Proteomics analysis of mouse aortas

1211 Aortas from *Sm22α-Ubr4^{KO}* and littermate control mice were carefully dissected, cleaned from
1212 the surrounding tissues, and divided in half at the level of the diaphragm into the thoracic and
1213 abdominal aortas. The thoracic and abdominal aortas were then snap frozen into 2 separate
1214 cryovials on dry ice and stored at -80°C, prior to being processed in a single batch for analysis
1215 by mass spectrometry.

1216 Thoracic and abdominal aortic tissues from *Sm22α-Ubr4^{KO}* and littermate control mice
1217 were homogenized in guanidine HCl buffer (4M GuHCl, 50 mM sodium acetate, pH 5.8, 25 mM
1218 EDTA supplemented with Protease Inhibitor Cocktail) and shaken for 48 hours. Afterwards, the
1219 supernatant was transferred into new Eppendorf tubes and the protein concentrations were
1220 measured using a Nanodrop (Thermo Fisher Scientific, ND-1000) at 280 nm. From each
1221 sample, 20 µg of proteins were precipitated by adding 10x volume of 100% ethanol and
1222 incubated at -20°C overnight. After centrifuging at 16,000 g for 30 mins at 4°C, the supernatant
1223 was discarded and the pellet was dried using a SpeedVac (Thermo Fisher Scientific, Savant
1224 SPD131DDA) for 10 min. The pellet was resuspended in deglycosylation buffer (50 mM Tris, 50
1225 mM Sodium Acetate, 25 mM EDTA, pH 6.8) and the following enzymes were added: endo-α-N-
1226 acetylgalactosaminidase, β1,4-galactosidase, β-N-acetylglucosaminidase, α2-3,6,8,9-
1227 Neuraminidase (all from Merck-Millipore Glycoprotein Deglycosylation Kit, Cat No. 362280),

1228 Chondroitinase ABC (Sigma-Aldrich, C3667), Heparinase II (Sigma-Aldrich, H6512) and Endo-
1229 β 1,4-galactosidase (Sigma-Aldrich, G6920). Samples were incubated for 1 hour at 25°C,
1230 followed by 24 hours at 37°C in agitation, then dried using a SpeedVac. Subsequently, samples
1231 were reconstituted in ^{18}O -water containing N-Glycosidase F (PNGase F, from the Merck-
1232 Millipore Glycoprotein Deglycosylation Kit, Cat No. 362280), and incubated at 37°C with
1233 agitation for 24 hours.

1234 Proteins were denatured by 6M urea, 2M thiourea and reduced with 10 mM dithiothreitol
1235 at 37°C for 1 hour. Afterwards, proteins were alkylated by 50 mM iodoacetamide and incubated
1236 in the dark for 1 hour at room temperature. Next, proteins were precipitated by adding 10x
1237 volume of pre-chilled acetone and incubated at -20°C overnight. Samples were centrifuged at
1238 16,000 g at 4°C for 30 mins and the supernatant was discarded. The pellets were dried using a
1239 SpeedVac for 10 min and resuspended in 0.1M TEAB (pH 8.5). Protein samples were digested
1240 to peptides as described above. Peptide samples were injected and separated by an
1241 UltiMate3000 RSLCnano system (EASY-Spray C18 reversed phase column, 75 μm x 50 cm, 2
1242 μm , Thermo Fisher Scientific) using the following LC gradient: 0-1 min: 1% B; 1-6 min: 1-6% B;
1243 6-40 min: 6-18% B; 40-70 min: 18-35% B; 70-80 min: 35-45% B; 80-81min: 45-99% B; 81-89.8
1244 min: 99% B; 90-120 min: 1% B (A=0.1% formic acid in H_2O , B=80% ACN, 0.1% formic acid in
1245 H_2O). The separated peptides were analyzed on an Orbitrap Q Exactive HF Mass Spectrometer
1246 (Thermo Fisher) as described above.

1247 Raw files of the proteomic analysis for murine aortas were processed by Proteome
1248 Discoverer 2.4 (Thermo Fisher Scientific) and searched against UniProt/SwissProt mouse
1249 database (2021_01, 17063 protein entries) using Mascot 2.6.0 (Matrix Science). Trypsin was
1250 selected as enzyme for digestion and 2 missed cleavages were allowed. Carbamidomethylation
1251 on cysteines was selected as a static modification and oxidation on methionine, proline, lysine,
1252 and ^{18}O -deamidation on asparagine as dynamic modifications. Precursor ion mass tolerance
1253 was set at 10 ppm and for fragment ion at 20 milli mass unit (mmu). Protein identification FDR
1254 confidence was set to High and a minimum number of peptides per protein was 2. Precursor
1255 peak area was used for quantification and normalized to total peak area of each sample.

1256 Before applying formal statistical analysis and principal component analysis, data were
1257 pre-processed with a more advanced processing and statistical analysis pipeline using the
1258 Ebayes algorithm of the limma package.⁷³ Proteins with more than 30% missing values in all
1259 samples were filtered except when > 90% missing values occurred in one genotype and less
1260 than 10% missing values in the other genotype. In the latter case, zeros were imputed in the
1261 missing values of the genotype with more than 90% missing values. All remaining missing
1262 values were imputed with KNN-Impute method with k equal to 3 (default value). The relative
1263 quantities of the proteins were scaled using log₂ transformation. Volcano plots were generated
1264 with Prism software (version 9.2.0, GraphPad). Proteins with *P* value < 0.05 and fold change >
1265 1.5 or < -1.5 were highlighted as indicated.

1267 Single cell RNA sequencing (scRNAseq) of mouse arteries

1268 Aortic and carotid arteries tissue were harvested from female *tdT-Sm22 α -Ubr4^{KO}* mice (*Sm22 α -*
1269 *CreER^{T2};tdTomato;Ubr4^{fllox/fllox}*) and female control mice (*Sm22 α -CreER^{T2};tdTomato*), 8-9

1270 months after tamoxifen treatment. The scRNA-seq experiment has duplicated samples (WT_1,
1271 WT_2, KO_1, KO_2). Each sample has pooled aortic and carotid artery tissues from 2 mice. A
1272 total of 8 mice were used. Single cell suspensions were prepared as described previously⁷⁴ and
1273 fluorescence activated cell sorting (FACS) was performed to separate tdT⁺ and tdT⁻ cells.
1274 Sorted cells from 2 mice were pooled together into 1 sample. Duplicated tdT⁺ and tdT⁻ samples
1275 of each genotype underwent scRNAseq using the Chromium Single Cell 3' Library and Gel
1276 Bead Kit (v3.1 10x Genomics, Pleasanton, CA) and a Chromium X. Libraries were sequenced
1277 on an Illumina Novaseq 6000 at Genomics Shared Resource at the University of Colorado
1278 Anschutz Medical Campus. 50,000 reads per cell were obtained. Fastq files were aligned to
1279 GRCm39 reference (Ensembl, r104) using Cell Ranger 6.1.2. Scanpy 1.9.3 was used for the
1280 downstream analysis including quality control, normalization, clustering, based on best practices
1281 for scRNAseq.⁷⁵ Cells with less than 200 genes and genes expressed by less than 10 cells
1282 were filtered out. Cells with a percentage of mitochondrial counts exceeding 8% or with more
1283 than 7500 genes were filtered. In addition, when reporting differentially expressed genes, only
1284 genes with FDR < 0.05 and either more than 1.5-fold up- or 2/3 fold downregulation in
1285 expression levels were reported. Pseudobulk samples were created from the single-cell dataset
1286 for differential gene expression analysis using edgeR 3.42.4. GOBP enrichment analysis was
1287 performed using GSEAPy 1.0.5 with GO_Biological_Process_2021.gmt obtained from Enrichr
1288 gene-set library.

1289 Gene scoring analysis was conducted using the Scanpy Python package.⁷⁶ The function
1290 "score_genes" was utilized to score cells in the filtered and normalized gene expression matrix
1291 for enrichment of the 572 mouse orthologs of human SN-A genes which showed expression in
1292 the scRNAseq data. In brief, the score_genes tool computes cell-wise enrichment scores by
1293 calculating the average expression of gene sets of interest, subtracted against the average
1294 expression of a randomly sampled reference gene list. This analysis generates a score for each
1295 cell proportional to the enrichment of the SN-A network signature.

1296 The NCBI Gene Expression Omnibus database accession number for these scRNAseq
1297 data is GSE242708.

1298 Statistics for non-RNAseq and non-proteomics analyses

1300 No outliers were excluded from this study, except where specifically stated. For all *in vitro*
1301 experiments, at least 3 to 4 biological replicates were used. For *in vitro* data, unpaired Student's
1302 t test or 1-way ANOVA with post hoc Tukey's multiple comparison test was used as stated. For
1303 *in vivo* data, we first tested each dataset using the Shapiro-Wilk test to assess for normality of
1304 distribution. For normally distributed *in vivo* data, we then applied an F test to check whether the
1305 two groups were equal in variance. Unpaired Student's t test was applied in equal variance
1306 datasets and Unpaired t test with Welch's correction was applied in unequal variance datasets.
1307 For *in vivo* data that were not normally distributed, we applied a Mann-Whitney U test or
1308 Kruskal-Wallis test with Dunn's post hoc analysis, as appropriate. The specific test applied for
1309 each comparison is stated in each figure legend. Statistical analyses were performed using
1310 Prism 9, and a 2-sided *P* value of less than 0.05 was considered significant. All data are
1311 presented as mean ± SD.

1312 **Data Availability**

1313 ScRNAseq data are available at the NCBI Gene Expression Omnibus database, accession
1314 number GSE242708. Mass spectrometry proteomics data have been deposited to the
1315 ProteomeXchange Consortium via the PRIDE partner repository with the dataset identifiers
1316 PXD049359 (*UBR4* knockdown studies in both HASMCs and Bj-5ta fibroblasts) and
1317 PXD051750 (mouse aortas). Bulk RNAseq data for primary human fibroblasts from study
1318 subjects, and also both HASMCs and Bj-5ta fibroblasts, have been deposited in dbGaP under
1319 accession number phs003674.v1.p1. With respect to the bulk RNAseq data for primary human
1320 fibroblasts, of the 154 human subjects in this analysis, 62 did not provide consent to have their
1321 genomic data made publicly available. Therefore the human subject data available at dbGAP
1322 under accession phs003674.v1.p1 is from the 92 study participants who provided written
1323 informed consent to share their deidentified genomic data publicly.

1324
1325 **Code Availability**

1326 No original code was used or created for this study.

1327
1328 **Acknowledgements**

1329 This study was funded by the US National Institutes of Health (R01HL148167 to JCK, DKD,
1330 JWO, JLMB, KDC and MCMW-E) and additional philanthropic support. JCK also acknowledges
1331 research support from New South Wales health grant RG194194, the Bourne Foundation, Snow
1332 Medical and Agilent. JLMB acknowledges support from the Swedish Research Council (2018-
1333 02529 and 2022-00734), the Swedish Heart Lung Foundation (2017-0265 and 2020-0207), the
1334 Leducq Foundation AteroGen (22CVD04) and PlaQOmics (18CVD02) consortia; the National
1335 Institute of Health-National Heart Lung Blood Institute (NIH/NHLBI, R01HL164577;
1336 R01HL148167; R01HL148239, R01HL166428, and R01HL168174), American Heart
1337 Association Transformational Project Award 19TPA34910021, and from the CMD AMP fNIH
1338 program. JLMB also acknowledges the European Union's Horizon Europe (European
1339 Innovation Council) programme under grant agreement No 101115381. YX is supported by the
1340 NYC Train KUHR Consortium (National Institutes of Health grant TL1DK136048).

1341
1342 We acknowledge the assistance and technical expertise of the Microscopy and Advanced
1343 Bioimaging CoRE, the BioMedical Engineering and Imaging Institute, and the Center for
1344 Comparative Medicine and Surgery, of the Icahn School of Medicine at Mount Sinai. University
1345 of Colorado Shared Resources (SR) are supported by the National Cancer Institute through the
1346 Cancer Center Support Grant (P30CA06934).

1347
1348 We also acknowledge and thank all the participants in this study.

1349
1350 **Author Contributions Statement**

1351 V.d'E processed patient samples, performed the majority of in vitro studies, and coordinated in
1352 vivo studies. DK-D and JWO were responsible for coordination of clinical study enrolment and
1353 clinical aspects of this study, AK enrolled the majority of the subjects into the study and was

1354 assisted by EB. LM was the primary person responsible for conducting bioinformatics and
1355 network analyses, while initial network analyses were performed by SP. KH and JLMB oversaw
1356 and supervised bioinformatics and network analyses. SL conducted scRNAseq analyses, while
1357 MCMW-E oversaw and planned scRNAseq experiments. YX assisted with immunofluorescence
1358 confocal microscopy and with statistical analyses, and created all figures. BV was responsible
1359 for dissecting mice and for mounting and staining most mouse samples, while AN-K, RJW and
1360 KDC also assisted with mouse protocols and studies. MM planned and oversaw proteomics
1361 studies, while MF, TB and LES performed these experiments. AT performed most
1362 immunofluorescence confocal microscopy on human samples. KCM established the separate
1363 human clinical protocol under which the surplus arterial samples that were analyzed in Figs. 3h-
1364 o were procured, while AA, FF and SF were the surgeons who obtained those samples, and RB
1365 assisted with sample collection.⁴⁹ NBN ran the case-control FMD analysis¹⁷ and provided
1366 access to summary data from that study (Table 2), while AG assisted with data interpretation
1367 and analyses related to that study. YZ, EC and VC performed mouse echocardiography and
1368 ultrasound studies, while MGK oversaw these analyses and analyzed the data. JCK conceived
1369 of this study, supervised the experiments and research group, wrote and approved the final
1370 version of the manuscript, and was the primary person who secured funding. All authors
1371 contributed to drafting, editing and/or revising the manuscript.

1372

1373 **Competing Interests Statement**

1374 Jason Kovacic is the recipient of an Agilent Thought Leader Award (January 2022), which
1375 includes funding for research that is unrelated to the current manuscript. Kevin Costa (a Co-
1376 Investigator in this study) is the scientific Co-Founder of, receives financial compensation as the
1377 Chief Scientific Officer for, and holds equity in NovoHeart LTD (biotech company that focuses
1378 on using human stem cells and engineered human cardiac tissues for drug
1379 development/screening applications). The other authors have no conflicts of interest or
1380 relationships with industry to declare.

1381

1382

1383

1384

1385

Tables

1386

Table 1. Subject demographics.

<i>variable</i>	FMD patients (n=83)		Healthy controls (n=71)	
	<i>summary*</i>	<i>n</i>	<i>summary*</i>	<i>n</i>
Clinical				
Sex: female	83 (100.00%)	83	71 (100.00%)	71
Age at FMD diagnosis	52.4 [31.0 – 72.0]	83	-	
Age at study enrollment	55.8 [35.0 – 72.0]	83	52.10 [19.0 – 72.0]	71
Height (in)	64.4 [58.0 – 71.0]	83	65.7 [60.0 – 73.0]	69
Weight (lbs)	137.7 [100.0 – 208.0]	83	150.4 [105.0 – 240.0]	69
BMI	23.4 [18.3 – 33.6]	83	24.4 [18.6 – 38.7]	69
DM	2 (2.41%)	83	1 (1.45%)	69
HTN	48 (57.83%)	83	3 (4.35%)	69
Ever smoker	16 (19.28%)	83	14 (20.29%)	69
Medications				
ACE/ARB	28 (33.73%)	83	1 (1.45%)	69
Aspirin	62 (74.70%)	83	4 (2.13%)	69
Anticoagulation	6 (7.23%)	83	0 (0.00%)	69
Beta blocker	19 (22.89%)	83	2 (2.13%)	69
Current hormone therapy	8 (9.64%)	83	5 (7.25%)	69
Statin	30 (36.14%)	83	5 (7.25%)	69
Non-statin lipid lowering	11 (13.25%)	83	1 (1.41%)	71
Thyroid replacement	14 (16.87%)	83	9 (13.04%)	69
FMD vascular features				
Aneurysm [†]	26 (31.33%)	83		-
Dissection [†]	35 (42.17%)	83		-
TIA/CVA	13 (15.85%)	82		-
FMD arterial disease location				
Cervical (Carotid/Vertebral)	66 (79.52%)	83		-
Coronary [#]	5 (6.02%)	83		-
Iliac	7 (8.43%)	83		-
Intracranial [#]	9 (10.84%)	83		-
Mesenteric	15 (18.07%)	83		-
Renal	63 (75.90%)	83		-
FMD arterial bed involvement				
Total number of arterial beds involved	2.0 [1.0 – 5.0]	83		-

1387 Except where stated, all data are as at the time of study enrollment.

1388 * Total number of subjects with the described characteristic for yes/no features (percentage in parenthesis); median
1389 and min-max range for continuous features.1390 † Aneurysm or dissection are considered a manifestation of FMD only if multifocal (or focal) findings consistent with
1391 FMD are observed in a separate vascular bed.1392 # Due to the specific features of FMD in these vascular beds, 'coronary FMD' implies a coronary artery dissection,
1393 while 'intracranial FMD' implies an intracranial aneurysm. ACE = angiotensin converting enzyme inhibitor; ARB =
1394 angiotensin receptor blocker; BMI = body mass index; CVA = cerebrovascular accident; DM = diabetes; HTN =
1395 hypertension; statin = HMG-CoA reductase inhibitor; TIA = transient ischemic attack.

1396

1397 **Table 2. Co-expression networks and their associations with FMD.** 18 co-expression
1398 networks were identified in a pooled analysis of all primary fibroblast RNAseq data. In turn,
1399 these 18 networks comprised 3 supernetworks (SN-A, -B, -C). To determine which of these are
1400 associated with FMD we initially evaluated 3 factors: 1) The proportion of genes in each network
1401 that showed fibroblast DGE between FMD cases and controls; 2) Correlation of network gene
1402 expression with number of diseased vessels (controls = 0, FMD cases = 1 - 5) and enrichment
1403 of number of diseased vessels in each network; 3) The proportion of genes in each network
1404 which reached nominal significance ($P < 0.05$) in a 2016 case-control FMD analysis comprising
1405 249 FMD cases and 689 controls that evaluated 7,816,791 SNPs.¹⁷ As a subsequent and fourth
1406 analysis, we evaluated the proportion of genes in each network which reached nominal
1407 significance ($P < 0.05$) in a 2021 FMD GWAS meta-analysis comprising 1556 FMD cases and
1408 7100 controls that evaluated 5,483,710 SNPs.⁹ Significant P values are in bold. Results for SN-
1409 A, the only network or supernetwork that was associated with FMD by all 4 methods, are in red.

Co-expression network or supernetwork	Number of genes in the network	Network genes exhibiting DGE by FMD case-control status		Enrichment analysis of network genes by number of diseased vessels (controls = 0, FMD cases = 1 - 5)		Network gene enrichment in 2016 FMD case-control study (Kiando et al ¹⁷)			Network gene enrichment in 2021 FMD GWAS meta-analysis (Georges et al ⁹)		
		Number of genes in network showing DGE	Enrichment P value	Number of genes significant for number of diseased vessels	Enrichment P value	Number of network genes found in the case-control study	Number of network genes reaching $P < 0.05$ in the case-control study	P value for enrichment of network genes found in the case-control study at $P < 0.05$	Number of network genes found in the GWAS	Number of network genes reaching $P < 0.05$ in the GWAS	P value for enrichment of network genes found in the GWAS at $P < 0.05$
Cyan	136	65	2.2×10^{-16}	103	9.45×10^{-53}	95	28	0.9996	17	4	0.9936
Light cyan	78	0	1	10	0.8028	73	34	0.4993	72	27	0.7846
Tan	143	0	1	33	0.0148	138	93	3.76×10^{-7}	132	79	1.7×10^{-05}
Green	418	0	1	98	4.56×10^{-5}	396	216	0.00049	373	185	0.00103
<i>SN-A comprising the above 4 networks</i>	775	65	6.85×10^{-13}	244	9.69×10^{-25}	702	371	0.00026	594	295	1.57×10^{-7}
Blue	1376	8	1	144	1	1314	598	0.6116	1231	462	0.9959
Yellow	648	3	1	38	1	632	292	0.4566	597	230	0.9243
Grey60	58	8	0.00135	21	1.26×10^{-4}	53	16	0.9931	47	9	0.9997
Pink	256	123	2.2×10^{-16}	180	2.60×10^{-80}	239	79	1	192	56	0.9998
Brown	1176	4	1	119	1	1024	403	1	844	273	0.9999
Salmon	139	0	1	11	0.9978	132	57	0.7598	126	41	0.9831
<i>SN-B the above 6 networks</i>	3653	146	0.00057	513	0.9908	3394	1445	0.9993	3037	1071	0.9994
Green-yellow	175	1	0.9985	9	1	167	75	0.6286	155	68	0.2949
Turquoise	1391	10	1	90	1	1320	712	5.34×10^{-8}	1236	550	0.0204
Red	302	24	0.00057	160	1.30×10^{-47}	282	134	0.3168	262	95	0.9593
Black	271	9	0.6686	38	0.8002	255	92	0.9993	236	80	0.9919
Light green	37	2	0.3988	3	0.9446	35	16	0.5738	33	10	0.9315
Purple	182	2	0.991	27	0.6608	173	90	0.06446	170	71	0.4921
Magenta	196	0	1	25	0.8936	179	63	0.9983	160	48	0.9988
Midnight blue	135	3	0.8766	11	0.9967	126	46	0.9861	108	31	0.9976
<i>SN-C comprising the above 8 networks</i>	2689	51	0.9988	363	0.9976	2537	1228	0.0167	2360	953	0.0830

1410 **Figure Legends**

1411 **Figure 1. SN-A is an important gene regulatory co-expression supernetwork governing**
1412 **FMD. a**, Catheter-based angiographic image of typical multifocal FMD ('string-of-beads')
1413 affecting the renal artery. **b**, Catheter-based angiographic image of FMD in a different patient
1414 demonstrating typical multifocal renal FMD with aneurysmal involvement (arrow). Image in b
1415 reproduced with permission.⁷⁷ **c**, Overview of study and data analysis workflow. DGE,
1416 differential gene expression; GWAS, genome-wide association study; WGCNA, weighted gene
1417 co-expression network analysis. The human schematic was from Servier Medical Art, which is
1418 licensed under CC BY 4.0. **d**, Volcano plot of primary fibroblast DGE between FMD cases
1419 versus matched controls. Selected genes were individually labeled (full results in
1420 Supplementary Table 1). Blue and purple data points represent the 349 transcripts that were
1421 significantly different after multiple comparison testing. **e**, Top 10 GO terms for terms based on
1422 *P* values of DGE between FMD cases and matched controls for genes showing upregulated
1423 gene expression, with these 10 GO terms all showing positive enrichment (full results in
1424 Supplementary Table 2). GOBP, GO biological process; GOMF, molecular function; GOCC, GO
1425 cellular component. **f**, Top 10 GO terms for terms based on *P* values of DGE between FMD
1426 cases and matched controls for genes showing downregulated gene expression, with these GO
1427 terms showing 2 with negative fold enrichment and 8 with positive enrichment (full results in
1428 Supplementary Table 3).

1429
1430 **Figure 2. Visual representation of SN-A, its GO terms, and green and cyan sub-networks.**
1431 **a**, Visual representation of SN-A (complete list of all genes in SN-A is provided in
1432 Supplementary Table 4). The top 14 key drivers are labeled as indicated (complete list of SN-A
1433 key drivers is provided in Supplementary Table 6). **b**, Top 10 GO terms (by Bonferroni *P* value)
1434 of genes in SN-A (full results in Supplementary Table 5). **c**, Alternate visual representation of
1435 SN-A. The top 14 key drivers are labeled as indicated. Note that the current software used to
1436 create network visualizations does not permit all genes in each network to be represented, and
1437 less than half of the 775 genes in SN-A are shown in either 2a or 2c. **d**, Visualization of the
1438 green network. The green network is one of the 4 networks that comprise SN-A and includes
1439 *UBR4*, which is indicated by a red arrow. **e**, Visualization of the cyan network. The cyan network
1440 is another of the 4 networks that comprise SN-A. Note that of the 4 networks that comprise SN-
1441 A, three are quite small. Specifically, and as stated in Table 2, green has 418 genes (including
1442 *UBR4*), but cyan, light cyan and tan have only 136, 78 and 143 genes respectively. Mainly due
1443 to size, it is only technically possible to create network visualizations for the green and cyan
1444 modules.

1445
1446 **Figure 3. *UBR4* is a key driver of SN-A and shows robust expression in SMCs of adult**
1447 **human arteries. a-c**, Expression levels of the top 14 key drivers of SN-A in GTEx aorta
1448 (n=224), tibial artery (n=332) and coronary artery samples (n=133), respectively. CPM = counts
1449 per million mapped reads. Statistical comparison of these expression levels as well as details of
1450 the box plots are presented in Supplementary Table 7, with levels of *UBR4* being consistently
1451 higher than all other key driver genes in all 3 tissues ($P < 4 \times 10^{-8}$ for all comparisons). **d**,

1452 Volcano plot of DGE between *UBR4-kd* Bj-5ta fibroblasts and scramble control cells. Selected
1453 genes were labeled including *UBR4* (full results in Supplementary Table 8). Blue and purple
1454 data points, as well as *UBR4* in red, represent the transcripts that were significantly different
1455 after multiple comparison testing. n=6 per group. **e**, Top 10 GO terms (by Bonferroni *P* value)
1456 for genes showing upregulated DGE when comparing *UBR4-kd* Bj-5ta fibroblasts and control
1457 cells (full results in Supplementary Table 9). **f**, Top 10 GO terms (by Bonferroni *P* value) for
1458 genes showing downregulated DGE when comparing *UBR4-kd* Bj-5ta fibroblasts and control
1459 cells (full results in Supplementary Table 10). **g**, Hypergeometric test comparing the 'expected'
1460 (dark blue column) versus 'observed' (light blue column) number of transcripts showing altered
1461 expression levels for genes in SN-A, based on knockdown of *UBR4* in Bj-5ta fibroblasts (i.e.,
1462 based on data in Supplementary Table 8). Knockdown of *UBR4* in Bj-5ta fibroblasts resulted in
1463 a substantially greater 'observed' number of genes with altered expression in SN-A ($P = 2.23 \times$
1464 10^{-165}). See also Extended Data Figure 5e showing the same analysis performed in HASMCs.
1465 **h-i**, Representative immunofluorescence staining images for SM22 α (green), UBR4 (red) and
1466 DAPI-stained nuclei (blue), in adult human internal mammary artery (IMA, h) and renal artery
1467 (RA, i), showing robust expression of UBR4 in adult human vascular SMCs. **j-k**, Representative
1468 immunofluorescence staining images for PDGFR α (green), UBR4 (red) and DAPI-stained nuclei
1469 (blue), in adult human IMA (j) and RA (k), corroborating the robust expression of UBR4 in adult
1470 human vascular SMCs. **l-m**, Representative immunofluorescence staining images for CD31
1471 (green), UBR4 (red) and DAPI-stained nuclei (blue), in adult human IMA (l) and RA (m),
1472 showing that adult human arterial endothelial cells also express UBR4. **n-o**, Representative
1473 immunofluorescence staining images for CD90 (green), UBR4 (red) and DAPI-stained nuclei
1474 (blue), in adult human IMA (n) and RA (o), showing expression of UBR4 in adventitial
1475 fibroblasts. For h-o scale bars: 30 μ m. L = lumen; M = media; A = adventitia. Smaller panels to
1476 the right are digital enlargements of the area demarcated by the dashed boxes in the adjacent
1477 merged images. Each immunofluorescence staining microscopy experiment and antibody
1478 combination shown in 3h-o was independently repeated a minimum of 3 occasions.

1479

1480 **Figure 4. *In vivo* perturbation of SN-A by SMC-specific *Ubr4* knockout in female mice**
1481 **(*Sm22 α -Ubr4^{KO}*) recapitulates the arterial dilation phenotype of FMD.** All images, tissues
1482 and data in this Figure, with the exception of 4e, are from female mice examined 5 months after
1483 tamoxifen administration (mice were then 6 months of age). **a**, Breeding and generation of
1484 *Sm22 α -Ubr4^{KO}* mice (*Sm22 α -CreERT²;Ubr4^{fllox/fllox}*). Mice schematics were from Servier Medical
1485 Art, which is licensed under CC BY 4.0. **b**, Representative immunofluorescence staining images
1486 for UBR4 (red), and DAPI-stained nuclei (blue) in the ascending aorta from *Sm22 α -Ubr4^{KO}* and
1487 littermate control mice. Scale bars: 100 μ m. **c**, Representative immunofluorescence staining
1488 images for UBR4 (red), SM22 α (green) and DAPI-stained nuclei (blue) in the ascending aorta
1489 from control and *Sm22 α -Ubr4^{KO}* mice. Smaller adjacent panels are digital enlargements of the
1490 area demarcated by the dashed boxes in the larger merged images. Scale bars: 20 μ m. Each
1491 immunofluorescence staining microscopy experiment and antibody combination was
1492 independently repeated a minimum of 3 occasions. **d**, Representative in situ fluorescent
1493 hybridization images for UBR4 (red), SM22 α (green) and DAPI-stained nuclei (blue) in the

1494 ascending aorta from control and *Sm22 α -Ubr4^{KO}* mice. Smaller adjacent panels are digital
1495 enlargements of the area demarcated by the dashed boxes in the larger merged images. Scale
1496 bars: 20 μ m. **e**, Gene expression levels of *Ubr4* by qRT-PCR in whole mouse aorta from *Sm22 α -*
1497 *Ubr4^{KO}* and littermate control mice at 7 weeks after tamoxifen administration (11 weeks of age).
1498 n=5, both groups. **f**, Representative echocardiographic images of the aortic root and thoracic
1499 aorta of *Sm22 α -Ubr4^{KO}* mice and littermate controls. These images are relevant to panels g-k.
1500 AoAn, aortic annulus; SOV, sinus of Valsalva; STJ, sino-tubular junction; AoAsc, ascending
1501 aorta; AoDesc, descending (thoracic) aorta. Scale bars: 1mm. **g-k**, Comparisons of aortic
1502 annulus, sinus of Valsalva, sino-tubular junction, ascending aorta and descending (thoracic)
1503 aortic dimensions, respectively. n=10 controls vs. 11 *Sm22 α -Ubr4^{KO}* for 4g-j, and 7 controls vs.
1504 8 *Sm22 α -Ubr4^{KO}* for 4k. **l**, Representative echocardiographic images of the abdominal aorta of
1505 *Sm22 α -Ubr4^{KO}* mice and littermate controls. Scale bars: 500 μ m. **m**, Comparison of abdominal
1506 aortic diameter of *Sm22 α -Ubr4^{KO}* mice and littermate controls. n=10 controls vs. 11 *Sm22 α -*
1507 *Ubr4^{KO}*. **n**, Representative histopathological images of ascending aortic sections of *Sm22 α -*
1508 *Ubr4^{KO}* mice and littermate controls using hematoxylin and eosin staining. These images are
1509 relevant to panels o-t. Scale bars: 100 μ m. **o-t**, Comparisons of ascending aorta inner perimeter
1510 length, outer perimeter length (medial/adventitial boundary), medial area, calculated lumen area
1511 (assuming the vessel was circular in cross-section), tortuosity of the elastic laminae (EL
1512 tortuosity index) and number of EL, respectively. n=8 controls vs. 9 *Sm22 α -Ubr4^{KO}* for 4o-r, 10
1513 controls vs. 10 *Sm22 α -Ubr4^{KO}* for 4s, and 10 controls vs. 9 *Sm22 α -Ubr4^{KO}* for 4t. **u**,
1514 Representative histopathological images of ascending aortic sections of *Sm22 α -Ubr4^{KO}* mice
1515 and littermate controls using Van Gieson's stain for EL staining. These images are relevant to
1516 panel v. Scale bars: 100 μ m. **v**, Comparison of breaks in the EL for the ascending aorta of
1517 *Sm22 α -Ubr4^{KO}* mice and littermate controls. n=8 controls vs. 10 *Sm22 α -Ubr4^{KO}*. **w**,
1518 Representative histopathological images of ascending aortic sections of *Sm22 α -Ubr4^{KO}* mice
1519 and littermate controls using Masson's trichrome staining to demonstrate collagen content.
1520 Scale bars: 100 μ m. These images are relevant to panel x. **x**, Statistical comparison of w for
1521 collagen content. n=10 controls vs. 7 *Sm22 α -Ubr4^{KO}* mice. All mice shown in this Figure
1522 received an identical course of tamoxifen administration (knockout mice and littermate controls)
1523 that was also the same as administered to mice shown in Figs. 5 and 6. Based on the
1524 distribution and variance of each group, all analyses were performed using unpaired Student's t
1525 test except 4g, 4k, 4m, 4t and 4v that were performed with Mann-Whitney test. * $P\leq 0.05$;
1526 ** $P\leq 0.01$; *** $P\leq 0.001$; **** $P\leq 0.0001$. Purple columns represent control groups, orange columns
1527 represent *Sm22 α -Ubr4^{KO}* groups. Additional statistical information regarding the analyses used
1528 in this Figure are provided in Supplementary Table 36.

1529
1530 **Figure 5. In vivo perturbation of SN-A by SMC-specific *Ubr4* knockout in male *SMMHC-***
1531 ***Ubr4^{KO}* mice validates an arterial dilation phenotype.** All images, tissues and data in this
1532 Figure are from male mice examined 5 months after tamoxifen administration (mice were then 6
1533 months of age). **a**, Breeding and generation of *SMMHC-Ubr4^{KO}* mice (*SMMHC-*
1534 *CreER^{T2};Ubr4^{flox/flox}*). Mice schematics were from Servier Medical Art, which is licensed under
1535 CC BY 4.0. **b**, Representative immunofluorescence staining for UBR4 (red), and DAPI-stained

1536 nuclei (blue) in the ascending aorta from *SMMHC-Ubr4^{KO}* and littermate control mice. Scale
1537 bars: 100µm. Immunofluorescence staining was independently repeated on 2 occasions. **c**,
1538 Representative echocardiographic images of the aortic root and thoracic aorta of *SMMHC-*
1539 *Ubr4^{KO}* and littermate control mice. These images are relevant to panels d-h. Scale bars: 1 mm.
1540 **d-h**, Comparisons of aortic annulus, sinus of Valsalva, sino-tubular junction, ascending aorta
1541 and descending (thoracic) aortic dimensions, respectively. n=5 controls vs. 6 *SMMHC-Ubr4^{KO}*
1542 for 5d-f, and 4 controls vs. 6 *SMMHC-Ubr4^{KO}* for 5g,h. **i**, Representative echocardiographic
1543 images of the abdominal aorta from *SMMHC-Ubr4^{KO}* and littermate controls. Scale bars:
1544 500µm. **j**, Comparison of abdominal aortic diameter of *SMMHC-Ubr4^{KO}* mice and littermate
1545 controls. n=5 controls vs. 6 *SMMHC-Ubr4^{KO}*. **k**, Representative histopathological images of
1546 ascending aortic sections of *SMMHC-Ubr4^{KO}* and littermate control mice using hematoxylin and
1547 eosin staining. These images are relevant to panels l-q. Scale bars: 100 µm. **l-q**, Comparisons
1548 of ascending aorta inner perimeter length, outer perimeter length (medial/adventitial boundary),
1549 medial area, calculated lumen area (assuming the vessel was circular in cross-section),
1550 tortuosity of the EL and number of EL, respectively. n=7 for both groups for 5l-q. **r**,
1551 Representative histopathological images of ascending aortic sections of *SMMHC-Ubr4^{KO}* mice
1552 and littermate controls using Van Gieson's stain for EL staining. These images are relevant to
1553 panel s. Scale bars: 100 µm. **s**, Comparison of EL breaks for the ascending aorta of *SMMHC-*
1554 *Ubr4^{KO}* mice and littermate controls. n=10 controls vs. 10 *Sm22α-Ubr4^{KO}*. **t**, Representative
1555 histopathological images of ascending aortic sections of *SMMHC-Ubr4^{KO}* mice and littermate
1556 controls using Masson's trichrome staining for collagen content. Scale bars: 100 µm. These
1557 images are relevant to panel u. **u**, Statistical comparison of t. n=10 controls vs. 8 *SMMHC-*
1558 *Ubr4^{KO}* mice. Based on the distribution and variance of each group, all analyses were
1559 performed using unpaired Student's t test except 5j that was performed with Mann-Whitney test,
1560 and 5g and 5n that were performed with Welch's t test. * $P \leq 0.05$; ** $P \leq 0.01$; *** $P \leq 0.001$;
1561 **** $P \leq 0.0001$. Green columns represent control groups, blue columns represent *SMMHC-*
1562 *Ubr4^{KO}* groups. Additional statistical information regarding the analyses used in this Figure are
1563 provided in Supplementary Table 36.

1564
1565 **Figure 6. Single cell RNA sequencing (scRNAseq) of arterial tissues from *tdT-Sm22α-***
1566 ***Ubr4^{KO}* and control mice confirms that SMC-specific *Ubr4* knockout leads to changes in**
1567 **extracellular collagen/matrix and also in specific SMC clusters.** ScRNAseq of *tdT-Sm22α-*
1568 *Ubr4^{KO}* and control mice (*Sm22α-CreERT²;tdTomato;Ubr4^{flox/flox}* and *Sm22α-CreERT²;tdTomato*
1569 mice, respectively) was performed with n=2 mice per group (a total of n=8 mice were used for
1570 this entire analysis). **a**, Uniform Manifold Approximation and Projection (UMAP) showing
1571 annotation of differing cell clusters. EC, endothelial cells; SMC, smooth muscle cells; FB,
1572 fibroblasts; Prog, progenitor cells; Mac, macrophages; DC, dendritic cells; TC, T cells; Unk,
1573 unknown. **b**, UMAP colored by the tdTomato (tdT) fluorescence of the cells (Red, tdT positive
1574 [tdT⁺]; Blue, tdT negative [tdT⁻]), confirming that tdT⁺ cells mostly comprised SMCs. **c**, UMAP
1575 colored by genotype of the cells, with the total dots representing all cells identified across *tdT-*
1576 *Sm22α-Ubr4^{KO}* and control mice in both tdT⁺ and tdT⁻ cells, and turquoise dots representing
1577 those cells identified only in control mice (both tdT⁺ and tdT⁻ cells). WT (wild type) = cells from

1578 control mice. **d**, UMAP colored by genotype of the cells, with the total dots representing all cells
1579 identified across *tdT-Sm22α-Ubr4^{KO}* and control mice in both tdT⁺ and tdT⁻ cells (as also in c),
1580 and orange dots representing those cells identified only in *tdT-Sm22α-Ubr4^{KO}* mice (both tdT⁺
1581 and tdT⁻ cells). Ko (knockout) = cells from *tdT-Sm22α-Ubr4^{KO}* mice. **e**, Volcano plot showing
1582 select DGE between *tdT-Sm22α-Ubr4^{KO}* and control mice among all SMC clusters in the
1583 scRNAseq data. **f**, GOBP enrichment for downregulated genes in SMCs of *tdT-Sm22α-Ubr4^{KO}*
1584 versus control mice. **g**, Dotplot showing select differentially expressed genes in the scRNAseq
1585 data that overlap with genes in SN-A. All cells in the scRNAseq data were scored using mouse
1586 orthologs of SN-A genes to generate an SN-A score, which is shown in the dotplot. **h**, Volcano
1587 plot showing select DGE between *tdT-Sm22α-Ubr4^{KO}* and control mice among tdT⁺ fibroblasts.
1588 **i**, GOBP enrichment for upregulated genes in tdT⁺ fibroblasts of *Sm22α-Ubr4^{KO}* versus control
1589 mice. STK, serine/threonine kinase. **j**, Volcano plot showing select DGE between *tdT-Sm22α-*
1590 *Ubr4^{KO}* versus control mice among tdT⁻ fibroblasts. **k**, GOBP enrichment for upregulated genes
1591 in tdT⁻ fibroblasts of *tdT-Sm22α-Ubr4^{KO}* versus control mice.
1592

1593
1594
1595
1596
1597
1598
1599
1600
1601
1602
1603
1604
1605
1606
1607
1608
1609
1610
1611
1612
1613
1614
1615
1616
1617
1618
1619
1620
1621
1622
1623
1624
1625
1626
1627
1628
1629
1630
1631
1632
1633
1634
1635
1636
1637
1638
1639
1640

References

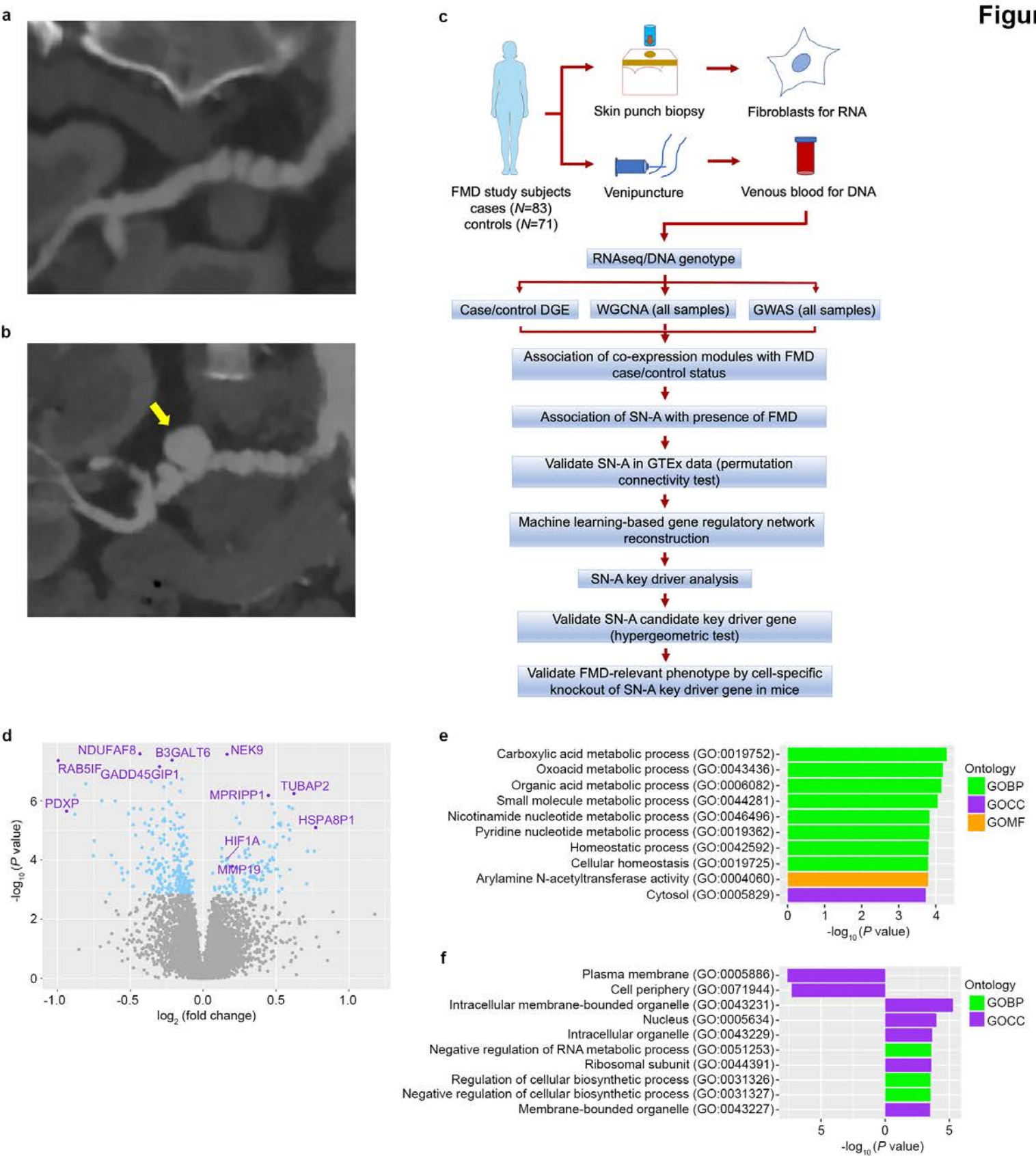
1. Sottiurai, V.S., Fry, W.J. & Stanley, J.C. Ultrastructure of medial smooth muscle and myofibroblasts in human arterial dysplasia. *Arch Surg* **113**, 1280-8 (1978).
2. Olin, J.W. *et al.* The United States Registry for Fibromuscular Dysplasia: results in the first 447 patients. *Circulation* **125**, 3182-90 (2012).
3. Pappaccogli, M. *et al.* The European/International Fibromuscular Dysplasia Registry and Initiative (FEIRI)-clinical phenotypes and their predictors based on a cohort of 1000 patients. *Cardiovasc Res* **117**, 950-959 (2021).
4. Gornik, H.L. *et al.* First International Consensus on the diagnosis and management of fibromuscular dysplasia. *Vasc Med* **24**, 164-189 (2019).
5. Hendricks, N.J. *et al.* Is fibromuscular dysplasia underdiagnosed? A comparison of the prevalence of FMD seen in CORAL trial participants versus a single institution population of renal donor candidates. *Vasc Med* **19**, 363-7 (2014).
6. Plouin, P.F. *et al.* Fibromuscular dysplasia. *Orphanet J Rare Dis* **2**, 28-35 (2007).
7. Leadbetter, W.F. & Burkland, C.R. Hypertension in unilateral renal disease. *J Urol* **39**, 611-626 (1938).
8. Olin, J.W. *et al.* Fibromuscular dysplasia: state of the science and critical unanswered questions: a scientific statement from the American Heart Association. *Circulation* **129**, 1048-78 (2014).
9. Georges, A. *et al.* Genetic investigation of fibromuscular dysplasia identifies risk loci and shared genetics with common cardiovascular diseases. *Nat Commun* **12**, 6031 (2021).
10. Stanley, J.C., Gewertz, B.L., Bove, E.L., Sottiurai, V. & Fry, W.J. Arterial fibrodysplasia. Histopathologic character and current etiologic concepts. *Arch Surg* **110**, 561-6 (1975).
11. Bruno, R.M. *et al.* Deep Vascular Phenotyping in Patients With Renal Multifocal Fibromuscular Dysplasia. *Hypertension* **73**, 371-378 (2019).
12. Kadian-Dodov, D. *et al.* Dissection and Aneurysm in Patients With Fibromuscular Dysplasia: Findings From the U.S. Registry for FMD. *J Am Coll Cardiol* **68**, 176-85 (2016).
13. Schwartz, A.M. *et al.* Aortic Dimensions Are Larger in Patients With Fibromuscular Dysplasia. *J Am Heart Assoc* **11**, e023858 (2022).
14. Katz, A.E. *et al.* Fibromuscular Dysplasia and Abdominal Aortic Aneurysms Are Dimorphic Sex-Specific Diseases With Shared Complex Genetic Architecture. *Circ Genom Precis Med* **15**, e003496 (2022).
15. Michelis, K.C., Olin, J.W., Kadian-Dodov, D., d'Escamard, V. & Kovacic, J.C. Coronary artery manifestations of fibromuscular dysplasia. *J Am Coll Cardiol* **64**, 1033-46 (2014).
16. Guill, C.K., Benavides, D.C., Rees, C., Fenves, A.Z. & Burton, E.C. Fatal mesenteric fibromuscular dysplasia: a case report and review of the literature. *Arch Intern Med* **164**, 1148-53 (2004).
17. Kiando, S.R. *et al.* PHACTR1 Is a Genetic Susceptibility Locus for Fibromuscular Dysplasia Supporting Its Complex Genetic Pattern of Inheritance. *PLoS Genet* **12**, e1006367 (2016).
18. Georges, A. *et al.* Rare loss-of-function mutations of PTGIR are enriched in fibromuscular dysplasia. *Cardiovasc Res* **117**, 1154-1165 (2021).
19. Olin, J.W. *et al.* A Plasma Proteogenomic Signature for Fibromuscular Dysplasia. *Cardiovasc Res* (2019).
20. Richer, J. *et al.* A Novel Recurrent COL5A1 Genetic Variant Is Associated With a Dysplasia-Associated Arterial Disease Exhibiting Dissections and Fibromuscular Dysplasia. *Arterioscler Thromb Vasc Biol* **40**, 2686-2699 (2020).

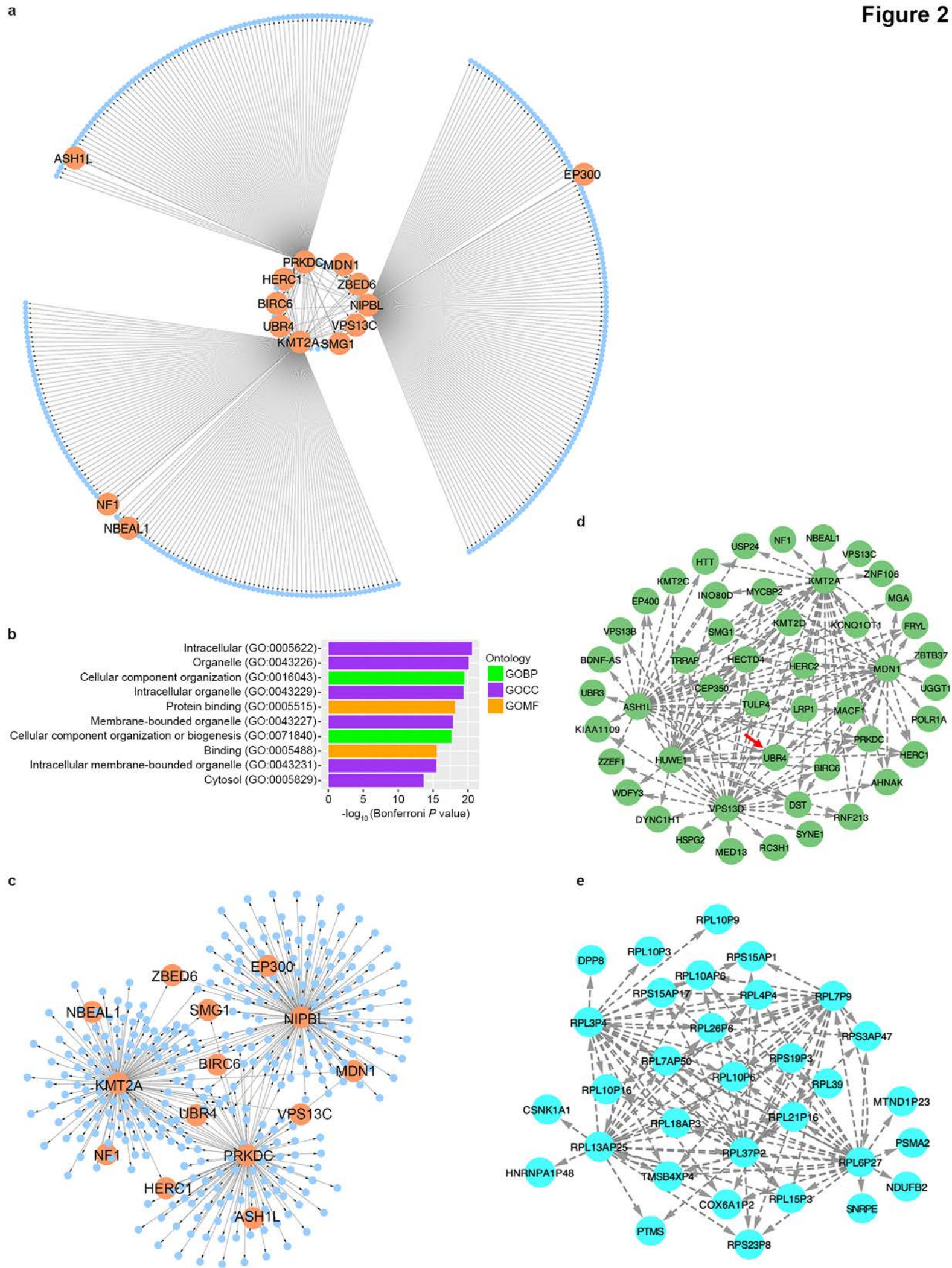
- 1641 21. Bjorkegren, J.L.M., Kovacic, J.C., Dudley, J.T. & Schadt, E.E. Genome-wide significant
1642 loci: how important are they? Systems genetics to understand heritability of coronary
1643 artery disease and other common complex disorders. *J Am Coll Cardiol* **65**, 830-845
1644 (2015).
- 1645 22. Zeng, L. *et al.* Contribution of Gene Regulatory Networks to Heritability of Coronary
1646 Artery Disease. *J Am Coll Cardiol* **73**, 2946-2957 (2019).
- 1647 23. Koplev, S. *et al.* A mechanistic framework for cardiometabolic and coronary artery
1648 diseases. *Nat Cardiovasc Res* **1**, 85-100 (2022).
- 1649 24. Ma, L. *et al.* Multiple independent mechanisms link gene polymorphisms in the region of
1650 ZEB2 with risk of coronary artery disease. *Atherosclerosis* **311**, 20-29 (2020).
- 1651 25. Hao, K. *et al.* Integrative Prioritization of Causal Genes for Coronary Artery Disease. *Circ*
1652 *Genom Precis Med* **15**, e003365 (2022).
- 1653 26. Ma, L. *et al.* The HDAC9-associated risk locus promotes coronary artery disease by
1654 governing TWIST1. *PLoS Genet* **18**, e1010261 (2022).
- 1655 27. Talukdar, H.A. *et al.* Cross-Tissue Regulatory Gene Networks in Coronary Artery
1656 Disease. *Cell Syst* **2**, 196-208 (2016).
- 1657 28. GTEx Consortium. Human genomics. The Genotype-Tissue Expression (GTEx) pilot
1658 analysis: multitissue gene regulation in humans. *Science* **348**, 648-60 (2015).
- 1659 29. McCormack, L.J., Poutasse, E.F., Meaney, T.F., Noto, T.J., Jr. & Dustan, H.P. A
1660 pathologic-arteriographic correlation of renal arterial disease. *Am Heart J* **72**, 188-98
1661 (1966).
- 1662 30. Uhlen, M. *et al.* Proteomics. Tissue-based map of the human proteome. *Science* **347**,
1663 1260419 (2015).
- 1664 31. Heidt, S.T., Ganesh, S.K., Liu, P., Froehlich, J.B. & Kline-Rogers, E. Bilateral internal
1665 mammary artery fibromuscular dysplasia discovered upon evaluation for reconstructive
1666 breast surgery. *Vasc Med* **20**, 487-8 (2015).
- 1667 32. Nakaya, T. *et al.* p600 Plays Essential Roles in Fetal Development. *PLoS One* **8**, e66269
1668 (2013).
- 1669 33. Tasaki, T. *et al.* UBR box N-recognin-4 (UBR4), an N-recognin of the N-end rule
1670 pathway, and its role in yolk sac vascular development and autophagy. *Proc Natl Acad*
1671 *Sci U S A* **110**, 3800-5 (2013).
- 1672 34. Nakatani, Y. *et al.* p600, a unique protein required for membrane morphogenesis and cell
1673 survival. *Proc Natl Acad Sci U S A* **102**, 15093-8 (2005).
- 1674 35. Chakraborty, R. *et al.* Promoters to Study Vascular Smooth Muscle. *Arterioscler Thromb*
1675 *Vasc Biol* **39**, 603-612 (2019).
- 1676 36. O'Brien, B.J., Martin, K.A. & Offermanns, S. "Cre"ating New Tools for Smooth Muscle
1677 Analysis. *Arterioscler Thromb Vasc Biol* **43**, 212-214 (2023).
- 1678 37. Deaton, R.A. *et al.* A New Autosomal Myh11-CreER(T2) Smooth Muscle Cell Lineage
1679 Tracing and Gene Knockout Mouse Model-Brief Report. *Arterioscler Thromb Vasc Biol*
1680 **43**, 203-211 (2023).
- 1681 38. Bulik-Sullivan, B.K. *et al.* LD Score regression distinguishes confounding from
1682 polygenicity in genome-wide association studies. *Nat Genet* **47**, 291-5 (2015).
- 1683 39. Schadt, E.E. & Bjorkegren, J.L. NEW: network-enabled wisdom in biology, medicine, and
1684 health care. *Sci Transl Med* **4**, 115rv1 (2012).
- 1685 40. Barabasi, A.L., Gulbahce, N. & Loscalzo, J. Network medicine: a network-based
1686 approach to human disease. *Nat Rev Genet* **12**, 56-68 (2011).

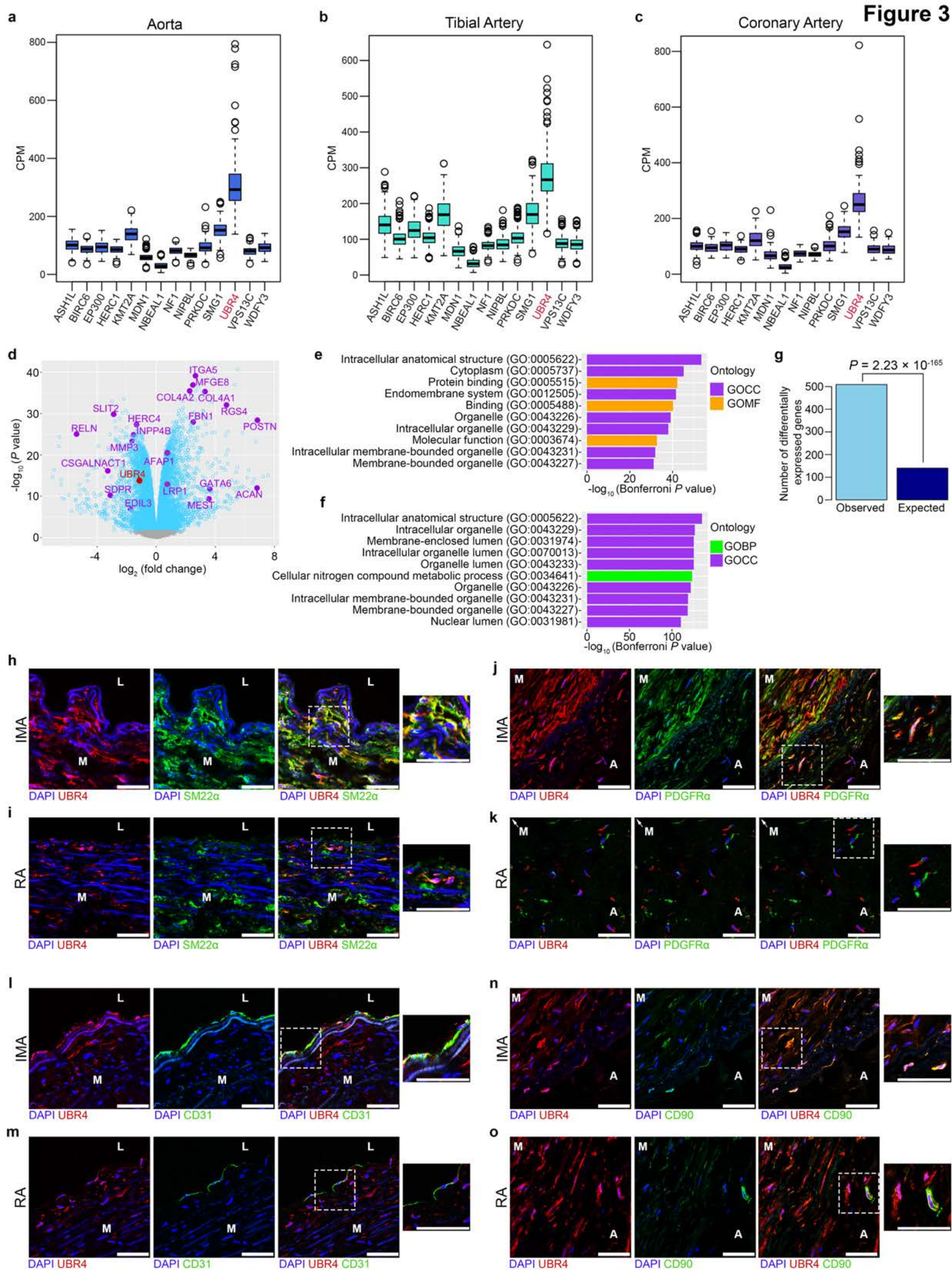
- 1687 41. Ganesh, S.K. *et al.* Clinical and biochemical profiles suggest fibromuscular dysplasia is a
1688 systemic disease with altered TGF-beta expression and connective tissue features.
1689 *FASEB J* **28**, 3313-24 (2014).
- 1690 42. Latosinska, A. *et al.* Increased Collagen Turnover Is a Feature of Fibromuscular
1691 Dysplasia and Associated With Hypertrophic Radial Remodeling: A Pilot, Urine
1692 Proteomic Study. *Hypertension* **79**, 93-103 (2022).
- 1693 43. Kim, S.T. *et al.* The N-recognin UBR4 of the N-end rule pathway is required for
1694 neurogenesis and homeostasis of cell surface proteins. *PLoS One* **13**, e0202260 (2018).
- 1695 44. Hunt, L.C. *et al.* Antagonistic control of myofiber size and muscle protein quality control
1696 by the ubiquitin ligase UBR4 during aging. *Nat Commun* **12**, 1418 (2021).
- 1697 45. Hunt, L.C. *et al.* A Key Role for the Ubiquitin Ligase UBR4 in Myofiber Hypertrophy in
1698 Drosophila and Mice. *Cell Rep* **28**, 1268-1281 e6 (2019).
- 1699 46. Wang, Y. *et al.* Burden of Rare Genetic Variants in Spontaneous Coronary Artery
1700 Dissection With High-risk Features. *JAMA Cardiology* (2022).
- 1701 47. Adlam, D. *et al.* Genome-wide association meta-analysis of spontaneous coronary artery
1702 dissection identifies risk variants and genes related to artery integrity and tissue-
1703 mediated coagulation. *Nat Genet* **55**, 964-972 (2023).
- 1704 48. Tarr, I. *et al.* Exploring the Genetic Architecture of Spontaneous Coronary Artery
1705 Dissection Using Whole-Genome Sequencing. *Circ Genom Precis Med* **15**, e003527
1706 (2022).
- 1707 49. Michelis, K.C. *et al.* CD90 Identifies Adventitial Mesenchymal Progenitor Cells in Adult
1708 Human Medium- and Large-Sized Arteries. *Stem Cell Reports* **11**, 242-257 (2018).
- 1709 50. Price, A.L. *et al.* Principal components analysis corrects for stratification in genome-wide
1710 association studies. *Nat Genet* **38**, 904-9 (2006).
- 1711 51. Andrews, S. FastQC: a quality control tool for high throughput sequence data. 2010
1712 <http://www.bioinformatics.babraham.ac.uk/projects/fastqc/>.
- 1713 52. Dobin, A. *et al.* STAR: ultrafast universal RNA-seq aligner. *Bioinformatics* **29**, 15-21
1714 (2013).
- 1715 53. Leek, J.T., Johnson, W.E., Parker, H.S., Jaffe, A.E. & Storey, J.D. The sva package for
1716 removing batch effects and other unwanted variation in high-throughput experiments.
1717 *Bioinformatics* **28**, 882-3 (2012).
- 1718 54. Robinson, M.D. & Oshlack, A. A scaling normalization method for differential expression
1719 analysis of RNA-seq data. *Genome Biol* **11**, R25 (2010).
- 1720 55. Ritchie, M.E. *et al.* limma powers differential expression analyses for RNA-sequencing
1721 and microarray studies. *Nucleic Acids Res* **43**, e47 (2015).
- 1722 56. Ashburner, M. *et al.* Gene ontology: tool for the unification of biology. The Gene Ontology
1723 Consortium. *Nat Genet* **25**, 25-9 (2000).
- 1724 57. Mi, H., Muruganujan, A., Ebert, D., Huang, X. & Thomas, P.D. PANTHER version 14:
1725 more genomes, a new PANTHER GO-slim and improvements in enrichment analysis
1726 tools. *Nucleic Acids Res* **47**, D419-D426 (2019).
- 1727 58. Langfelder, P. & Horvath, S. WGCNA: an R package for weighted correlation network
1728 analysis. *BMC Bioinformatics* **9**, 559 (2008).
- 1729 59. Huynh-Thu, V.A., Irrthum, A., Wehenkel, L. & Geurts, P. Inferring regulatory networks
1730 from expression data using tree-based methods. *PLoS One* **5**(2010).
- 1731 60. Makinen, V.P. *et al.* Mergeomics: Integrative network analysis of omics data. R package
1732 version 1.10.0. (2018).
- 1733 61. Finucane, H.K. *et al.* Partitioning heritability by functional annotation using genome-wide
1734 association summary statistics. *Nat Genet* **47**, 1228-35 (2015).

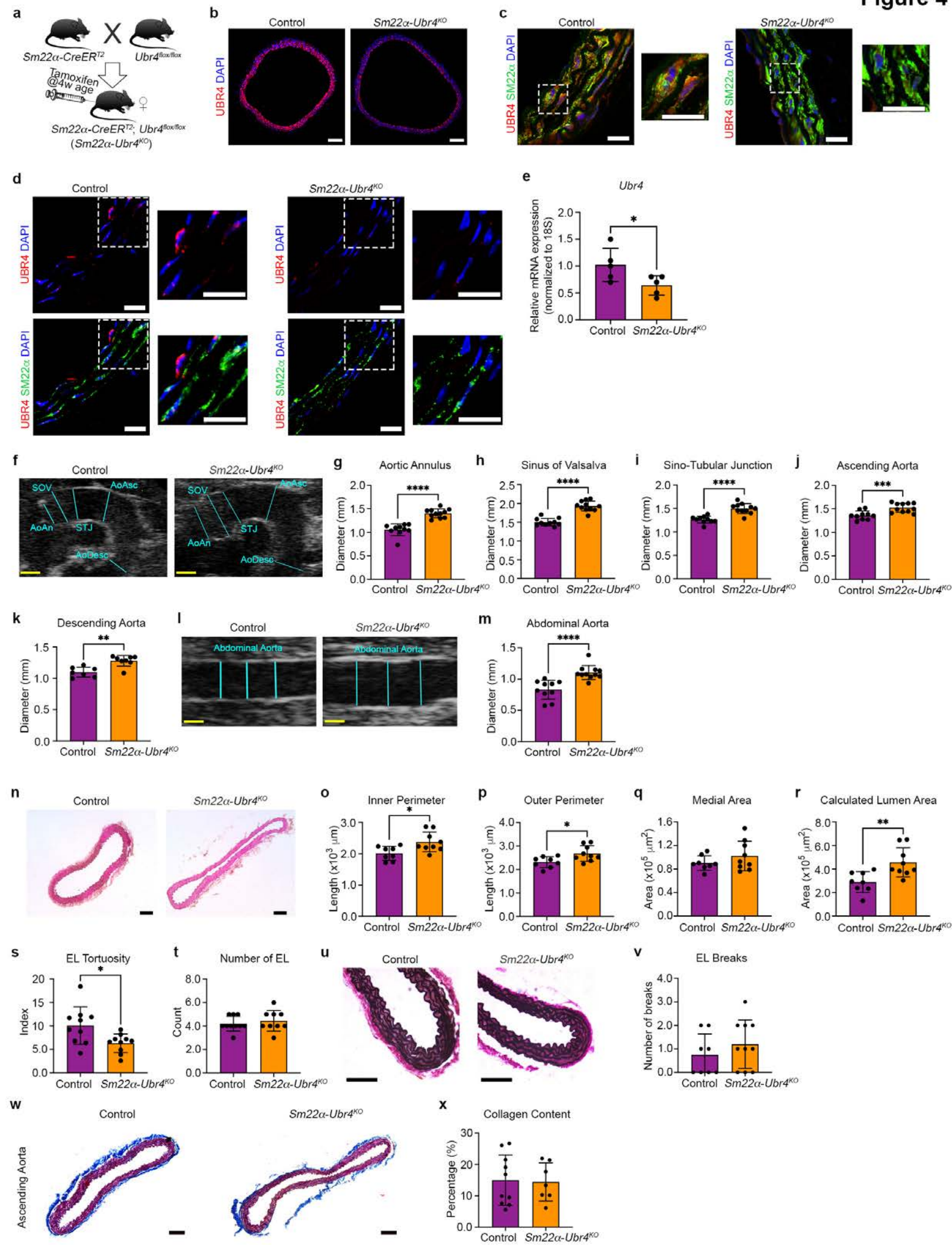
- 1735 62. Teufel, F. *et al.* SignalP 6.0 predicts all five types of signal peptides using protein
1736 language models. *Nat Biotechnol* **40**, 1023-1025 (2022).
- 1737 63. Shao, X. *et al.* MatrisomeDB 2.0: 2023 updates to the ECM-protein knowledge database.
1738 *Nucleic Acids Res* **51**, D1519-D1530 (2023).
- 1739 64. Feil, S., Hofmann, F. & Feil, R. SM22alpha modulates vascular smooth muscle cell
1740 phenotype during atherogenesis. *Circ Res* **94**, 863-865 (2004).
- 1741 65. Kühbandner, S. *et al.* Temporally controlled somatic mutagenesis in smooth muscle.
1742 *Genesis* **28**, 15-22 (2000).
- 1743 66. Wirth, A. *et al.* G12-G13-LARG-mediated signaling in vascular smooth muscle is required
1744 for salt-induced hypertension. *Nat Med* **14**, 64-8 (2008).
- 1745 67. Madisen, L. *et al.* A robust and high-throughput Cre reporting and characterization
1746 system for the whole mouse brain. *Nat Neurosci* **13**, 133-40 (2010).
- 1747 68. Evrard, S.M. *et al.* Endothelial to mesenchymal transition is common in atherosclerotic
1748 lesions and is associated with plaque instability. *Nat Commun* **7**, 11853 (2016).
- 1749 69. Evangelista, A. *et al.* Echocardiography in aortic diseases: EAE recommendations for
1750 clinical practice. *Eur J Echocardiogr* **11**, 645-58 (2010).
- 1751 70. Gouma, E. *et al.* A simple procedure for estimation of total body surface area and
1752 determination of a new value of Meeh's constant in rats. *Lab Anim* **46**, 40-5 (2012).
- 1753 71. Lindsey, M.L., Kassiri, Z., Virag, J.A.I., de Castro Bras, L.E. & Scherrer-Crosbie, M.
1754 Guidelines for measuring cardiac physiology in mice. *Am J Physiol Heart Circ Physiol*
1755 **314**, H733-H752 (2018).
- 1756 72. Morris, S.A. *et al.* Increased vertebral artery tortuosity index is associated with adverse
1757 outcomes in children and young adults with connective tissue disorders. *Circulation* **124**,
1758 388-96 (2011).
- 1759 73. Smyth, G.K. Linear models and empirical bayes methods for assessing differential
1760 expression in microarray experiments. *Stat Appl Genet Mol Biol* **3**, Article3 (2004).
- 1761 74. Lu, S. *et al.* Smooth muscle-derived progenitor cell myofibroblast differentiation through
1762 KLF4 downregulation promotes arterial remodeling and fibrosis. *JCI Insight* **5**(2020).
- 1763 75. Heumos, L. *et al.* Best practices for single-cell analysis across modalities. *Nat Rev Genet*
1764 **24**, 550-572 (2023).
- 1765 76. Wolf, F.A., Angerer, P. & Theis, F.J. SCANPY: large-scale single-cell gene expression
1766 data analysis. *Genome Biol* **19**, 15 (2018).
- 1767 77. Kim, E.S.H., Saw, J., Kadian-Dodov, D., Wood, M. & Ganesh, S.K. FMD and SCAD:
1768 Sex-Biased Arterial Diseases With Clinical and Genetic Pleiotropy. *Circ Res* **128**, 1958-
1769 1972 (2021).

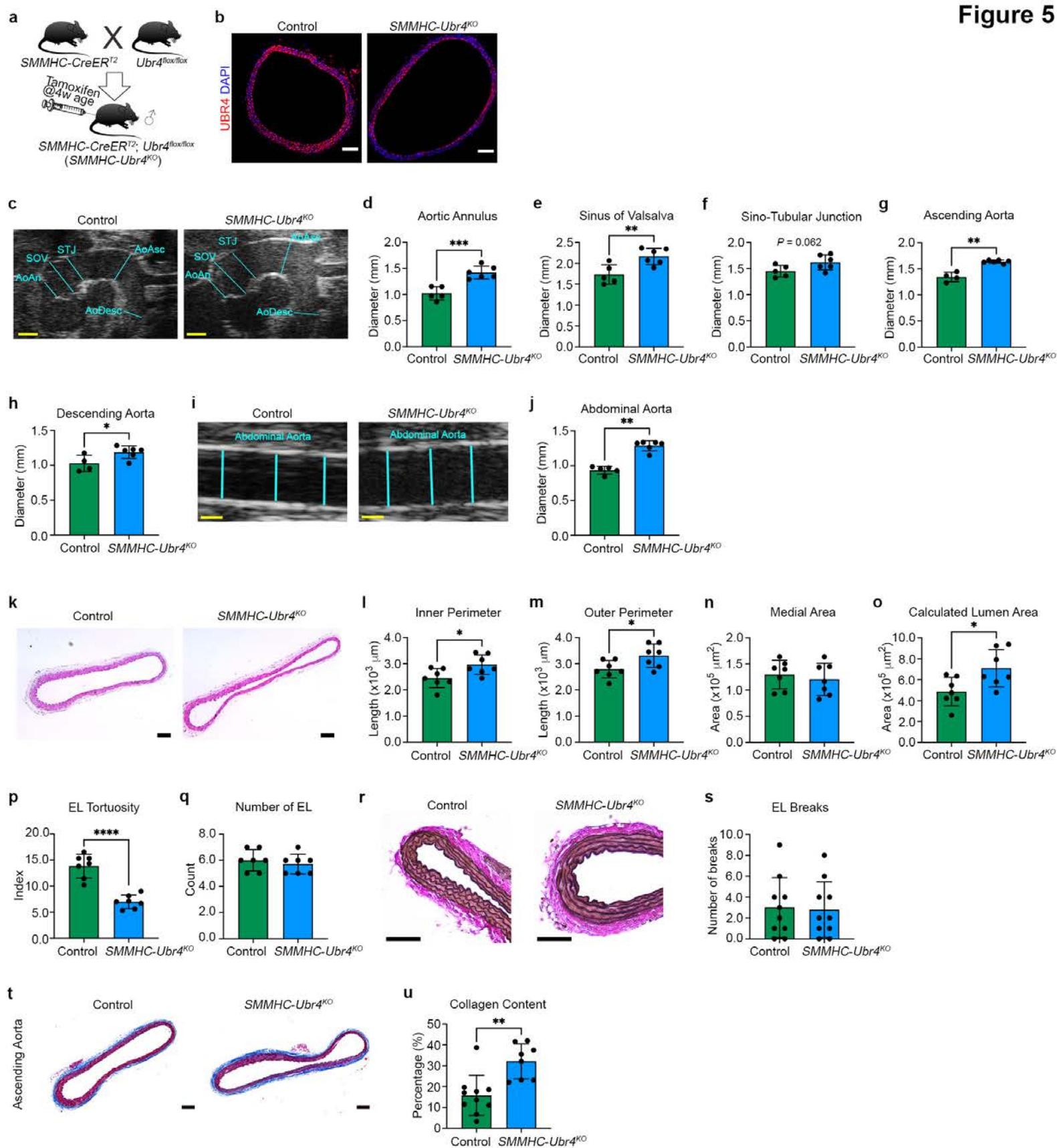
1770

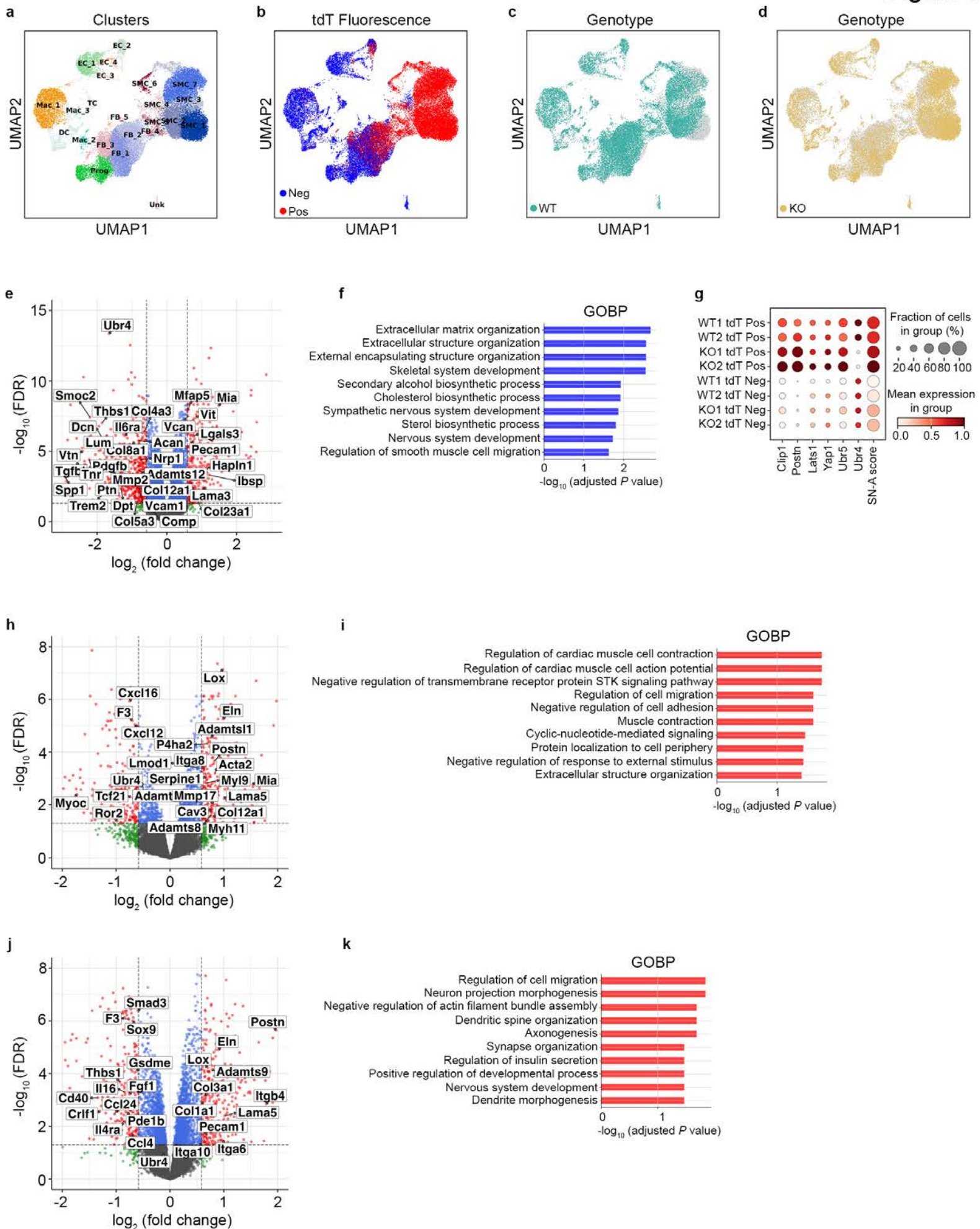


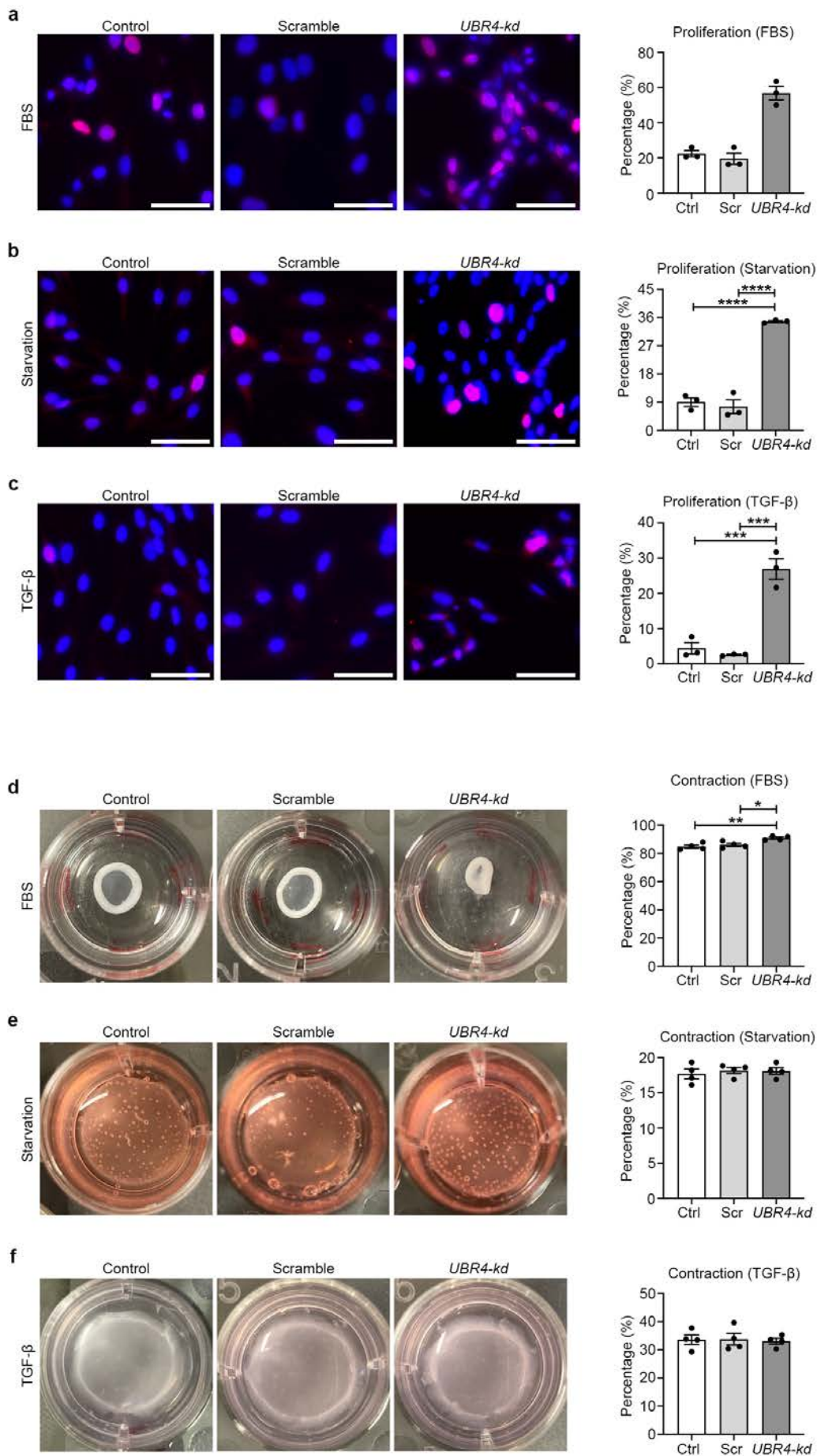




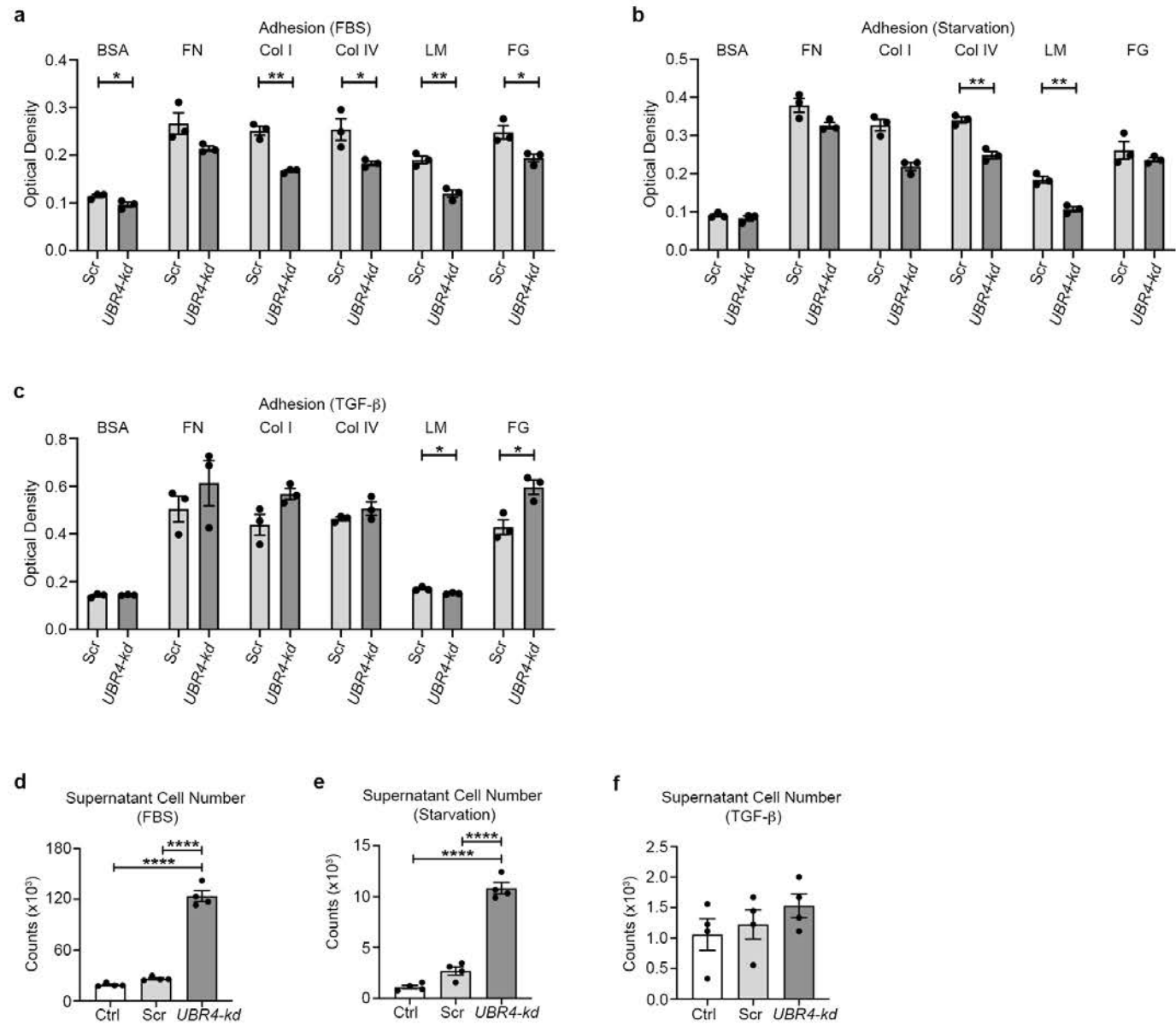




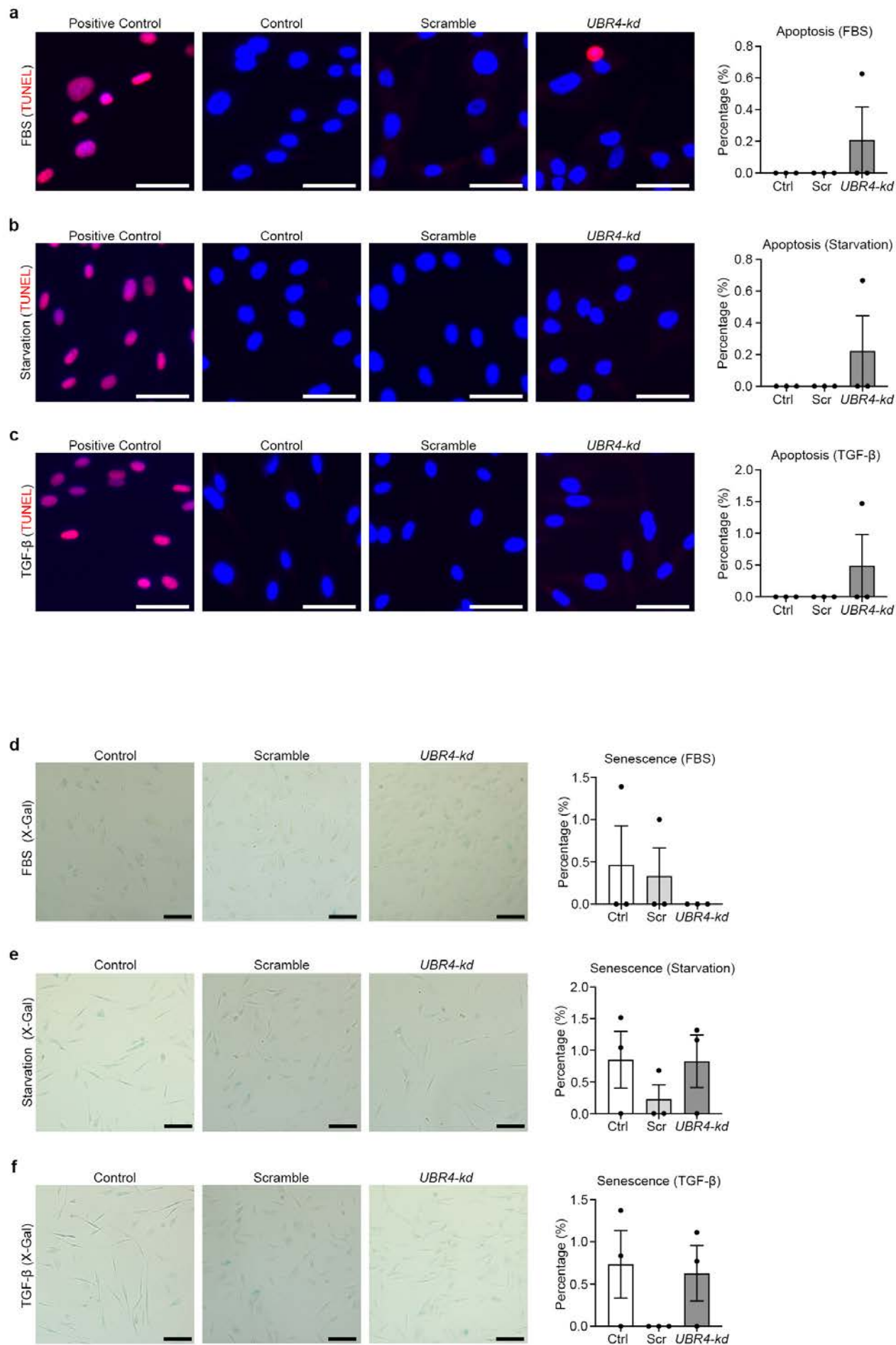




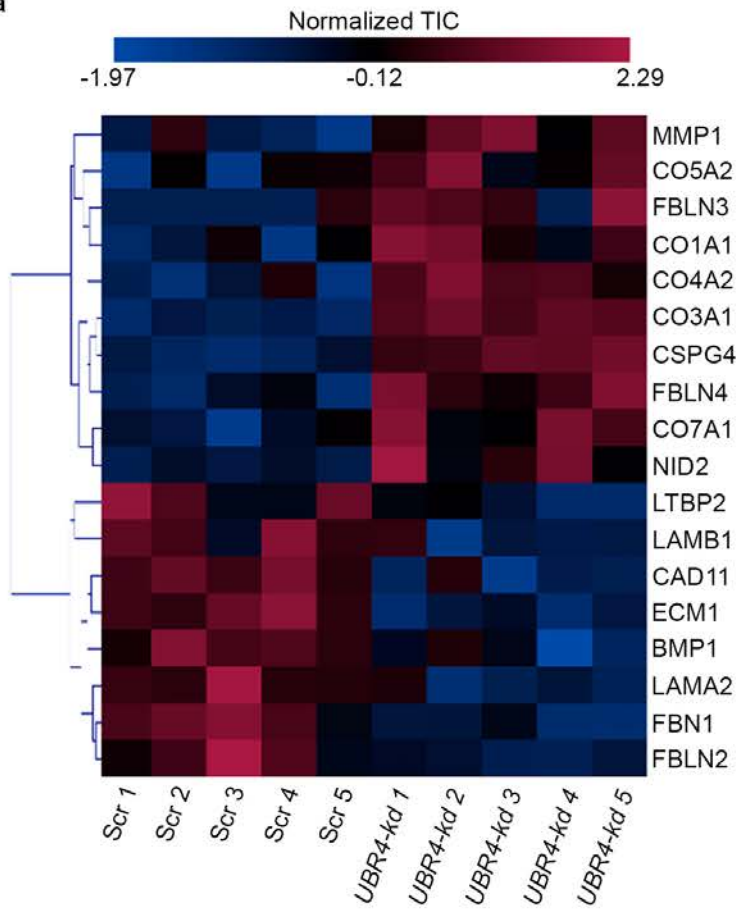
Extended Data Fig 2

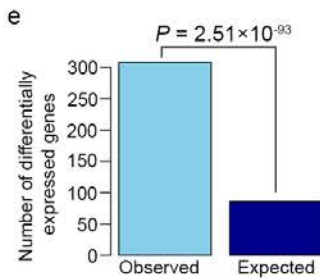
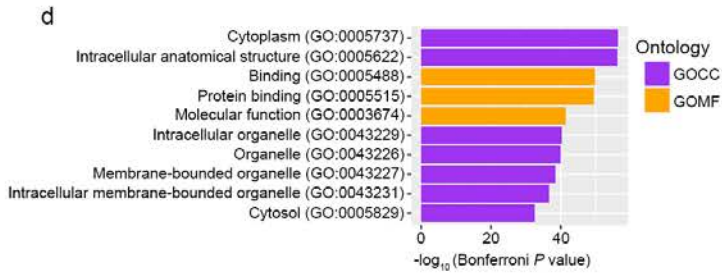
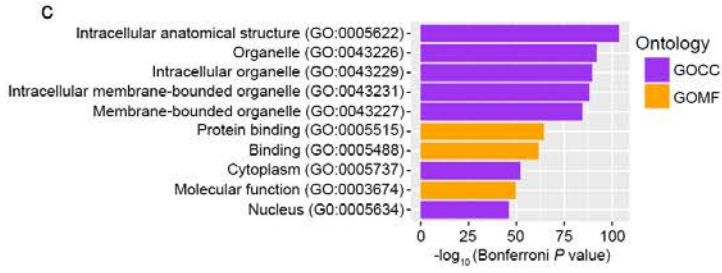
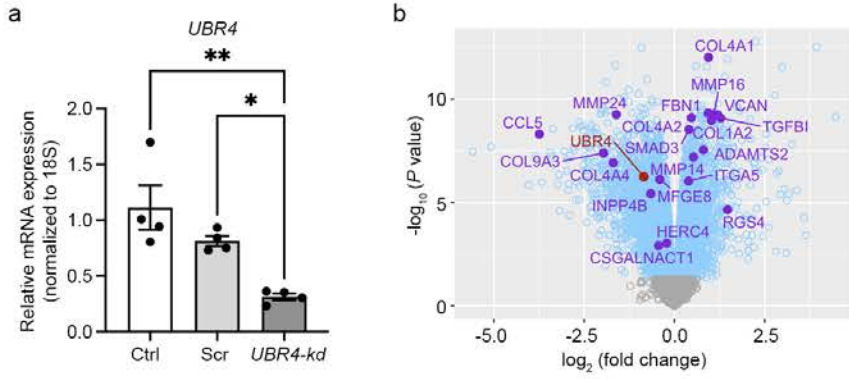


Extended Data Fig 3

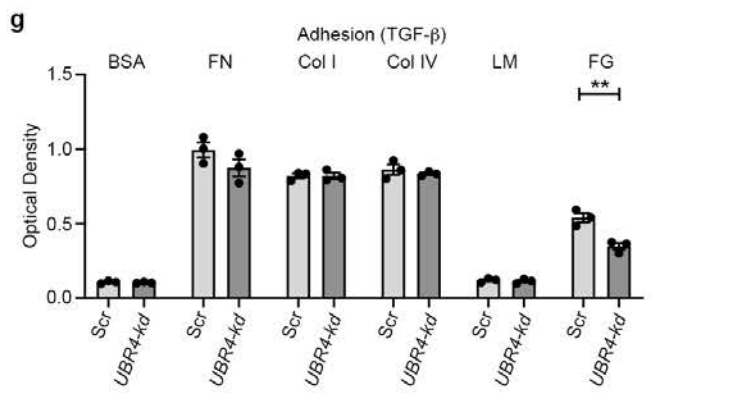
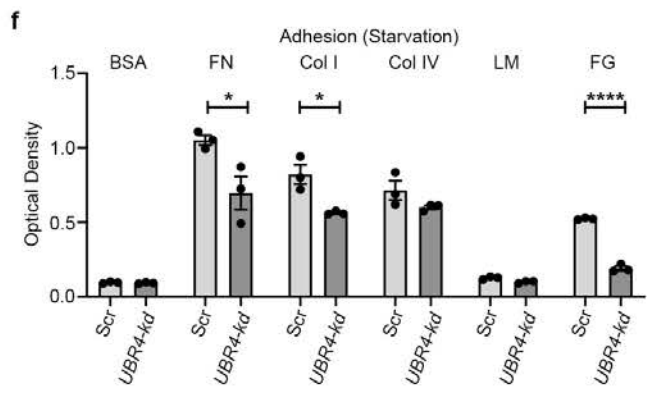
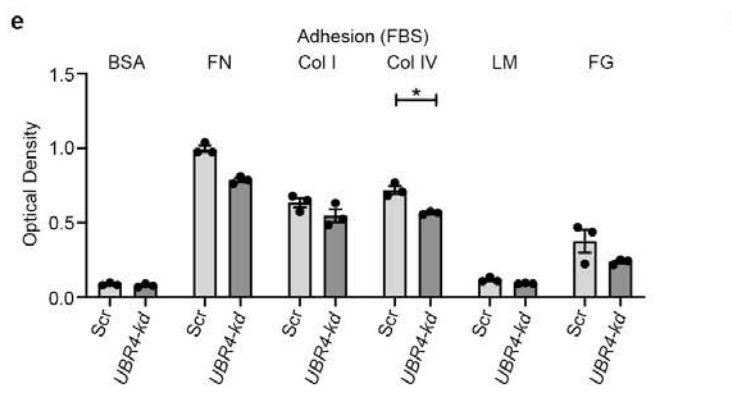
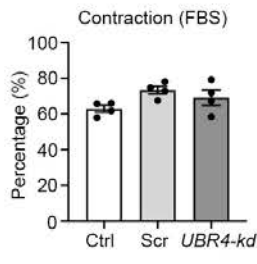
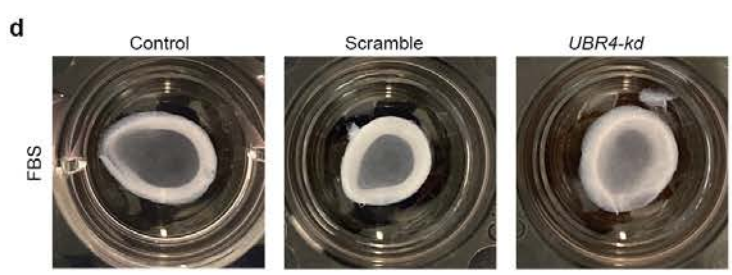
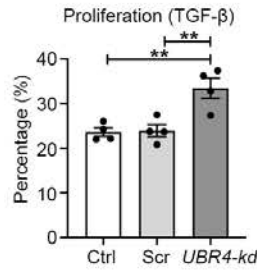
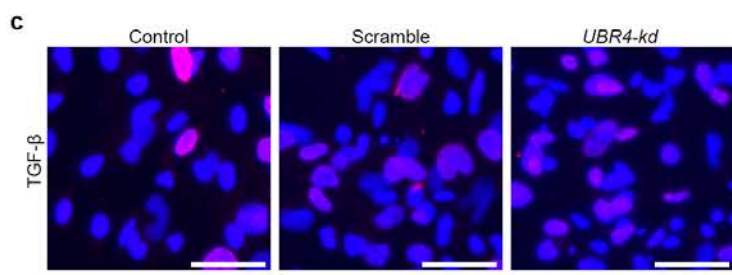
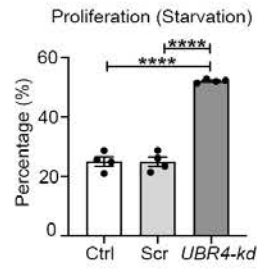
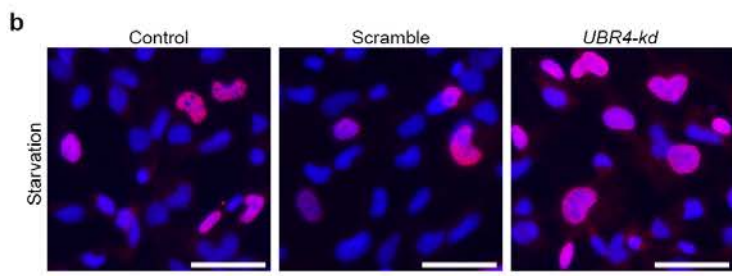
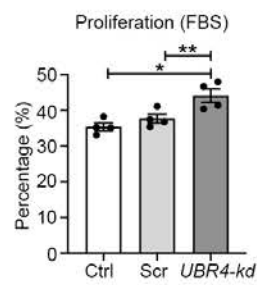
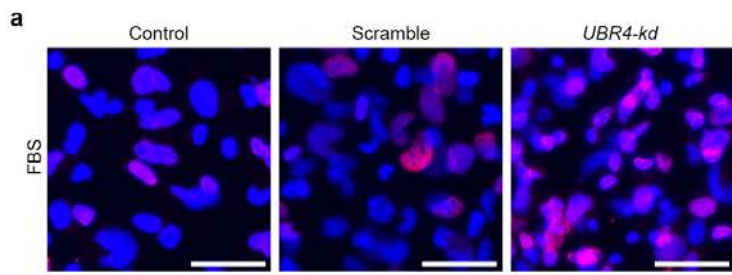


a

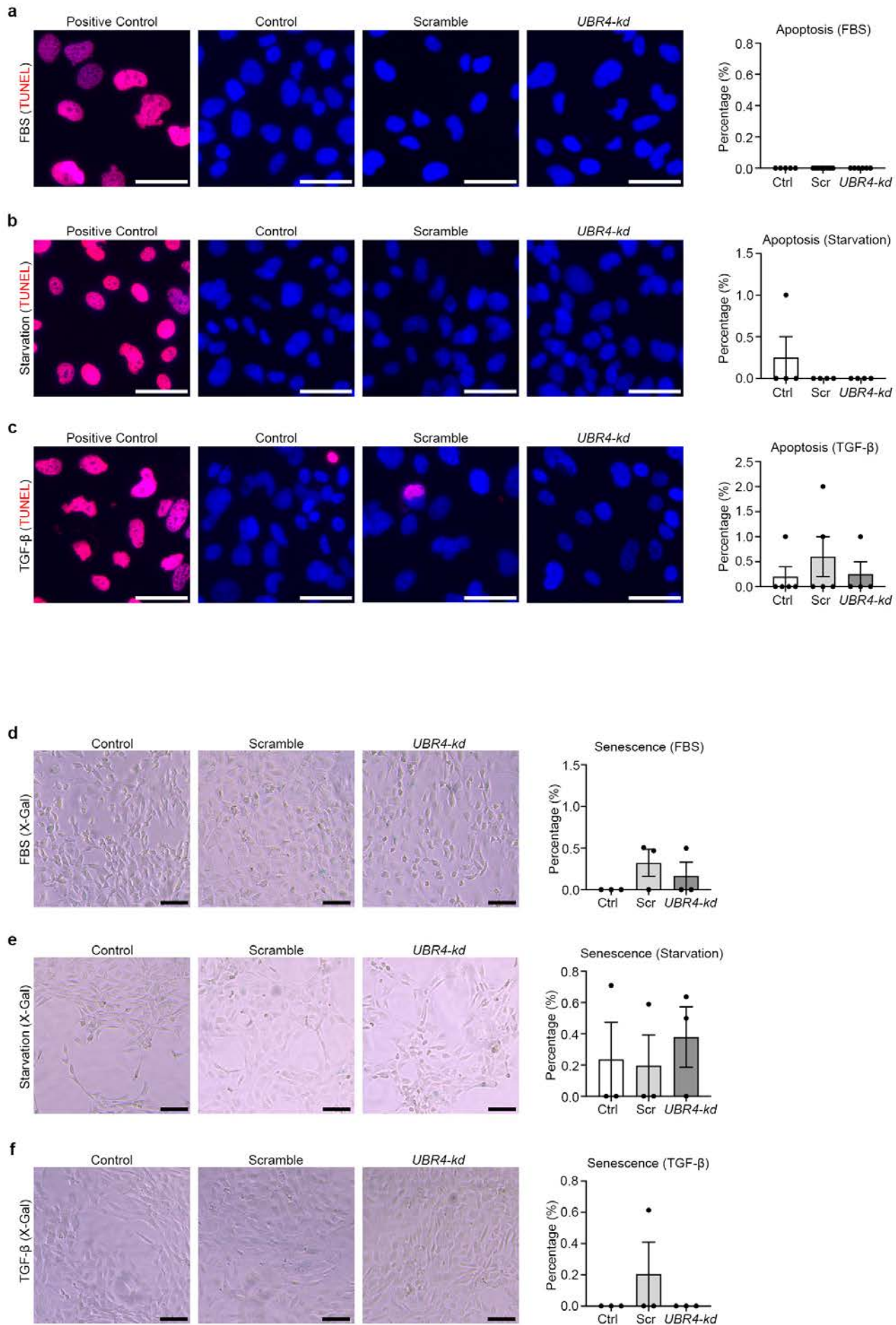


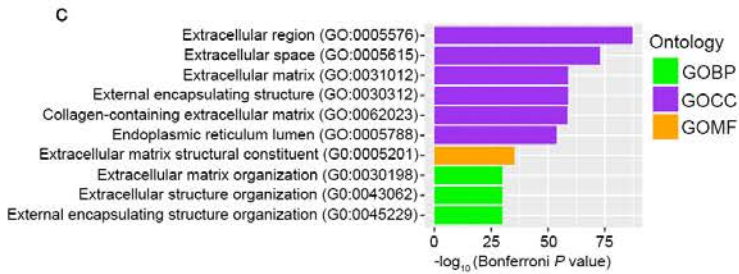
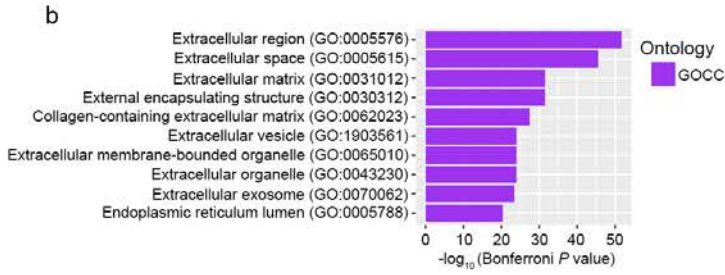
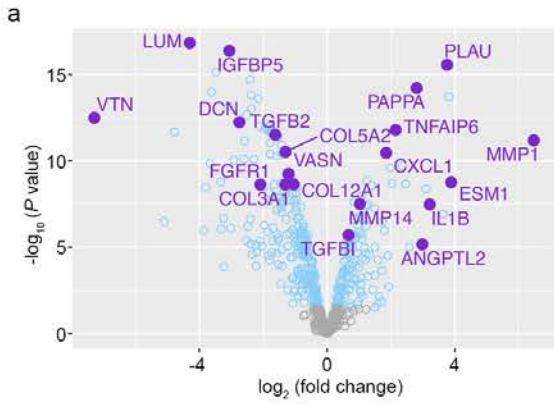


Extended Data Fig 6



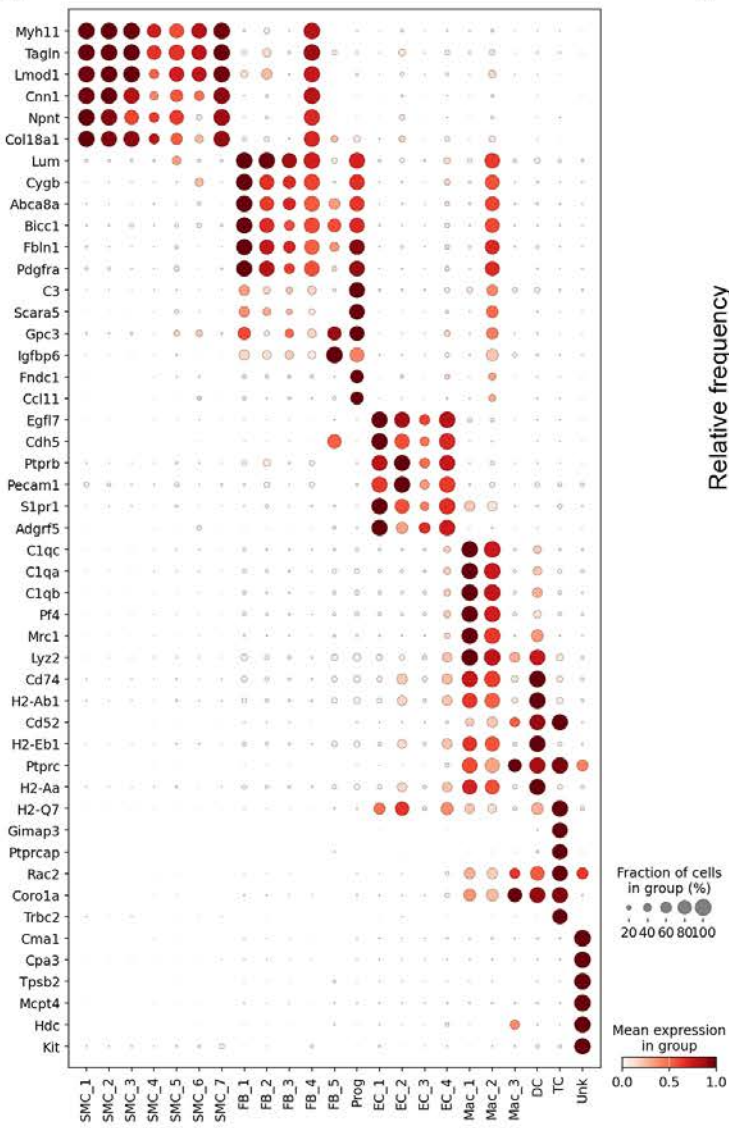
Extended Data Fig 7



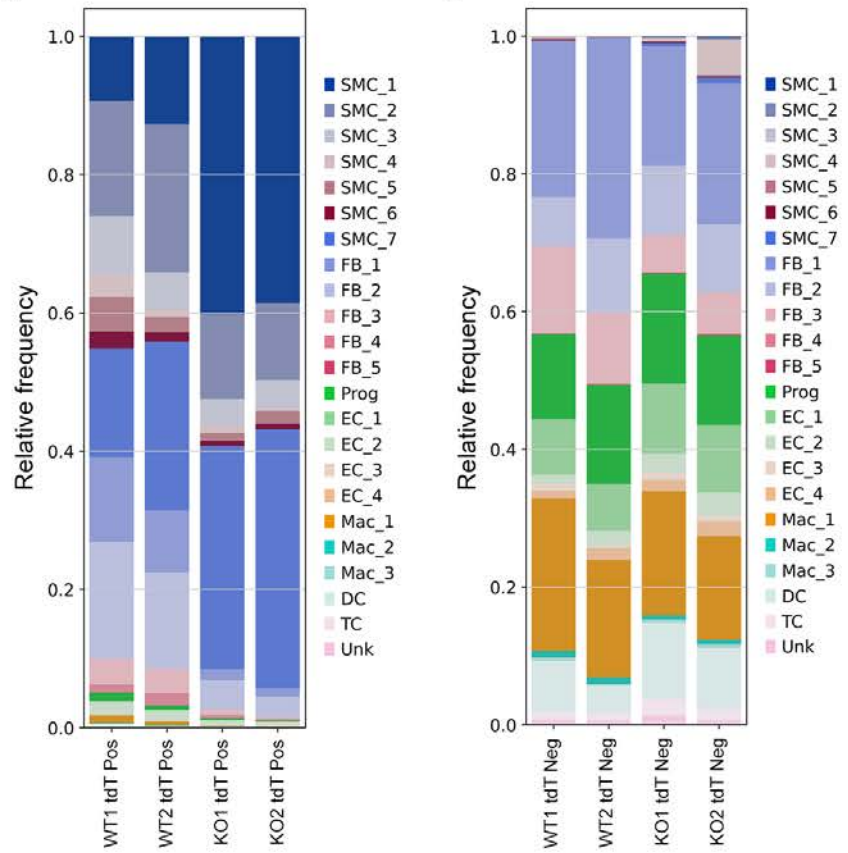


Extended Data Fig 9

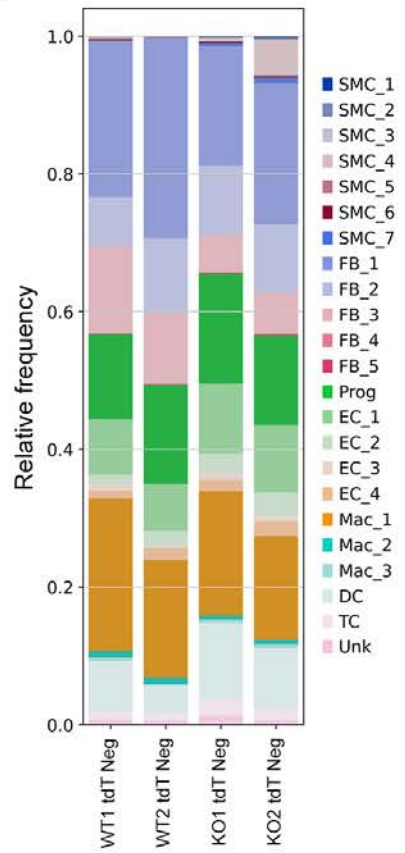
a



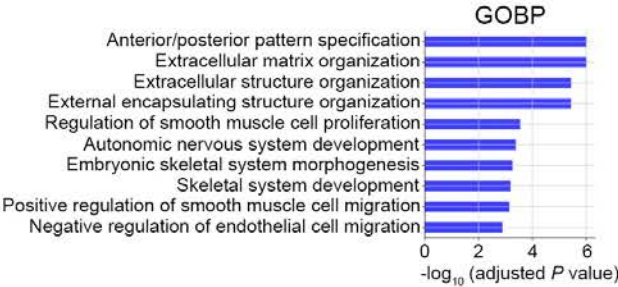
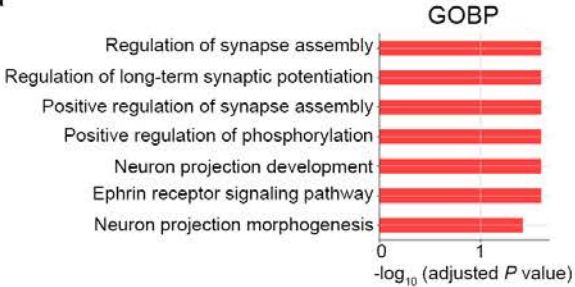
b



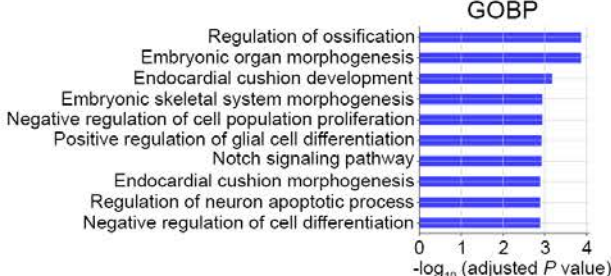
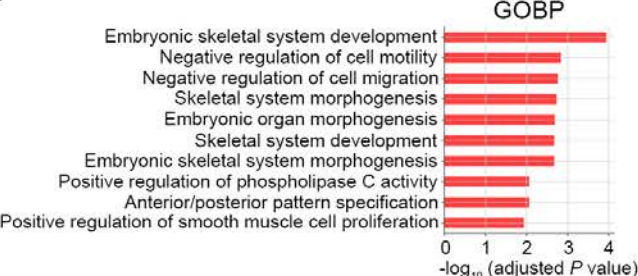
c



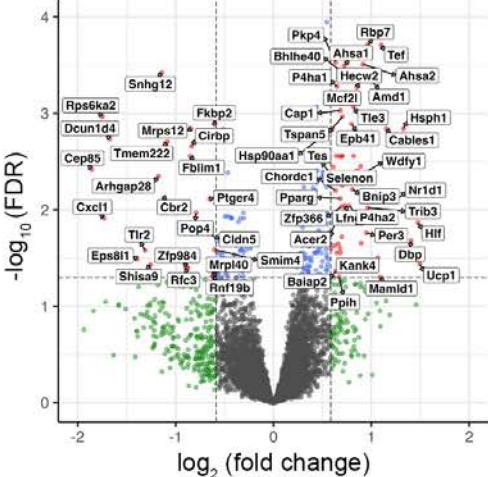
a



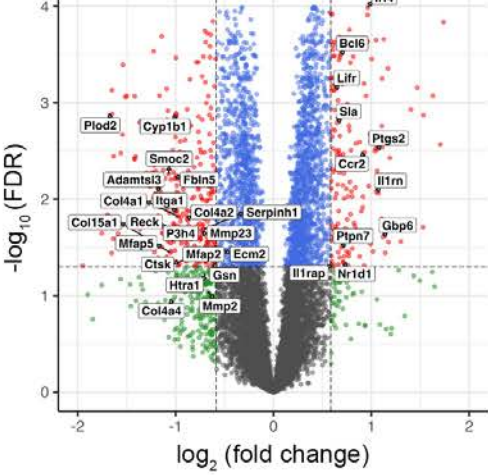
b



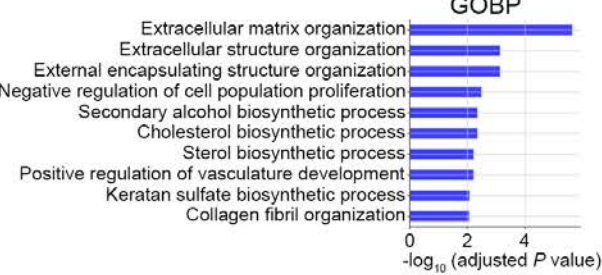
c



d



e



**Supplementary Table 36. Details of statistical tests used and specific statistical methods.
Primary Figures Statistical Method Summary**

Figure Number	Statistical Method Used	Statistical Method Detail	
		Normal distributed	Equal Variance
Figure 4			
a			
b			
c			
d			
e	Unpaired t test	Y	Y
f			
g	Mann-Whitney test	N	
h	Unpaired t test	Y	Y
i	Unpaired t test	Y	Y
j	Unpaired t test	Y	Y
k	Mann-Whitney test	N	
l			
m	Mann-Whitney test	N	
n			
o	Unpaired t test	Y	Y
p	Unpaired t test	Y	Y
q	Unpaired t test	Y	Y
r	Unpaired t test	Y	Y
s	Unpaired t test	Y	Y
t	Mann-Whitney test	N	
u			
v	Mann-Whitney test	N	
w			
x	Unpaired t test	Y	Y
Figure 5			
a			
b			
c			
d	Unpaired t test	Y	Y
e	Unpaired t test	Y	Y
f	Unpaired t test	Y	Y
g	Welch's t test	Y	No (F test P = 0.04)
h	Unpaired t test	Y	Y
i			
j	Mann-Whitney test	N	
k			
l	Unpaired t test	Y	Y

m	Unpaired t test	Y	Y
n	Unpaired t test	Y	Y
o	Unpaired t test	Y	Y
p	Unpaired t test	Y	Y
q	Unpaired t test	Y	Y
r			
s	Unpaired t test	Y	Y
t			
u	Unpaired t test	Y	Y

Extended Data Figures Statistical Method Summary

Figure Number	Statistical Method Used	Statistical Method Detail	
		Normal distributed	Equal Variance
Extended Data Figure 1			
a	Kruskal-Wallis test	N	
b	Ordinary one-way ANOVA	Y	
v	Ordinary one-way ANOVA	Y	
d	Ordinary one-way ANOVA	Y	
e	Ordinary one-way ANOVA	Y	
f	Ordinary one-way ANOVA	Y	

Extended Data Figure 2

a			
BSA	Unpaired t test	Y	Y
FN	Unpaired t test	Y	Y
Col I	Unpaired t test	Y	Y
Col IV	Unpaired t test	Y	Y
LM	Unpaired t test	Y	Y
FG	Unpaired t test	Y	Y

b				
BSA	Unpaired t test	Y		Y
FN	Unpaired t test	Y		Y
Col I	Mann-Whitney test	N		
Col IV	Unpaired t test	Y		Y
LM	Unpaired t test	Y		Y
FG	Unpaired t test	Y		Y
c				
BSA	Unpaired t test	Y		Y
FN	Unpaired t test	Y		Y
Col I	Unpaired t test	Y		Y
Col IV	Unpaired t test	Y		Y
LM	Unpaired t test	Y		Y
FG	Unpaired t test	Y		Y
d	Ordinary one-way ANOVA	Y		
e	Ordinary one-way ANOVA	Y		
f	Ordinary one-way ANOVA	Y		

Extended Data Figure 3

a	Kruskal-Wallis test	N		
b	Kruskal-Wallis test	N		
c	Kruskal-Wallis test	N		
d	Kruskal-Wallis test	N		
e	Kruskal-Wallis test	N		
f	Kruskal-Wallis test	N		

Extended Data Figure 5

a Ordinary one-way ANOVA Y

Extended Data Figure 6

a Ordinary one-way ANOVA Y

b Ordinary one-way ANOVA Y

c Ordinary one-way ANOVA Y

d Ordinary one-way ANOVA Y

e				
BSA	Unpaired t test	Y		Y
FN	Mann-Whitney test	N		
Col I	Unpaired t test	Y		Y
Col IV	Unpaired t test	Y		Y
LM	Unpaired t test	Y		Y
FG	Unpaired t test	Y		Y
f				
BSA	Unpaired t test	Y		Y
FN	Unpaired t test	Y		Y
Col I	Unpaired t test	Y		Y
Col IV	Unpaired t test	Y		Y
LM	Mann-Whitney test	N		
FG	Unpaired t test	Y		Y
g				
BSA	Unpaired t test	Y		Y
FN	Unpaired t test	Y		Y
Col I	Unpaired t test	Y		Y
Col IV	Unpaired t test	Y		Y
LM	Unpaired t test	Y		Y
FG	Unpaired t test	Y		Y

Extended Data Figure 7

a	All values were zero and no statistical is needed	N
b	Kruskal-Wallis test	N
c	Kruskal-Wallis test	N
d	Kruskal-Wallis test	N
e	Kruskal-Wallis test	N
f	Kruskal-Wallis test	N

Supplemental Figures Statistical Method Summary

Figure Number	Statistical Method Used	Statistical Method Detail	
		Normal distributed	Equal Variance

Suppl. Figure 2

a	Ordinary one-way ANOVA	Y	
b			

Suppl. Figure 3

a	Unpaired t test	Y	Y
b			
Heart	Unpaired t test	Y	Y
Lungs	Unpaired t test	Y	Y
c	Mann-Whitney test	N	
d	Unpaired t test	Y	Y
e	Unpaired t test	Y	Y
f	Unpaired t test	Y	Y
g	Mann-Whitney test	N	
h	Mann-Whitney test	N	
i			

LVESV	Unpaired t test	Y	Y
LVEDV	Mann-Whitney test	N	
j	Unpaired t test	Y	Y
k	Unpaired t test	Y	Y
l	Unpaired t test	Y	Y
m	Mann-Whitney test	N	
n	Unpaired t test	Y	Y
o			
LVESVI	Unpaired t test	Y	Y
LVEDVI	Mann-Whitney test	N	
p	Mann-Whitney test	N	

Suppl. Figure 4

a	Unpaired t test	Y	Y
b	Unpaired t test	Y	Y
c	Unpaired t test	Y	Y
d	Mann-Whitney test	N	
e	Unpaired t test	Y	Y
f	Mann-Whitney test	N	
g	Welch's t test	Y	No (F test P = 0.0056)
h	Welch's t test	Y	No (F test P = 0.0041)
i	Unpaired t test	Y	Y
j			
WBC	Unpaired t test	Y	Y
NEU	Mann-Whitney test	N	
LYMPH	Unpaired t test	Y	Y
k			
MONO	Mann-Whitney test	N	
EO	Unpaired t test	Y	Y
BASO	Mann-Whitney test	N	
l			
ASL	Unpaired t test	Y	Y
ALT	Mann-Whitney test	N	
m			
ALP	Unpaired t test	Y	Y
GGT	N/A	N/A	N/A
n			
Total	Mann-Whitney test	N	
Direct	Welch's t test	Y	No (F test P <0.0001)
Indirect	Mann-Whitney test	N	
o			
BUN	Unpaired t test	Y	Y
Creatinine	Mann-Whitney test	N	

p	Mann-Whitney test	N	
q			
Cholesterol	Unpaired t test	Y	Y
TG	Unpaired t test	Y	Y
r			
Total Protein	Unpaired t test	Y	Y
Albumin	Unpaired t test	Y	Y
Globulin	Unpaired t test	Y	Y
s	Unpaired t test	Y	Y
t	Welch's t test	Y	No (F test P = 0.0190)
u			
Calcium	Unpaired t test	Y	Y
Phosphorus	Welch's t test	Y	No (F test P = 0.0053)
Magnesium	Unpaired t test	Y	Y

Suppl. Figure 5

a			
b	Unpaired t test	Y	Y
c	Unpaired t test	Y	Y
d	Mann-Whitney test	N	
e	Unpaired t test	Y	Y
f	Unpaired t test	Y	Y
g	Mann-Whitney test	N	
h			
i	Mann-Whitney test	N	
j			
k	Unpaired t test	Y	Y
l			
m	Unpaired t test	Y	Y
n			
o	Unpaired t test	Y	Y
p			
q	Unpaired t test	Y	Y

Suppl. Figure 6

a			
b	Unpaired t test	Y	Y
c	Unpaired t test	Y	Y
d	Mann-Whitney test	N	
e	Unpaired t test	Y	Y
f	Unpaired t test	Y	Y
g	Mann-Whitney test	N	
h			

i	Mann-Whitney test	N	
j			
k	Unpaired t test	Y	Y

Suppl. Figure 8

a	Unpaired t test	Y	Y
b			
Heart	Unpaired t test	Y	Y
Lungs	Unpaired t test	Y	Y
c	Mann-Whitney test	N	
d	Mann-Whitney test	N	
e	Unpaired t test	Y	Y
f	Unpaired t test	Y	Y
g	Unpaired t test	Y	Y
h	Unpaired t test	Y	Y
i			
LVESV	Unpaired t test	Y	Y
LVEDV	Unpaired t test	Y	Y
j	Mann-Whitney test	N	
k	Unpaired t test	Y	Y
l	Unpaired t test	Y	Y
m	Unpaired t test	Y	Y
n	Welch's t test	Y	No (F test P = 0.037)
o			
LVESVI	Welch's t test	Y	No (F test P = 0.0229)
LVEDVI	Unpaired t test	Y	Y
p	Unpaired t test	Y	Y
q	Unpaired t test	Y	Y
r	Welch's t test	Y	No (F test P = 0.0378)
s	Unpaired t test	Y	Y
t	Mann-Whitney test	N	
u	Mann-Whitney test	N	
v	Unpaired t test	Y	Y

Suppl. Figure 9

a			
b	Unpaired t test	Y	Y
c	Unpaired t test	Y	Y
d	Unpaired t test	Y	Y
e	Unpaired t test	Y	Y
f	Mann-Whitney test	N	
g	Unpaired t test	Y	Y
h			

i	Unpaired t test	Y	Y
---	-----------------	---	---

Suppl. Figure 10

a			
b	Unpaired t test	Y	Y
c	Unpaired t test	Y	Y
d	Unpaired t test	Y	Y
e	Unpaired t test	Y	Y
f	Unpaired t test	Y	Y
g	Mann-Whitney test	N	
h			
i	Mann-Whitney test	N	

Suppl. Figure 11

a			
b	Unpaired t test	Y	Y
c	Mann-Whitney test	N	
d	Mann-Whitney test	N	
e	Unpaired t test	Y	Y
f	Unpaired t test	Y	Y
g	Mann-Whitney test	N	
h			
i	Mann-Whitney test	N	

Suppl. Figure 12

a	Unpaired t test	Y	Y
b			
Heart	Mann-Whitney test	N	
Lungs	Mann-Whitney test	N	
c	Mann-Whitney test	N	
d	Mann-Whitney test	N	
e	Unpaired t test	Y	Y
f	Unpaired t test	Y	Y
g	Unpaired t test	Y	Y
h	Mann-Whitney test	N	
i			
LVESV	Unpaired t test	Y	Y
LVEDV	Mann-Whitney test	N	
j	Unpaired t test	Y	Y
k	Unpaired t test	Y	Y
l	Welch's t test	Y	No (F test P = 0.0382)
m	Unpaired t test	Y	Y
n	Unpaired t test	Y	Y

o				
LVESVI	Unpaired t test	Y		Y
LVEDVI	Unpaired t test	Y		Y
p	Unpaired t test	Y		Y

Suppl. Figure 13

a	Mann-Whitney test	N		
b	Mann-Whitney test	N		
c	Mann-Whitney test	N		
d	Unpaired t test	Y		Y
e	Mann-Whitney test	N		
f	Unpaired t test	Y		Y
g	Unpaired t test	Y		Y
h	Unpaired t test	Y		Y
i	Unpaired t test	Y		Y
j				
WBC	Unpaired t test	Y		Y
NEU	Unpaired t test	Y		Y
LYMPH	Mann-Whitney test	N		
k				
MONO	Mann-Whitney test	N		
EO	Unpaired t test	Y		Y
BASO	Mann-Whitney test	N		

Suppl. Figure 14

a				
b	Unpaired t test	Y		Y
c	Unpaired t test	Y		Y
d	Unpaired t test	Y		Y
e	Unpaired t test	Y		Y
f	Unpaired t test	Y		Y
g	Mann-Whitney test	N		
h				
i	Mann-Whitney test	N		
j				
k	Mann-Whitney test	N		
l				
m	Unpaired t test	Y		Y
n				
o	Unpaired t test	Y		Y
p				
q	Unpaired t test	Y		Y

Suppl. Figure 15

a			
b	Unpaired t test	Y	Y
c	Welch's t test	Y	No (F test P = 0.0136)
d	Unpaired t test	Y	Y
e	Unpaired t test	Y	Y
f	Unpaired t test	Y	Y
g	Mann-Whitney test	N	
h			
i	Unpaired t test	Y	Y
j			
k	Welch's t test	Y	No (F test P <0.0001)

Sample Size (Biological replicates)			P Value Note	P Value
Control	Scramble	KD/KO		
All replicates are biological				

5		5		0.0462
10		11		<0.0001
10		11		<0.0001
10		11		<0.0001
10		11		0.0010
7		8		0.0037
10		11		<0.0001
8		9		0.0156
8		9		0.0198
8		9		0.2396
8		9		0.0065
10		10		0.0150
10		9		0.5856
8		10		0.4108
10		7		0.8754

All replicates are biological

5		6		0.0005
5		6		0.0085
5		6		0.0623
4		6		0.0049
4		6		0.0383
5		6		0.0043
7		7		0.0225

7	7	0.0296
7	7	0.5657
7	7	0.0220
7	7	<0.0001
7	7	0.5098
10	10	0.8733
10	8	0.0016

Sample Size (Biological replicates)

Control	Scramble	KD/KO		P Value
All replicates are biological				Adj. P
3	3	3	Ctrl vs. Scramble	>0.9999
			Ctrl vs. UBR4 KO	0.2209
			Scramble vs. UBR4	0.076
3	3	3	Ctrl vs. Scramble	0.7849
			Ctrl vs. UBR4 KO	<0.0001
			Scramble vs. UBR4	<0.0001
3	3	3	Ctrl vs. Scramble	0.7797
			Ctrl vs. UBR4 KO	0.0004
			Scramble vs. UBR4	0.0003
4	4	4	Ctrl vs. Scramble	0.6933
			Ctrl vs. UBR4 KO	0.0059
			Scramble vs. UBR4	0.0205
4	4	4	Ctrl vs. Scramble	0.8171
			Ctrl vs. UBR4 KO	0.8657
			Scramble vs. UBR4	0.9949
4	4	4	Ctrl vs. Scramble	0.9961
			Ctrl vs. UBR4 KO	0.9733
			Scramble vs. UBR4	0.9499

All replicates are biological

3	3	3	0.0415
3	3	3	0.0851
3	3	3	0.0010
3	3	3	0.0377
3	3	3	0.0029
3	3	3	0.0296

3	3	3	0.3598
3	3	3	0.0577
3	3	3	0.1000
3	3	3	0.0016
3	3	3	0.0019
3	3	3	0.3534

3	3	3	0.6617
3	3	3	0.3749
3	3	3	0.0591
3	3	3	0.2091
3	3	3	0.0194
3	3	3	0.0180

Adj. P

4	4	4	Ctrl vs. Scramble 0.4037
			Ctrl vs. UBR4 KO <0.0001
			Scramble vs. UBR4 I <0.0001
4	4	4	Ctrl vs. Scramble 0.0573
			Ctrl vs. UBR4 KO <0.0001
			Scramble vs. UBR4 I <0.0001
4	4	4	Ctrl vs. Scramble 0.8699
			Ctrl vs. UBR4 KO 0.3642
			Scramble vs. UBR4 I 0.6365

All replicates are biological

Adj. P

3	3	3	Ctrl vs. Scramble >0.9999
			Ctrl vs. UBR4 KO 0.6620
			Scramble vs. UBR4 I 0.6620
3	3	3	Ctrl vs. Scramble >0.9999
			Ctrl vs. UBR4 KO 0.6620
			Scramble vs. UBR4 I 0.6620
3	3	3	Ctrl vs. Scramble >0.9999
			Ctrl vs. UBR4 KO 0.6620
			Scramble vs. UBR4 I 0.6620
3	3	3	Ctrl vs. Scramble >0.9999
			Ctrl vs. UBR4 KO 0.9223
			Scramble vs. UBR4 I >0.9999
3	3	3	Ctrl vs. Scramble 0.7287
			Ctrl vs. UBR4 KO >0.9999
			Scramble vs. UBR4 I 0.7287
3	3	3	Ctrl vs. Scramble 0.3074
			Ctrl vs. UBR4 KO >0.9999

Scramble vs. UBR4 | 0.5743

Replicates in 8a are biological Adj. P

4	4	4	Ctrl vs. Scramble	0.2328
			Ctrl vs. UBR4 KO	0.0028
			Scramble vs. UBR4	0.0385

All replicates are biological Adj. P

4	4	4	Ctrl vs. Scramble	0.5271
			Ctrl vs. UBR4 KO	0.0052
			Scramble vs. UBR4	0.0279
4	4	4	Ctrl vs. Scramble	0.9994
			Ctrl vs. UBR4 KO	<0.0001
			Scramble vs. UBR4	<0.0001
4	4	4	Ctrl vs. Scramble	0.9873
			Ctrl vs. UBR4 KO	0.0050
			Scramble vs. UBR4	0.0063
4	4	4	Ctrl vs. Scramble	0.0891
			Ctrl vs. UBR4 KO	0.3542
			Scramble vs. UBR4	0.6175

Non Adj. P

3	3	3		0.4045
3	3	3		0.1000
3	3	3		0.1832
3	3	3		0.0044
3	3	3		0.0613
3	3	3		0.1479
3	3	3		0.6064
3	3	3		0.0376
3	3	3		0.0168
3	3	3		0.1545
3	3	3		0.1000
3	3	3		<0.0001
3	3	3		0.6867
3	3	3		0.1880
3	3	3		0.9991
3	3	3		0.4885
3	3	3		0.6353
3	3	3		0.0076

All replicates are biological			Adj. P
5	8	6	Ctrl vs. Scramble >0.9999 Ctrl vs. UBR4 KO >0.9999 Scramble vs. UBR4 I >0.9999
4	4	4	Ctrl vs. Scramble 0.6620 Ctrl vs. UBR4 KO 0.6620 Scramble vs. UBR4 I >0.9999
5	5	4	Ctrl vs. Scramble >0.9999 Ctrl vs. UBR4 KO >0.9999 Scramble vs. UBR4 I >0.9999
3	3	3	Ctrl vs. Scramble 0.3327 Ctrl vs. UBR4 KO >0.9999 Scramble vs. UBR4 I >0.9999
3	3	3	Ctrl vs. Scramble >0.9999 Ctrl vs. UBR4 KO >0.9999 Scramble vs. UBR4 I >0.9999
3	3	3	Ctrl vs. Scramble 0.6620 Ctrl vs. UBR4 KO >0.9999 Scramble vs. UBR4 I 0.6620

Sample Size (Biological replicates)			P Value
Control	Scramble	KD/KO	Adj. P
4	4	4	Ctrl vs. Scramble 0.9843 Ctrl vs. UBR4 KO 0.0034 Scramble vs. UBR4 I 0.0043

10		11	0.6800
7		6	0.8403
7		6	0.5005
7		3	>0.9999
10		11	0.676
10		12	0.2745
10		12	0.3308
10		12	0.3376
9		10	0.3451

10	11	0.2327
10	11	0.6539
10	11	<0.0001
10	11	0.0380
10	11	0.0010
10	11	0.0295
10	11	0.0022
10	11	0.2128
10	11	0.7045
10	11	0.9177



7	7	0.3036
7	7	0.3872
7	7	0.8018
7	7	0.1282
7	7	0.1852
7	7	0.1544
7	7	0.0381
7	7	0.0466
7	7	0.4125
7	7	0.3952
7	7	0.0973
7	7	0.4451
7	7	0.6329
7	7	0.6464
7	7	0.2739
7	7	0.4609
7	7	0.3333
7	7	0.0745
7	6	N/A (>0.9999)
7	7	0.8689
7	6	0.3559
7	7	>0.9999
7	7	0.5218
7	7	0.4615

7	7	0.6200
7	7	0.3628
7	5	0.9370
7	7	0.9130
7	6	0.6679
7	6	0.6955
7	7	0.4364
7	7	0.4425
7	7	0.6901
7	7	0.6986
7	7	0.6047

12	13	0.0001
12	13	0.0002
12	13	0.2945
12	13	0.0001
12	13	0.0285
12	13	0.0516
10	10	0.582
9	10	0.4570
8	5	0.4537
6	6	0.8205
5	5	0.4502

8	9	0.0524
8	9	0.1425
8	9	0.2766
8	9	0.0570
10	11	0.0168
10	11	0.6699

12	8	0.2009
----	---	--------

7	7	0.7969
---	---	--------

12	16	0.9933
----	----	--------

11	15	0.5355
----	----	--------

11	15	0.1579
----	----	--------

8	8	0.8912
---	---	--------

11	14	0.8823
----	----	--------

11	15	0.0004
----	----	--------

11	15	0.0002
----	----	--------

11	15	0.0002
----	----	--------

7	9	0.1041
---	---	--------

11	14	0.0178
----	----	--------

11	14	0.9633
----	----	--------

11	14	<0.0001
----	----	---------

11	14	0.1400
----	----	--------

11	14	0.1140
----	----	--------

11	14	0.2387
----	----	--------

11	14	0.0055
----	----	--------

11	14	0.0072
----	----	--------

11	14	0.9767
----	----	--------

11	14	0.0018
----	----	--------

11	14	0.0011
----	----	--------

11	14	<0.0001
----	----	---------

11	15	<0.0001
----	----	---------

11	13	<0.0001
----	----	---------

10	12	<0.0001
----	----	---------

11	15	<0.0001
----	----	---------

5	6	<0.0001
---	---	---------

5	6	<0.0001
---	---	---------

5	6	0.3361
---	---	--------

5	6	<0.0001
---	---	---------

6	8	0.0426
---	---	--------

6	8	0.1348
---	---	--------

7	9	0.6568
---	---	--------

9	12	0.0005
9	12	0.0020
9	12	0.7281
9	12	0.0007
6	12	<0.0001
6	12	0.2330

7	14	0.6357
---	----	--------

10	12	<0.0001
10	12	0.0020
10	12	0.2829
10	12	<0.0001
7	10	0.0001
7	10	0.6372

8	11	0.9039
---	----	--------

16	14	0.1574
----	----	--------


16	14	0.7343
16	13	0.2529
5	6	0.7944
5	6	0.1255
5	6	0.8271
5	6	0.3575
5	6	0.8152
5	6	0.0823

4	6	0.3143
4	6	0.4762
4	6	0.0704
4	3	0.1836
4	6	0.2501
4	6	0.3102
4	6	0.2575

4	6	0.2515
4	6	0.7235
4	6	0.1271

5	6	>0.9999
5	6	0.7554
5	6	0.7922
5	6	0.9014
5	6	0.8355
5	6	0.8242
5	6	0.4482
5	6	0.2959
5	6	0.4000
6	7	0.8476
6	6	0.3262
5	6	0.5368
5	6	0.3074
5	6	0.6416
5	6	>0.9999

11	8	0.0231
11	8	0.0455
11	8	0.1376
11	8	0.0247
10	8	<0.0001
10	8	0.3416
9	8	0.1222
9	10	0.0133
5	5	0.8482
5	5	0.3985
5	5	0.8592



8	9	0.0001
4	6	0.0021
8	9	0.6146
8	9	<0.0001
9	9	<0.0001
9	9	>0.9999
8	9	0.6729
8	8	0.0441

Error Bars	One-sided or two-sided	Adjusted Multiple Comparisons
------------	------------------------	-------------------------------

Mean +/- SD 2-sided

Mean +/- SD 2-sided

Mean +/- SD 2-sided

Mean +/- SD 2-sided

Mean +/- SD 2-sided

Mean +/- SD 2-sided

Mean +/- SD 2-sided

Mean +/- SD 2-sided

Mean +/- SD 2-sided

Mean +/- SD 2-sided

Mean +/- SD 2-sided

Mean +/- SD 2-sided

Mean +/- SD 2-sided

Mean +/- SD 2-sided

Mean +/- SD 2-sided

Mean +/- SD 2-sided

Mean +/- SD 2-sided

Mean +/- SD 2-sided

Mean +/- SD 2-sided

Mean +/- SD 2-sided

Mean +/- SD 2-sided

Mean +/- SD 2-sided

Mean +/- SEM 2-sided
Mean +/- SEM 2-sided
Mean +/- SEM 2-sided
Mean +/- SEM 2-sided
Mean +/- SEM 2-sided
Mean +/- SEM 2-sided

Mean +/- SEM 2-sided
Mean +/- SEM 2-sided
Mean +/- SEM 2-sided
Mean +/- SEM 2-sided
Mean +/- SEM 2-sided
Mean +/- SEM 2-sided

Mean +/- SEM 2-sided Yes - Tukey's multiple comparisons
2-sided
2-sided

Mean +/- SEM 2-sided Yes - Tukey's multiple comparisons
2-sided
2-sided

Mean +/- SEM 2-sided Yes - Tukey's multiple comparisons
2-sided
2-sided

Mean +/- SEM 2-sided Yes - Dunn's multiple comparisons
2-sided

Mean +/- SEM 2-sided Yes - Dunn's multiple comparisons
2-sided
2-sided

Mean +/- SEM 2-sided Yes - Dunn's multiple comparisons
2-sided
2-sided

Mean +/- SEM 2-sided Yes - Dunn's multiple comparisons
2-sided
2-sided

Mean +/- SEM 2-sided Yes - Dunn's multiple comparisons
2-sided
2-sided

Mean +/- SEM 2-sided Yes - Dunn's multiple comparisons
2-sided

2-sided

Mean +/- SEM 2-sided Yes - Tukey's multiple comparisons

Mean +/- SEM 2-sided Yes - Tukey's multiple comparisons

2-sided

2-sided

Mean +/- SEM 2-sided Yes - Tukey's multiple comparisons

2-sided

2-sided

Mean +/- SEM 2-sided Yes - Tukey's multiple comparisons

2-sided

2-sided

Mean +/- SEM 2-sided

2-sided

2-sided

Mean +/- SEM 2-sided

Mean +/- SEM 2-sided

Mean +/- SEM 2-sided

Mean +/- SEM 2-sided

Mean +/- SEM 2-sided

Mean +/- SEM 2-sided

Mean +/- SEM 2-sided

Mean +/- SEM 2-sided

Mean +/- SEM 2-sided

Mean +/- SEM 2-sided

Mean +/- SEM 2-sided

Mean +/- SEM 2-sided

Mean +/- SEM 2-sided

Mean +/- SEM 2-sided

Mean +/- SEM 2-sided

Mean +/- SEM 2-sided

Mean +/- SEM 2-sided

Mean +/- SEM 2-sided

Mean +/- SD	2-sided
Mean +/- SD	2-sided
Mean +/- SD	2-sided
Mean +/- SD	2-sided
Mean +/- SD	2-sided
Mean +/- SD	2-sided
Mean +/- SD	2-sided

Mean +/- SD	2-sided
Mean +/- SD	2-sided
Mean +/- SD	2-sided

Mean +/- SD	2-sided
Mean +/- SD	2-sided
Mean +/- SD	2-sided
Mean +/- SD	2-sided
Mean +/- SD	2-sided
Mean +/- SD	2-sided
Mean +/- SD	2-sided
Mean +/- SD	2-sided
Mean +/- SD	2-sided

Mean +/- SD	2-sided
Mean +/- SD	2-sided
Mean +/- SD	2-sided

Mean +/- SD	2-sided
Mean +/- SD	2-sided
Mean +/- SD	2-sided

Mean +/- SD	2-sided
Mean +/- SD	2-sided

Mean +/- SD	2-sided
Mean +/- SD	2-sided

Mean +/- SD	2-sided
Mean +/- SD	2-sided
Mean +/- SD	2-sided

Mean +/- SD	2-sided
Mean +/- SD	2-sided

Mean +/- SD 2-sided

Mean +/- SD 2-sided

Mean +/- SD 2-sided

Mean +/- SD 2-sided

Mean +/- SD 2-sided

Mean +/- SD 2-sided

Mean +/- SD 2-sided

Mean +/- SD 2-sided

Mean +/- SD 2-sided

Mean +/- SD 2-sided

Mean +/- SD 2-sided

Mean +/- SD 2-sided

Mean +/- SD 2-sided

Mean +/- SD 2-sided

Mean +/- SD 2-sided

Mean +/- SD 2-sided

Mean +/- SD 2-sided

Mean +/- SD 2-sided

Mean +/- SD 2-sided

Mean +/- SD 2-sided

Mean +/- SD 2-sided

Mean +/- SD 2-sided

Mean +/- SD 2-sided

Mean +/- SD 2-sided

Mean +/- SD 2-sided

Mean +/- SD 2-sided

Mean +/- SD 2-sided

Mean +/- SD 2-sided

Mean +/- SD 2-sided

Mean +/- SD 2-sided

Mean +/- SD 2-sided

Mean +/- SD 2-sided

Mean +/- SD 2-sided

Mean +/- SD 2-sided

Mean +/- SD 2-sided

Mean +/- SD 2-sided

Mean +/- SD 2-sided

Mean +/- SD 2-sided

Mean +/- SD 2-sided

Mean +/- SD 2-sided

Mean +/- SD 2-sided

Mean +/- SD 2-sided

Mean +/- SD 2-sided

Mean +/- SD 2-sided

Mean +/- SD 2-sided

Mean +/- SD 2-sided

Mean +/- SD 2-sided

Mean +/- SD 2-sided

Mean +/- SD 2-sided

Mean +/- SD 2-sided

Mean +/- SD 2-sided

Mean +/- SD 2-sided

Mean +/- SD 2-sided

Mean +/- SD 2-sided

Mean +/- SD 2-sided

Mean +/- SD 2-sided

Mean +/- SD 2-sided

Mean +/- SD 2-sided

Mean +/- SD 2-sided

Mean +/- SD 2-sided

Mean +/- SD 2-sided

Mean +/- SD 2-sided

Mean +/- SD 2-sided

Mean +/- SD 2-sided

Mean +/- SD 2-sided

Mean +/- SD 2-sided

Mean +/- SD 2-sided

Mean +/- SD 2-sided

Mean +/- SD 2-sided

Mean +/- SD 2-sided

Mean +/- SD 2-sided

Mean +/- SD 2-sided

Mean +/- SD 2-sided

Mean +/- SD 2-sided

Mean +/- SD 2-sided

Mean +/- SD 2-sided

Mean +/- SD 2-sided

Mean +/- SD 2-sided

Mean +/- SD 2-sided

Mean +/- SD 2-sided

Mean +/- SD

Mean +/- SD 2-sided

Mean +/- SD 2-sided

Mean +/- SD 2-sided

Mean +/- SD 2-sided

Mean +/- SD 2-sided

Mean +/- SD 2-sided

Mean +/- SD 2-sided

Mean +/- SD 2-sided

Mean +/- SD 2-sided

Mean +/- SD 2-sided

Mean +/- SD 2-sided

Mean +/- SD	2-sided
Mean +/- SD	2-sided
Mean +/- SD	2-sided

Mean +/- SD	2-sided
Mean +/- SD	2-sided
Mean +/- SD	2-sided
Mean +/- SD	2-sided
Mean +/- SD	2-sided
Mean +/- SD	2-sided
Mean +/- SD	2-sided
Mean +/- SD	2-sided
Mean +/- SD	2-sided

Mean +/- SD	2-sided
Mean +/- SD	2-sided
Mean +/- SD	2-sided

Mean +/- SD	2-sided
Mean +/- SD	2-sided
Mean +/- SD	2-sided

Mean +/- SD	2-sided
Mean +/- SD	2-sided
Mean +/- SD	2-sided
Mean +/- SD	2-sided
Mean +/- SD	2-sided
Mean +/- SD	2-sided


Mean +/- SD	2-sided
-------------	---------

Mean +/- SD	2-sided
-------------	---------

Mean +/- SD	2-sided
-------------	---------

Mean +/- SD	2-sided
-------------	---------

Mean +/- SD	2-sided
-------------	---------



Mean +/- SD	2-sided
Mean +/- SD	2-sided
Mean +/- SD	2-sided
Mean +/- SD	2-sided
Mean +/- SD	2-sided
Mean +/- SD	2-sided

Mean +/- SD	2-sided
-------------	---------

Mean +/- SD	2-sided
-------------	---------